SYNTHESIS AND *IN SILICO* STUDIES OF QUINAZOLINONE DERIVATIVES AS PARP-1 INHIBITORS

Thesis submitted to the Central University of Punjab

For the award of

Master of Pharmacy (Medicinal Chemistry)

In

Department of Pharmaceutical Sciences and Natural Products

BY

SONIA VERMA

Supervisor

Dr. Pradeep Kumar

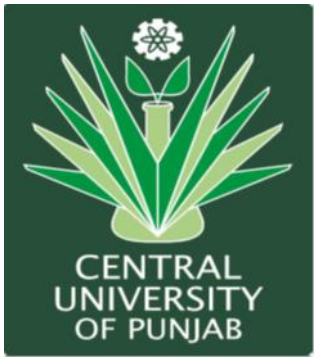

Department of Pharmaceutical Sciences and Natural Products

School of Basic and Applied Sciences

Central University of Punjab, Bathinda

May, 2018

DECLARATION

I declare that the thesis entitled **"SYNTHESIS AND *IN SILICO* STUDIES OF QUINAZOLINONE DERIVATIVES AS PARP-1 INHIBITORS"** has been prepared by me under the guidance of Dr. Pradeep Kumar, Assistant Professor, Department of Pharmaceutical Sciences and Natural Products, School of Basic and Applied Sciences, Central University of Punjab, Bathinda. No part of this thesis has formed the basis for the award of any degree or fellowship previously.

[Sonia Verma]
[Department of Pharmaceutical Sciences and Natural Products],
School of Basic and Applied Sciences,
Central University of Punjab, Bathinda - 151001.

Date:

CERTIFICATE

I certify that SONIA VERMA has prepared her thesis entitled **"SYNTHESIS AND *IN SILICO* STUDIES OF QUINAZOLINONE DERIVATIVES AS PARP-1 INHIBITORS",** for the award of M.Pharm. (Medicinal Chemistry) degree at the Central University of Punjab, under my guidance. She has carried out this work at the Department of Pharmaceutical Sciences and Natural Products, School of Basic and Applied Sciences, Central University of Punjab, Bathinda.

[Dr. Pradeep Kumar]
Assistant Professor
[Department of Pharmaceutical Sciences and Natural Products],
School of Basic and Applied Sciences,
Central University of Punjab, Bathinda -151001.

Date:

ABSTRACT

"Synthesis and *In silico* Studies of Quinazolinone Derivatives as PARP-1 Inhibitors"

Name of student	:	Sonia Verma
Registration number	:	16mpharm16
Degree for which submitted	:	M. Pharmacy (Medicinal Chemistry)
Name of supervisor	:	Dr. Pradeep Kumar
Name of Department	:	Department of Pharmaceutical Sciences and Natural Products
Name of school	:	Basic and Applied Sciences
Key words	:	Cancer, PARP-1, Quinazolinone

Cancer is one of the leading diseases responsible for high mortality rates worldwide. It develops when normal cells begin to grow out of control in particular part of the body. Cancer is a leading cause of death worldwide, accounting for 8.8 million deaths in 2015. According to WHO, the most common causes of cancer death are cancers of Lung (1.69 million deaths), Liver (788 000 deaths), Colorectal (774 000 deaths), Stomach (754 000 deaths) and Breast (571 000 deaths). PARP-1 is a ubiquitous zinc-finger DNA-binding enzyme that is activated by binding to DNA breaks and then catalyzes the synthesis of the branched polymer PAR using NAD^+ as the building block. PARP-1 has a crucial role in cell proliferation, survival, and death, due to its properties on regulation of multiple biological processes. Quinazolinone and its derivatives possess a large class of biologically active compounds that exhibited broad spectrum of biological activities such as anti-HIV, anticancer, antifungal, antibacterial, anticonvulsant, anti-inflammatory, antidepressant, antimalarial, antioxidant, antileukemic, and antileishmanial activities and other activities. In this study, we have synthesized quinazolinone derivatives and studied the in silico properties as PARP-1 inhibitors which indicated that quinazolinone derivatives were having good affinity towards active site of PARP-1. Out of all synthesized compounds, SVA-11 was having maximum dock score (-10.421).

(Sonia Verma) (Dr. Pradeep Kumar)

ACKNOWLEDGEMENT

This thesis is the end of my journey in obtaining my M. Pharmacy. This thesis has been kept on track and been seen through to the completion with the support, help and encouragement of numerous people including my well-wishers, my family, my friends and colleagues. At the end of my thesis I would like to thank all those people who made this thesis possible and an unforgettable experience for me.

I would first like to thank my thesis supervisor ***Dr. Pradeep Kumar****, Assistant Professor, Department of Pharmaceutical Sciences and Natural Products for his guidance, valuable advice, support and encouragement throughout my research work. The door to his office was always open whenever I ran into a trouble spot or had a question about my research or writing. He consistently allowed this to be my own work, but steered me in the right direction whenever he thought I needed it. It was a pleasure working with him.*

I would like to thank ***Dr. Raj Kumar, Associate Professor and Head, Dr. Vinod Kumar and Dr. Vikas Jaitak, Dr. Venkata Rao Kaki, Assistant Professors,*** *Department of Pharmaceutical Sciences and Natural Products for their guidance and support through all these years.*

I wish to express my warm and sincere thanks to ***Prof. (Dr.) R.K. Kohli, Vice chancellor and Prof. (Dr.) P. Ramarao, Dean Academic Affairs, Central University of Punjab, Bathinda*** *for providing me the necessary facilities for carrying out the research.*

*I am highly thankful to my seniors **Monika Chauhan, Ashish Sharma** and **Mohit Kumar** for their kind suggestions and support. This thesis would not have been possible without their guidance.*

*I am also very thankful to **Bhupinder Mittal** and **Ramit Singla** for helping and supporting me throughout my work. I would like to thank all my batchmates for sharing wonderful time and memories during the course. I would like to extend my thanks to **Mr. Rajesh Tiwari** for his time to time help in the lab.*

Sonia Verma

TABLE OF CONTENTS

Sr. No.	Content	Page No.
1.	Introduction (Chapter - 1)	1
2.	Review of literature (Chapter - 2)	5
3.	Rationale (Chapter - 3)	39
4.	Aim and Objectives (Chapter - 4)	43
5.	Materials and Methods (Chapter - 5)	47
6.	Results and Discussion (Chapter - 6)	61
7.	Conclusion	79
8.	References	83
9.	Appendices	91

LIST OF TABLES

Table No.	Table Description	Page No.
2.1	Expression level of PARP-1 in different carcinomas	9
2.2	FDA Approved PARP-1 inhibitors	16
2.3	PARP-1 inhibitors in clinical trials	17
2.4	Quinazolinone derivatives as PARP-1 inhibitors	36-37
6.1	List of synthesized compounds and their substitutions and percentage yield	65
6.2	Docking pose of the synthesized compounds and their dock score	68-71
6.3	ADME results of synthesized compounds	77

LIST OF FIGURES

Fig. No.	Description of figure	Page No.
1.1	Structure of PARP-1 (PDB ID: 5WTC)	4
2.1	Characteristic structure of PARP-1	8
2.2	DNA repair by base excision pathway	10
2.3	Role of PARP-1 in cancer	11
2.4	PARP-1 Inhibitors generations	12
2.5	First generation PARP-1 inhibitors	12
2.6	Second generation PARP-1 inhibitors	13
2.7	Third generation PARP1 inhibitors	14
2.8	Mechanism of actions of PARP-1 Inhibitors	15
2.9	Quinazoline derivatives as PARP-1 inhibitors	18
2.10	Representation of compound 5 binding mode with key residue	19
2.11	(a) Docking of compound 6 in the active site of PARP-1; (b) docking of compound 6 and Olaparib in the active site of PARP-1.	20
2.12	SAR of pyridazino[3,4,5-de]quinazolin-3(2H)-one derivatives	20

2.13	The docking model of core 2,3-dihydro-1H-[1,2]diazepino[4,5,6-cd]indole-1,4(6H)-dione binding to PARP-1	21
2.14	SAR of 2,3-dihydro-1H-[1,2]diazepino[4,5,6-cd]indole-1,4(6H)-dione derivatives	22
2.15	Molecular docking interactions of compound **13**	23
2.16	SAR studies of 1H-thieno[3,4-d]imidazole-4-carboxamide derivatives	24
2.17	Docked conformation of compound **15** into the active binding site of PARP-1	25
2.18	SAR of 5-fluorine-benzimidazole-4-carboxamide analogs	25
2.19	Molecular docking structure of compound **17**	26
2.20	SAR of cycloheptathieno[2,3-d]pyrimidines	27
2.21	SAR of quinazoline-2,4 (1H,3H)- dione derivatives	28
2.22	Molecular docking interactions of compound **18**	29
2.23	SAR of thiazolidine-2,4-dione analogs as PARP-1 inhibitors	29
2.24	Molecular docking interactions of general structure of (Z)-4-(3-carbamoylphenylamino)-4-oxobut-2-enyl amides	30
2.25	SAR of of (Z)-4-(3-carbamoylphenylamino)-4-oxobut-2-enyl amides	31
2.26	Molecular docking studies of thiazolidine-2,4-dione (TZD) derivatives	32

2.27	SAR studies of thiazolidine-2,4-dione (TZD) derivatives	32
2.28	Isomers of quinazolinone	33
2.29	Biological activities of Quinazolinones	34
2.30	Quinazolinone containing anticancer drugs available in the market	35
3.1	Rationale of quinazolinone derivatives as anticancer agents	41
3.2	Docking interaction of proposed molecule and standard inhibitor (Veliparib); Green – Proposed molecule and Pink – Standard inhibitor	42
4.1	Quinazolinone-based designed compounds	45
6.1	General scheme for the synthesis of designed compounds	63
6.2	Proposed mechanism of the designed scheme	64
6.3	Synthesized Compounds	66
6.4	2D interaction diagram of Veliparib	65
6.5	3D interaction diagram of Veliparib	72
6.6	3D interaction diagram of SVA-11	73
6.7	3D interaction diagram of SVA-7	74
6.8	3D interaction diagram of SVA-4	75
6.9	SAR of synthesized compounds on the basis of docking studies	76

LIST OF ABBREVIATIONS

Sr. No.	Full Form	Abbreviation
1.	Poly (ADP-ribose) polymerase-1	PARP-1
2.	DNA-binding domain	DBD
3.	Auto-modification domain	AD
4.	Catalytic domain	CAT
5.	Zinc finger	ZF
6.	Single-strand DNA breaks	SSBs
7.	Double-strand DNA breaks	DSBs
8.	Nuclear localization signal	NLS
9.	Breast-cancer-susceptibility protein-carboxy terminus	BRCT
10.	Helical subdomain	HD
11.	ADP-ribosyl transferase	ART
12.	Histidine	H
13.	Tyrosine	Y
14.	Glutamic acid	E
15.	Poly ADP-ribose	PAR
16.	Food and Drug Administration	FDA
17.	Structure Activity Relationship	SAR
18.	Thiazolidine-2,4-dione	TZD
19.	Protein Data Bank	PDB
20.	Coupling Constant	J
21.	Half Maximal Inhibitory Concentration	IC_{50}
22.	Reactive Oxygen Species	ROS
23.	Reactive Nitrogen Species	RNS
24.	Hertz	Hz
25.	Infrared	IR
26.	Melting Point	MP
27.	Micromolar	µM

28.	Nanomolar	Nm
29.	Tetramethylsilane	TMS
30.	Two Dimensional	2D
31.	Three Dimensional	3D
32.	Dimethyl Sulfoxide	DMSO
33.	Round Bottom Flask	RBF
34.	Ethyl Acetate	EtOAc
35.	Dichloromethane	DCM
36.	Thin Layer Chromatography	TLC
37.	Absorption, Distribution, Metabolism, And Excretion	ADME

CHAPTER - 1

INTRODUCTION

1. Introduction

1.1. Cancer

Cancer is a severe disease that is threatening human health and continues to be a prominent health problem over the world (Murtaugh et al., 2017). It is an abnormal growth of cells which tend to proliferate and spread in an uncontrolled manner (Cotter et al., 2017). Cancer is a complicated and dynamic disease characterized by significant hallmarks (Hanahan et al., 2011). They include strengthening proliferative signaling, evading growth inhibitors, preventing cell death, enabling continues reproduction of cells, inducing development of new blood vessels, activating invasion and metastasis, reprogramming of energy metabolism and evading immune destruction (De Mas et al., 2014). The transformation of a normal cell into the cancer cell occurs due to alteration of genes that regulate cell growth. The affected genes are of two types i.e. oncogenes that promote cell growth and reproduction of cell and the second one are tumor suppressor genes that inhibit or suppress the division and survival of cell growth. Cancer is caused by the relations between genetic susceptibility and environmental toxins (Laird, 2005). Cancer is a leading cause of death worldwide, accounting for 8.8 million deaths in 2015. According to WHO, the most common causes of cancer death are cancers of Lung (1.69 million deaths), Liver (788 000 deaths), Colorectal (774 000 deaths), Stomach (754 000 deaths) and Breast (571 000 deaths).

1.2. PARP-1

Poly (ADP-ribose) polymerase-1 (PARP-1) is a DNA-dependent ADP-ribosyl transferase. It is also known as poly (ADP-ribose) synthetase which is found in the nucleus (Jagtap et al., 2005). It is a ubiquitous zinc-finger DNA-binding enzyme that is activated by binding to DNA breaks and then catalyzes the synthesis of Poly (ADP-ribose) chains (PAR) using NAD^+ as a substrate (Gibson et al., 2012). The PARP family of enzymes contains 18 members. Out of those 18 proteins, PARP-1 and PARP-2 are considered to be up-regulated in different carcinomas (Schiewer et al., 2014). Recently many PARP-1 inhibitors have been approved for treatment of human malignancies such as olaparib, rucaparib, and niraparib. A few are under clinical investigation, such as olaparib (AZD2281), veliparib (ABT-888), and

rucaparib (AG-014699, PF-01367338), for the treatment of ovarian cancer, breast cancer, prostate cancer, pancreatic cancer, and unspecified solid tumors (Wang et al., 2017). PARP1 has a crucial role in cell proliferation, survival, and death, due to its properties on the regulation of multiple biological processes. PARP-1 and PARP-2 are mainly involved in DNA repair and DNA transcription processes. There is a range of malignant tissues which have revealed elevated expression of the PARP-1 protein, which may be correlated with deterioration, metastasis, and angiogenesis in tumors. The crystal structure of human PARP-1 (PDB ID: 5WTC) is shown in **Fig. 1.1.**

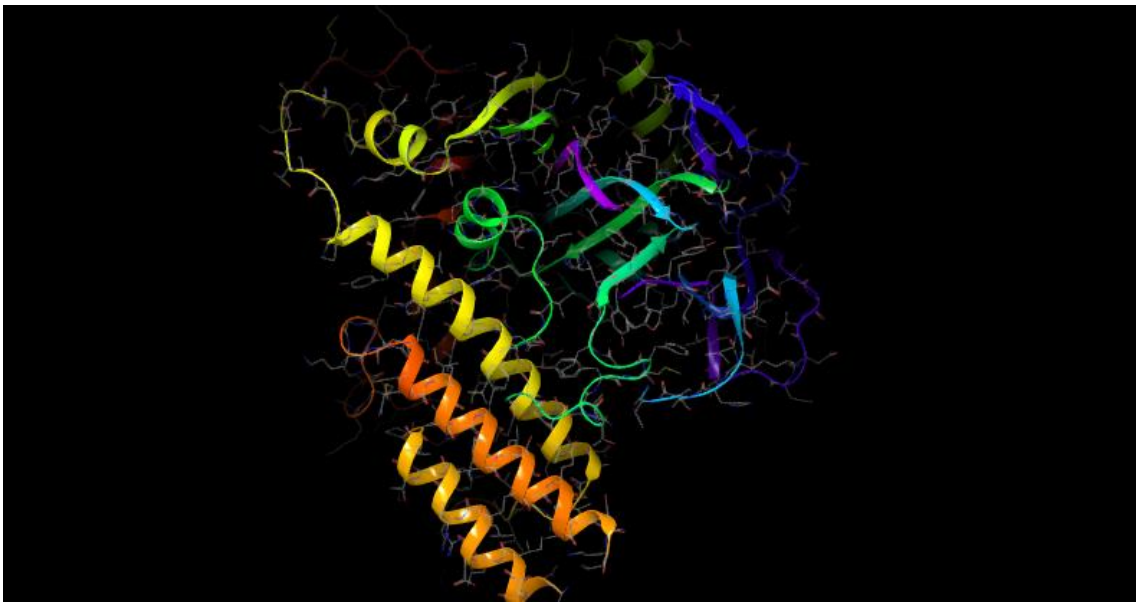

Figure 1.1: Structure of PARP-1 (PDB ID: 5WTC)

CHAPTER - 2

REVIEW OF LITERATURE

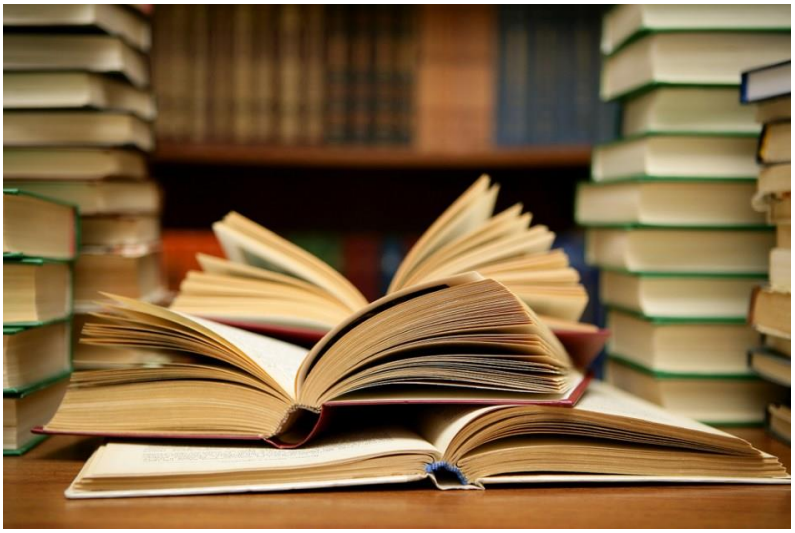

2. Review of literature

2.1. PARP-1

PARP-1 (EC 2.4.2.30), is a nuclear enzyme of PARP family which contains 18 members (Schiewer et al., 2014). Out of those 18 proteins, PARP-1 is the most widely studied (Rojo et al., 2011). It has a crucial role in cell proliferation, survival, and death, due to its properties on the regulation of multiple biological processes. PARP-1 is activated when DNA breaks and plays an important role in repairing the single strand DNA breaks (SSDs) via base excision repair (BER). The primary function of PARP-1 is to modify target proteins with ADP-ribose units using NAD^+ as a substrate. It possesses the ability to catalyze the transfer of multiple ADP-ribose units, resulting in the formation of Poly (ADP-ribose) [PAR] chains (Gibson et al., 2012).

2.2. Structural Insights of Poly (ADP-ribose) polymerase-1

PARP-1 involves four domains i.e. N-terminal DNA-binding domain (DBD), auto-modification domain (AD), WGR domain, and C-terminal catalytic domain (CAT) (Langelier et al., 2012).

2.2.1. N-terminal DNA-binding domain:

DBD comprises of two zinc fingers (ZF1 and ZF2) which are accountable for binding of PARP-1 to single and double-strand DNA breaks (SSBs, DSBs), and a nuclear localization signal (NLS) act as a DNA-nick sensor (Ali et al., 2012). In DBD, there is additional zinc finger (ZF3) which is established only in this isoform of PARP family except for other isoforms. It may be nonessential for DNA-binding but have a significant role in PARP-1 catalytic activity through conveying of “PARP1-DNA binding” signal to the catalytic domain (Rouleau et al., 2010).

2.2.2. Auto-modification domain:

The Auto-modification domain consists of a breast-cancer-susceptibility protein-carboxy terminus (BRCT) motif for auto-ADP ribosylation and mediates PARP1–protein interaction (Loeffler et al., 2011).

2.2.3. WGR domain:

WGR domain contains tryptophan-glycine-arginine motif which activate the enzymatic activity of the catalytic region (Langelier et al., 2012).

2.2.4. C-terminal catalytic domain (CAT):

Another domain of PARP-1 is CAT which consists of a helical subdomain (HD) and a conserved ADP-ribosyl transferase subdomain (ART) (Eustermann et al., 2015). ART is composed of vital amino acid residues i.e. histidine (H) and tyrosine (Y) residues which are crucial for NAD^+ binding, and a glutamic acid (E) residue for polymerase activity (Wang et al., 2017) **(Fig. 2.1).**

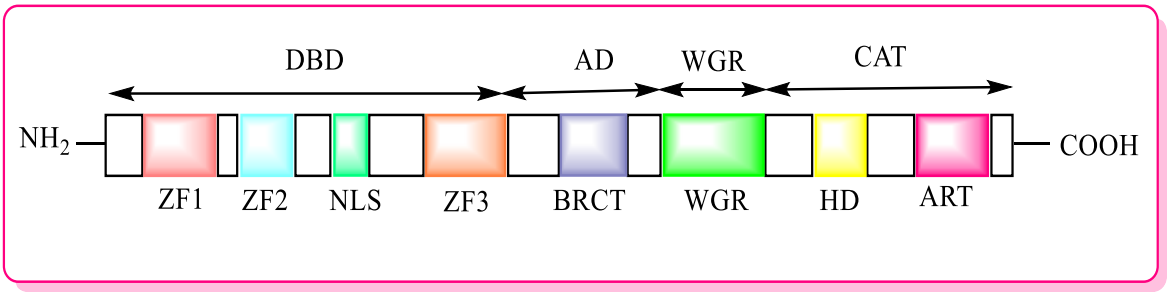

Figure 2.1: Characteristic structure of PARP-1

2.3. Poly (ADP-ribose) polymerase-1: Molecular Regulation in Carcinoma

PARP-1 has been identified in both the nucleus and cytoplasm of cancer cells. Investigation studies of PARP-1 expression level in various tumors are necessary to estimate the possible beneficial effects, and side effects of PARP-1 inhibitors on each type or subtype of cancers (Schiewer et al., 2012). A group of tumors has been associated with upregulated PARP-1 when compared to adjacent normal tissues (Wang et al., 2017). The expression level of PARP-1 in diverse carcinomas is given in **Table 2.1**:

Table 2.1: Expression level of PARP-1 in different carcinomas

CANCER TYPES	EXPRESSION OF PARP-1
Breast cancer	Up-regulated
Ovarian cancer	Up-regulated
Uterine cancer	Up-regulated
Lung cancer	Up-regulated
Skin cancer	Up-regulated
Non-Hodgkin's lymphoma	Up-regulated
Glioblastoma Multiforme	Up-regulated
Prostate cancer	Up-regulated
Ewing's Sarcoma	Up-regulated
Colorectal cancer	Up-regulated
Pediatric central nervous system cancer	Up-regulated
Testicular Germ cell tumor	Up-regulated

2.4. Poly (ADP-ribose) polymerase-1: Role in DNA Repair

PARP-1 is activated by DNA damage and participates in it by base excision repair trail. It gets triggered upon detection and binding to areas of single-strand damage by its zinc-finger DNA-binding domain (Schiewer et al., 2017). After binding to altered DNA, PARP-1 upsurges its catalytic activity and uses NAD^+ to produce polymers of poly ADP ribose (PAR) and transfers it to acceptor proteins, including PARP itself. This auto-poly ADP-ribosylation recruits several other proteins to the site of DNA-damage, commencing a repair complex (Kim et al., 2005). Ultimately, PARP-1 goes through a molecular modification that leads to its reduced affinity for DNA. Further, its release in the damaged site may be accessed by other repair complex proteins (Dziadkowiec et al., 2016). Additionally, overactivation of PARP-1 induces reduction of NAD^+ and ATP, resulting in cellular dysfunction and may cause necrosis or apoptosis **(Fig. 2.2)**.

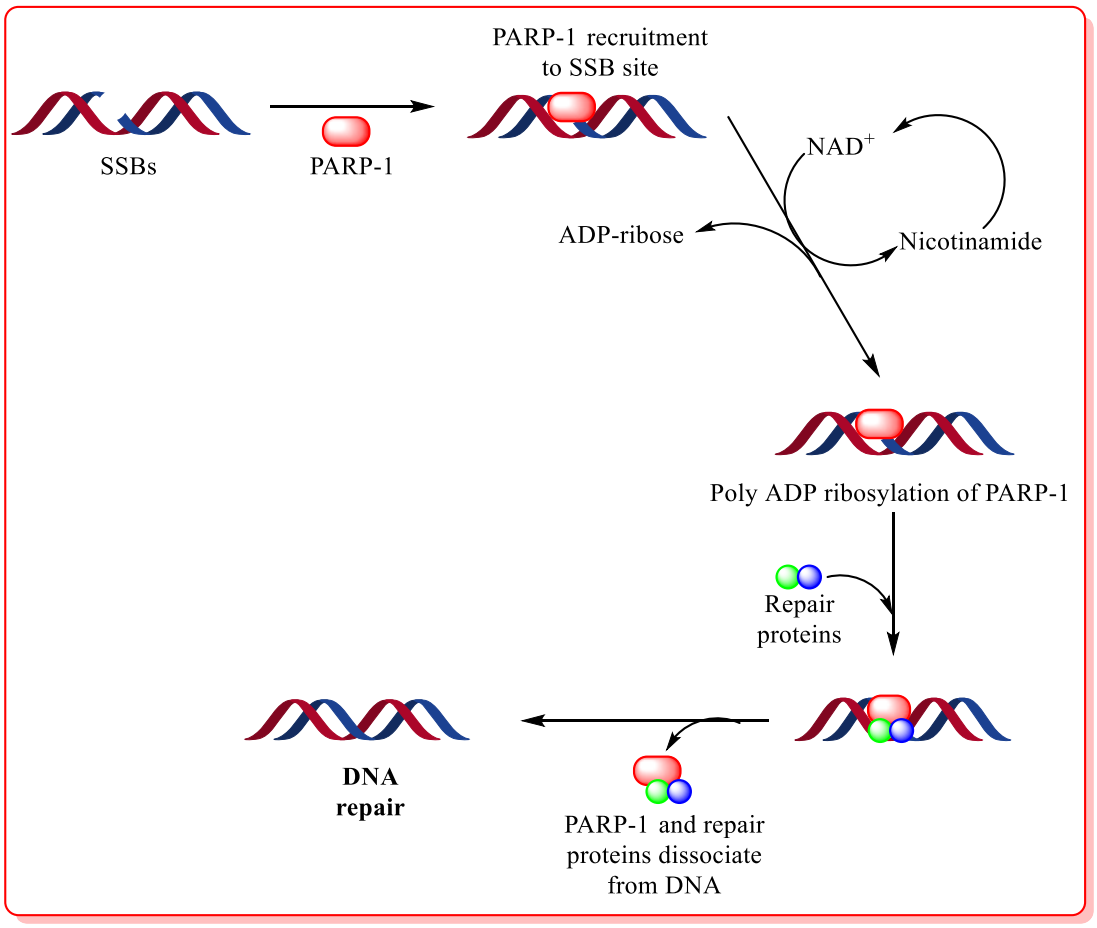

Figure 2.2: DNA repair by base excision pathway

2.5. Poly (ADP-ribose) polymerase-1: Role in Cancer

To survive, cancer cells will trigger PARP-1 to repair slightly damaged DNA by keeping DNA lesions. In case of extreme DNA lesions, normal PARP-1 activation leads to inadequate DNA repair, and thus causes cancer cell apoptosis. This may be an advantage of cancer cells in anticancer therapy because apoptosis cells will then be cleared by macrophages rapidly (Swindall et al., 2013). On the other hand, overactivation of PARP-1 leads to mutagenesis, metastasis, necrosis, and autophagy of tumors. Necrosis induces inflammation, which is another important carcinogenetic factor **(Fig. 2.3)** (Rouleau et al., 2010).

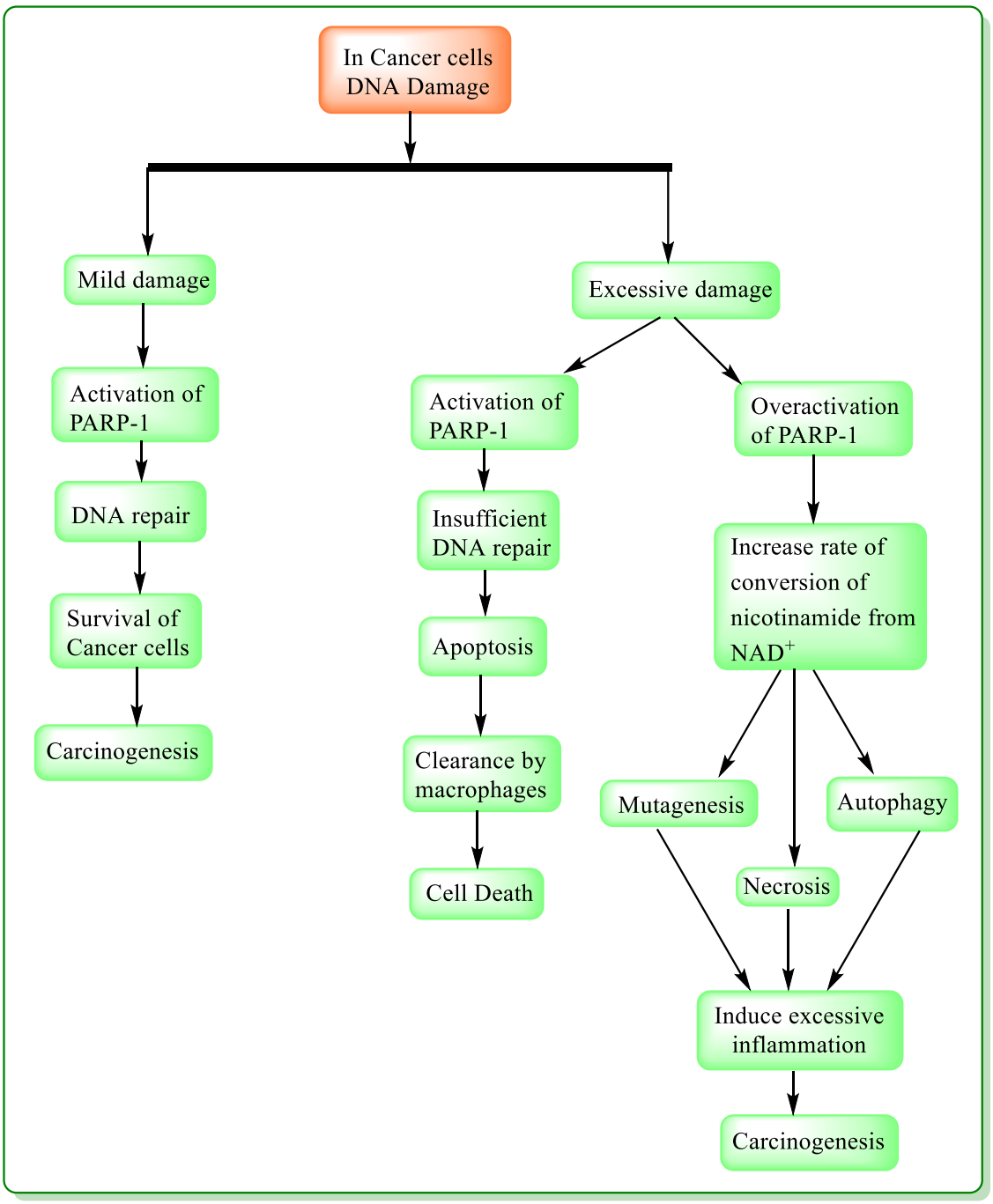

Figure 2.3: Role of PARP-1 in cancer

2.6. Poly (ADP-ribose) polymerase-1 Inhibitors

PARP-1 inhibitors are those which inhibits the PARP-1 activity. They are divided into three generations (Malyuchenko et al., 2015) which are as follows **(Fig. 2.4)**:

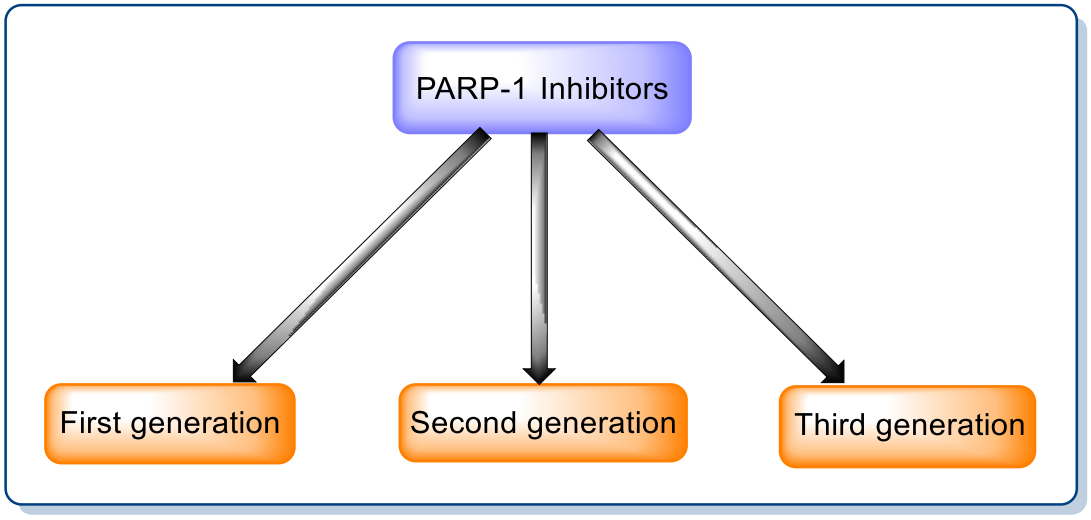

Figure 2.4: PARP-1 Inhibitors generations

2.6.1. First generation PARP-1 inhibitors:

This generation of PARP-1 inhibitors was developed on the observations that nicotinamide which is a second product of the PARP1-catalyzed reaction, causes reasonable inhibition of the reaction (Purnell et al., 1980). In this generation, N-atom was replaced via C-atom at the third position for the development of a class of benzamide analogs. Drug solubility was improved via substitution at the third position(Durkacz et al., 1980) **(Fig. 2.5)**.

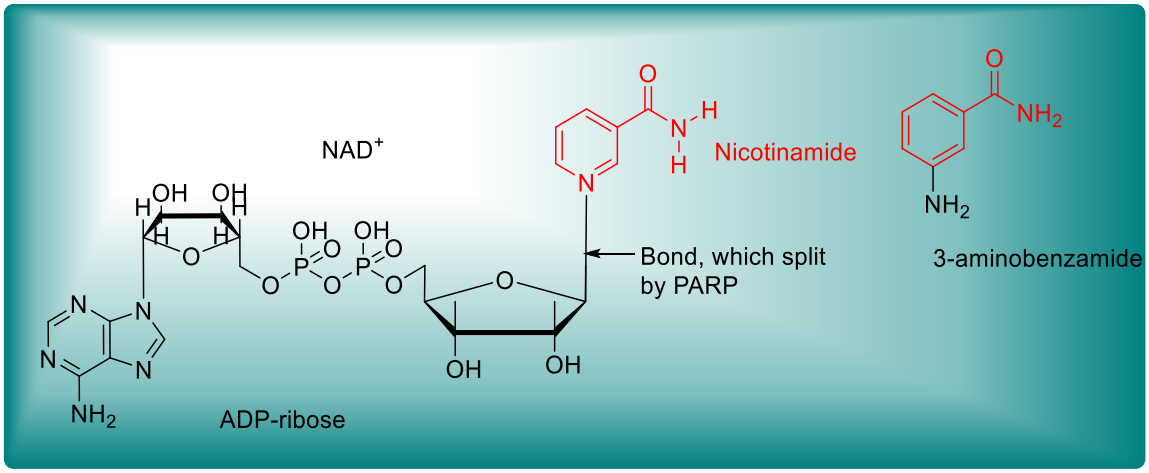

Figure 2.5: First generation PARP-1 inhibitors

2.6.2. Second generation PARP-1 inhibitors:

After the discovery of first-generation PARP-1 inhibitors, the more effective PARP-1 inhibitors were established on the basis of quinazoline analogs. This group of compounds was more operational and target-specific. The development of phenanthridinones from quinazolinone further led to the generation of PJ-34 and NU1025, which are in clinical trials. Both of these compounds are 50 times more effective PARP-1 inhibitors than 3-aminobenzamide (Malyuchenko et al., 2015). All of these compounds enclosed a carboxamide group in the second aromatic ring. The presence of carboxamide group is indispensable for escalating the activity of inhibitors. The crystallization of PARP-1 inhibitors established that the carboxamide group forms several H-bonds with Ser994-OG and Gly863-N in the catalytic domain of PARP-1. The interaction between the heterocycle of these inhibitors and the protein was strengthened by these types of bonding **(Fig. 2.6)** (Jagtap et al., 2005).

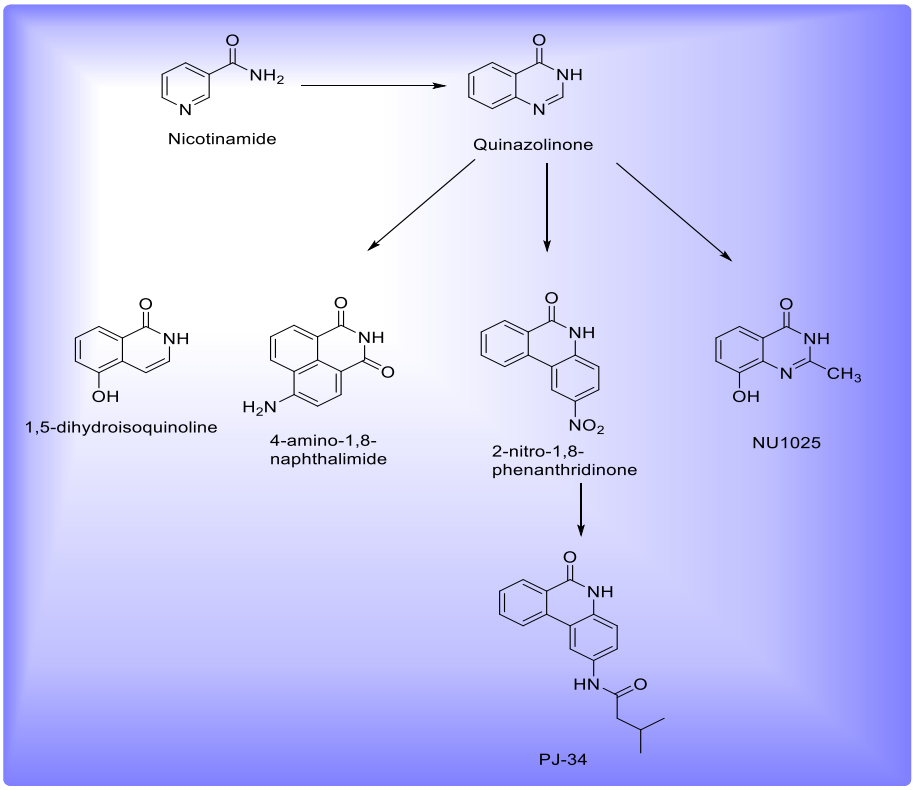

Figure 2.6: Second generation PARP-1 inhibitors

2.7.3 Third generation PARP-1 inhibitors:

The more potent third generation PARP-1 inhibitors were developed on the basis of benzimidazole analogs (Malyuchenko et al., 2015). At present, a number of benzimidazole-based PARP-1 inhibitors of the third generation have been synthesized. Many of them (e.g., rucaparib, iniparib, olaparib, veliparib, niraparib, talazoparib, CEP-9722, and E7016) are currently undergoing clinical trials **(Fig. 2.7).**

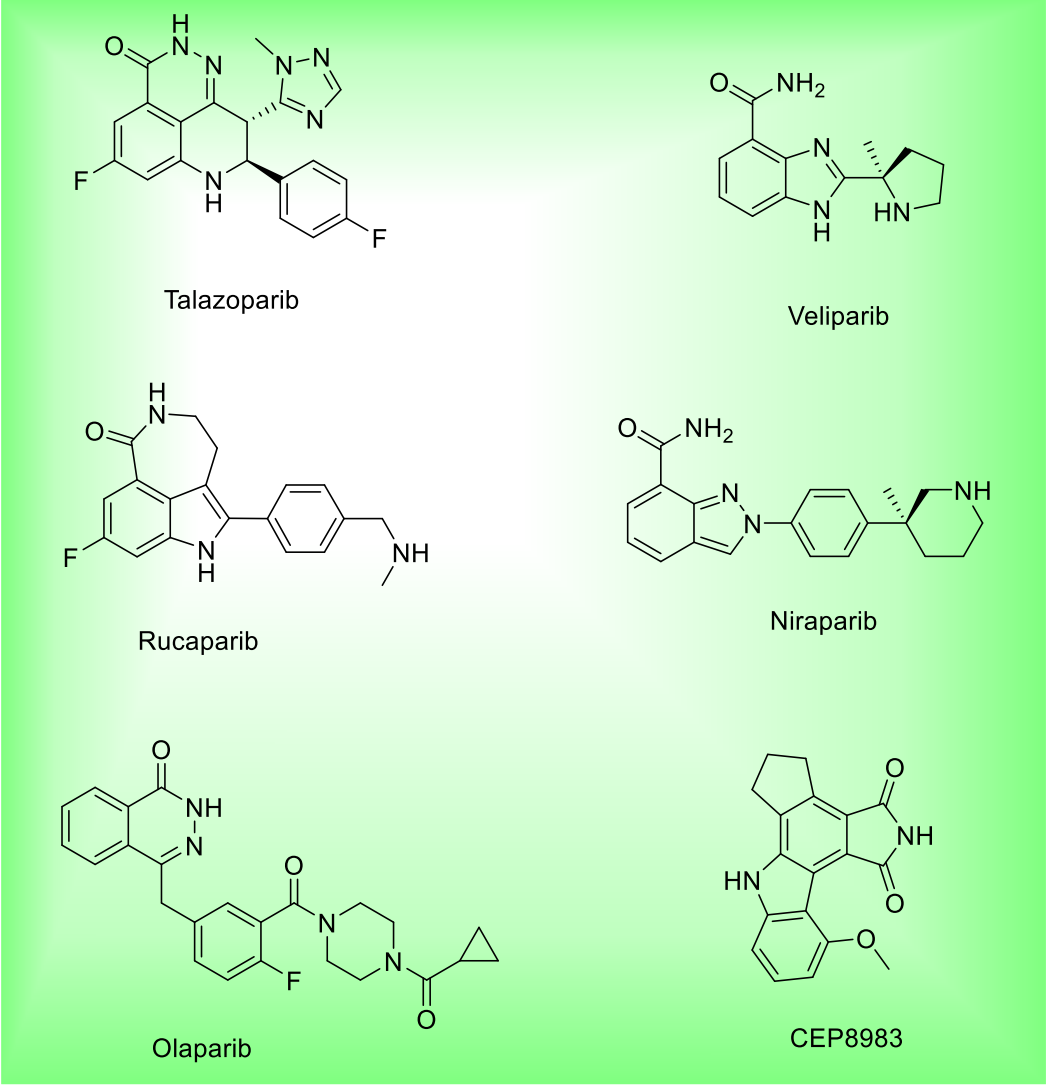

Figure 2.7: Third generation PARP-1 inhibitors

2.7. Mechanistic Insights of Poly (ADP-ribose) polymerase-1 Inhibitors

PARP-1 inhibitors inhibit the activity of PARP-1. The inhibition leads to stoppage of DNA repair. PARP-1 binds to single-strand and double-strand DNA breaks in response to DNA damage. PARP-1 inhibitors act as competitive inhibitors by competing with NAD^+ and inhibit the formation of PAR chains. (Scott et al., 2015). The PARP-1 activity is minimum when there is the lack of DNA damage **(Fig. 2.8)**. But, if there are DNA damages, PARP-1 gets activated. PARP-1 finds DNA breaks, which acts as a sensor and provides a prompt enrollment of repair proteins to the break site (Rouleau et al., 2010).

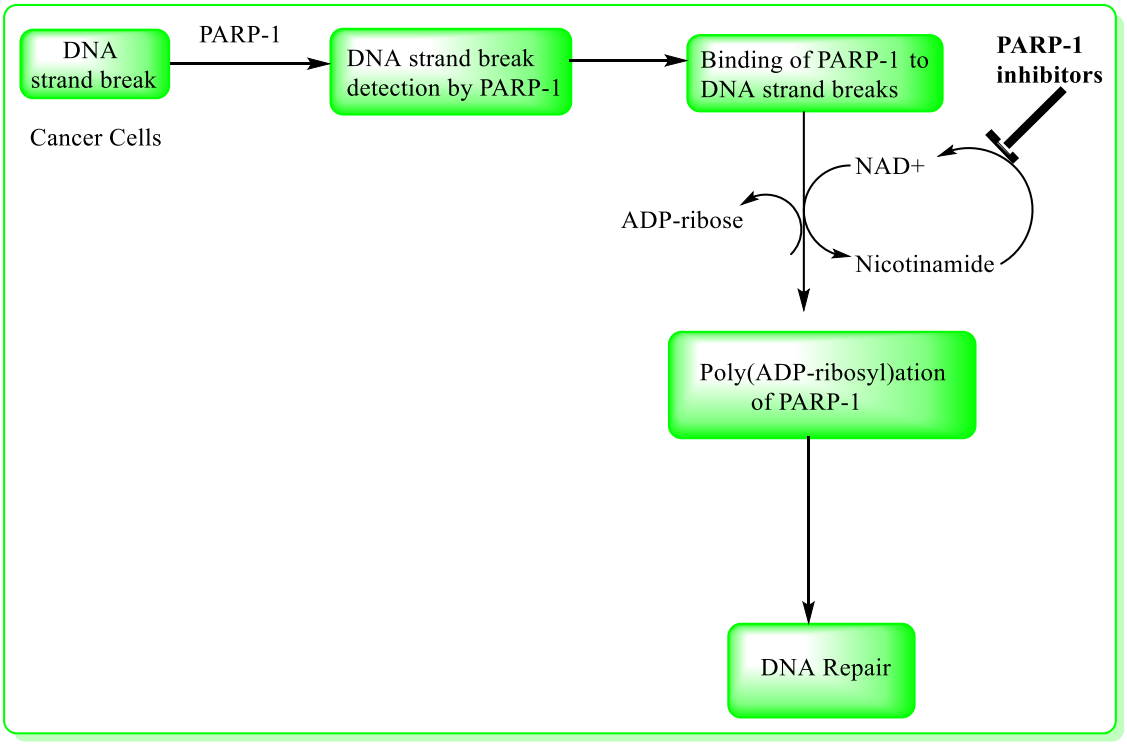

Figure 2.8: Mechanism of action of PARP-1 Inhibitors

2.8. FDA Approved Poly (ADP-ribose) polymerase-1 inhibitors

Olaparib and Rucaparib were approved for BRCA-mutated ovarian cancer patients by the FDA in 2014 and 2016, respectively, and then Niraparib was approved for the maintenance treatment of epithelial ovarian, fallopian tube or primary peritoneal cancer by the FDA in March 2017 (Yuan et al., 2017), are given as follows **(Table 2.2)**:.

Table 2.2: FDA Approved PARP-1 inhibitors

Sr. No.	Drugs	US FDA Approval (Year)	Cancer Type	Marketed As
1.	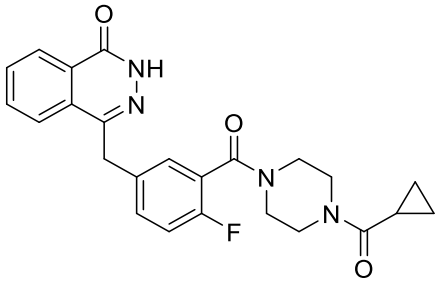 Olaparib	December, 2014	BRCA-mutated ovarian cancer	Lynparza
2.	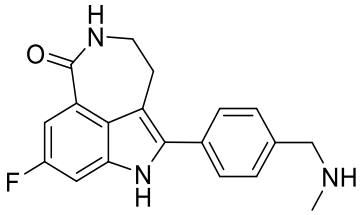 Rucaparib	December, 2016	BRCA-mutated ovarian cancer	Rubraca
3.	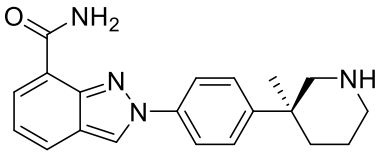 Niraparib	March, 2017	Epithelial ovarian, fallopian tube or primary peritoneal cancer	Zejula

2.9. Poly (ADP-ribose) polymerase-1 inhibitors in Clinical Trials:

PARP-1 inhibitors which are in clinical trials (Wang et al., 2017) are given as follows **(Table 2.3)**:

Table 2.3: PARP-1 inhibitors in clinical trials

Sr. No.	Drug	Structure	Cancer types	Phase	IC_{50}
1.	Olaparib	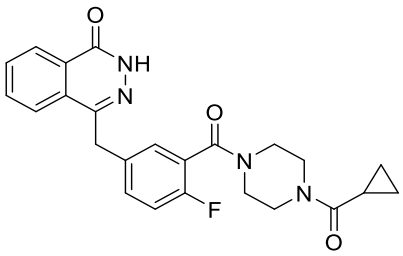	Ovarian Breast Prostate Pancreatic Gastric Lung	Phase 4 Phase 3 Phase 3 Phase 3 Phase 3 Phase 2	5nM
2.	Niraparib	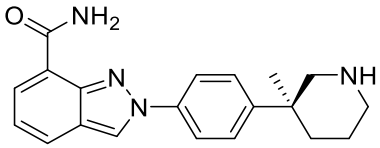	Ovarian Breast Fallopian tube Endometrial	Phase 3 Phase 3 Phase 2 Phase 2	3.2nM
3.	Rucaparib	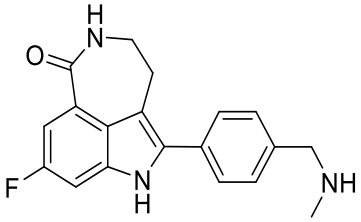	Ovarian Breast Fallopian tube Prostate Pancreatic	Phase 3 Phase 2 Phase 3 Phase 3 Phase 2	1.4nM
4.	Veliparib	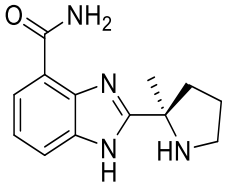	Ovarian Breast Lung	Phase 3 Phase 3 Phase 3	5.2nM
5.	Talazoparib	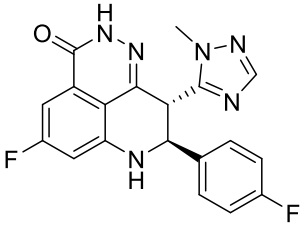	Ovarian Breast Prostate Endometrial	Phase 2 Phase 3 Phase 2 Phase 2	1.2nM

2.10. Current Trends in Poly (ADP-ribose) polymerase-1 Inhibitor Development:

2.10.1. From 2014

Giannini et al. in 2014 discovered quinazoline derivatives as a novel scaffold with the PARP-1 inhibitory profile. They tested various compounds out of which compound **5** was found to be a most potent PARP-1 inhibitor **(Fig. 2.9)**.

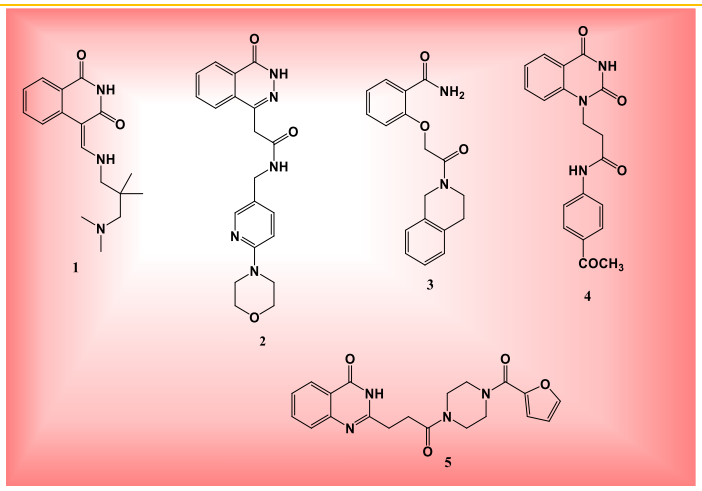

Compound	PARP-1 [IC_{50}(nM)]
1	87.4
2	49.8
3	42.9
4	87.6
5	28.5

Figure 2.9: Quinazoline derivatives as PARP-1 inhibitors

The molecular docking studies of compound **5** revealed that the presence of carbonyl group on propanoyl chain forms a strong hydrogen bond with S203 hydroxyl group. Compound **5** demonstrated numerous interactions with the PARP-1 enzyme. It inhibited the conversion of NAD^+ to nicotinamide (Giannini et al., 2014). The molecular docking interactions are shown in **Fig. 2.10** below:

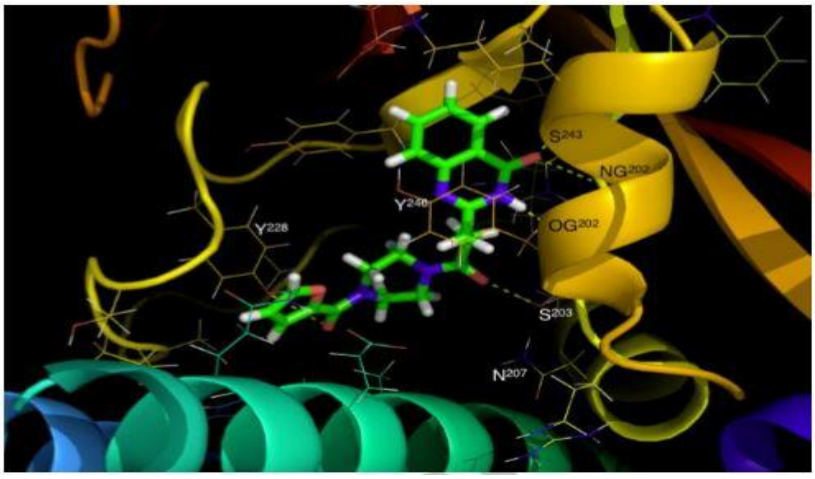

Figure 2.10: Representation of compound **5** binding mode with key residue (Giannini et al., 2014)

SAR studies discovered that presence of oxygen and nitrogen on the quinazoline ring are imperative for PARP-1 inhibition. The presence of carbonyl group on propanoyl chain of compound **5** plays an important role in hydrogen bond formation with the active cavity of PARP-1. From this SAR study authors concluded that substitution on the third position of Quinazoline ring is good for PARP-1 inhibition activity (Giannini et al., 2014).

2.10.2. From 2015

In 2015, Wang et al. designed and synthesized a series of pyridazino[3,4,5-de]quinazolin-3(2H)-one derivatives as PARP-1 inhibitors. The biological assessment studies discovered that compounds displayed good inhibitory PARP-1 activities. The molecular docking interactions exhibited were π- π interactions with Tyr246 and Tyr235. The carboxamide group of designed compounds was involved in key hydrogen bonding interactions with both Ser243 and Gly202 (Wang et al., 2015). The designed compounds showed better interactions with PARP-1 as compared to standard Olaparib as shown in **Fig. 2.11.**

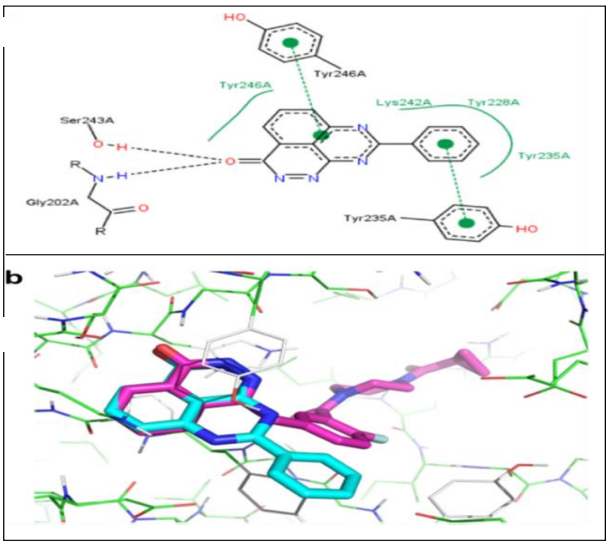

Figure 2.11: (a) Docking of compound **6** in the active site of PARP-1; (b) docking of compound **6** and Olaparib in the active site of PARP-1 (Wang et al., 2015).

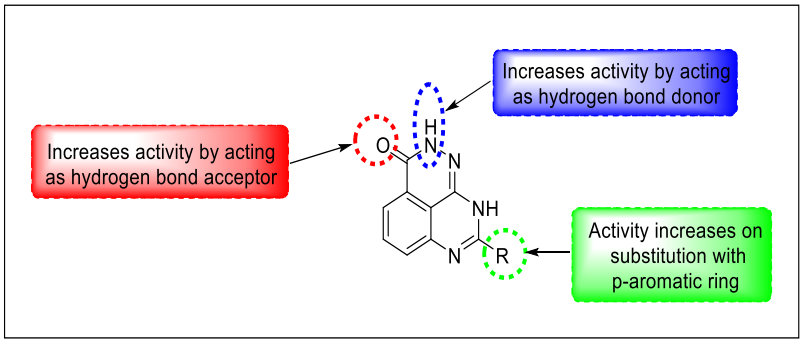

COMPOUND	R	IC_{50}(μM)
6	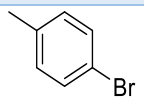	17.99
7	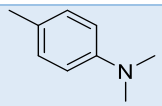	18.95
8	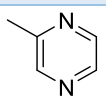	18.77
9	Benzamide	59.29

Figure 2.12: SAR of pyridazino[3,4,5-de]quinazolin-3(2H)-one derivatives

Out of various synthesized molecules, compound **6** displayed the best inhibition due to the existence of bromine on p-substitution to an aromatic ring (Wang et al., 2015). SAR studies validated that substitution on **R** with p-substituted aromatic ring escalates the activity and carboxamide group upsurges activity by participating in hydrogen bonding interactions as shown in **Fig. 2.12.**

Xie et al. in 2015, designed and synthesized 2,3-dihydro-1H-[1,2]diazepino[4,5,6-cd]indole-1,4(6H)-dione derivatives and assessed their inhibitory activities toward PARP-1 enzyme on two cell lines, MCF-7 cells, and the BRCA1-deficient MDA-MB-436 cells. They executed molecular docking studies of the designed compounds. Molecular docking studies discovered that carbonyl oxygen in 2,3-dihydro-1H-[1,2]diazepino[4,5,6-cd]indole-1,4(6H)-dione form a hydrogen bond with the side chain hydroxyl group of Ser904, while the double carboxamide hydrogen exhibited hydrogen bonding interaction with the backbone carbonyl oxygen of Gly863. The aromatic ring had π- π stacking interaction with the electron-rich phenyl rings of Tyr907 and Tyr 896 (Xie et al., 2015). The NH of indole showed hydrogen bonding interactions with Glu988 via a water molecule **(Fig. 2.13).**

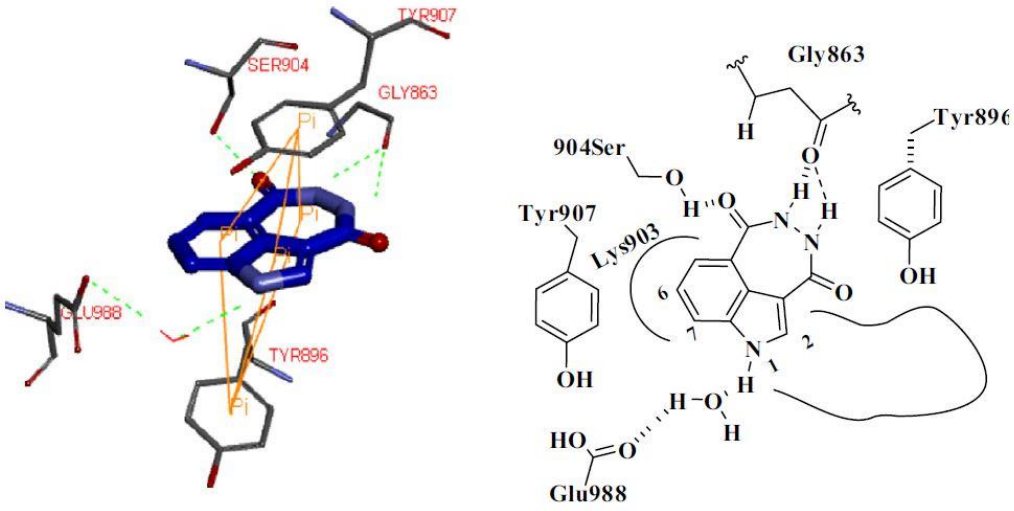

Figure 2.13: The docking model of core 2,3-dihydro-1H-[1,2]diazepino[4,5,6-cd]indole-1,4(6H)-dione binding to PARP-1 (Xie et al., 2015)

SAR studies of synthesized compounds revealed that substitution with ‘F’ atom at ‘X’ escalated the activity while substitution with ‘H’ will decrease the activity. Long alkyl chain substitution at R increased the activity by increasing the lipophilicity of the designed compounds (Xie et al., 2015). The oxygen of carboxamide increased activity by acting as hydrogen bond acceptor as shown in **Fig. 2.14.**

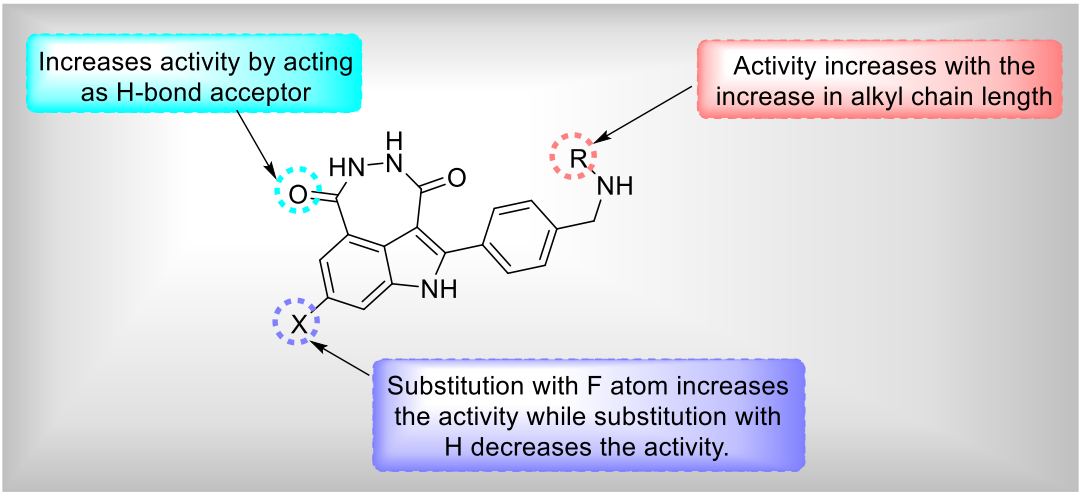

COMPOUND	R	IC_{50} (nM)	CC_{50} (MCF-7, μM)	CC_{50} (MDA-MB-436, BRCA-1, μM)
10	C_4H_9	2.416	25.87	5.454
11	C_3H_7	3.501	2.84	114.5
12	Rucaparib	0.8044	19.47	3.0

Figure 2.14: SAR of 2,3-dihydro-1H-[1,2]diazepino[4,5,6-cd]indole-1,4(6H)-dione derivatives

2.10.3. From 2016

In 2016, Wang et al. designed and synthesized 1H-thieno[3,4-d]imidazole-4-carboxamide derivatives and evaluated their biological activity for inhibition of PARP-1. They performed the molecular docking studies of designed compounds against the catalytic domain of human PARP-1. The designed compound showed hydrogen

bonding interactions with Gly-202 and Ser-243. Moreover, 1-NH of the thienoimidazole ring interacted via a water-mediated hydrogen bond with Glu-327. Thienoimidazole ring displayed a characteristic π-stacking interaction with Tyr-246 (Wang et al., 2016). The carboxamide group accomplished an optimal orientation through an intramolecular hydrogen bond for interacting with the key amino acids as shown in **Fig. 2.15.**

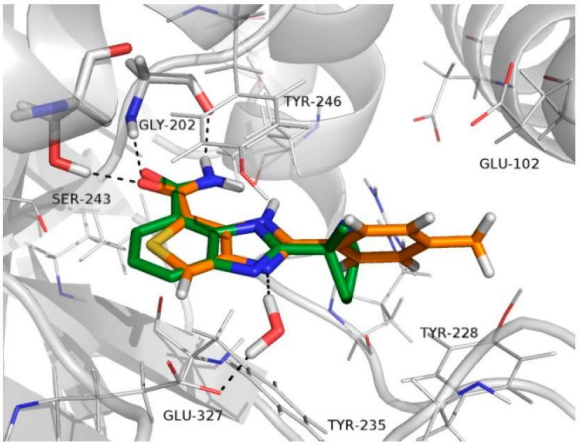

Figure 2.15: Molecular docking interactions of compound **13** (L. Wang et al., 2016)

Out of various synthesized molecules, compound **13** and **14** were best. Further, SAR studies showed that methyl group substitution on para-position escalated the activity whereas substitution on ortho and meta position declines the activity. Substitution with an electron withdrawing group on R reduced in activity **(Fig. 2.16)**. Authors concluded that substitution with alkyl groups increased anticancer potential (Wang et al., 2016).

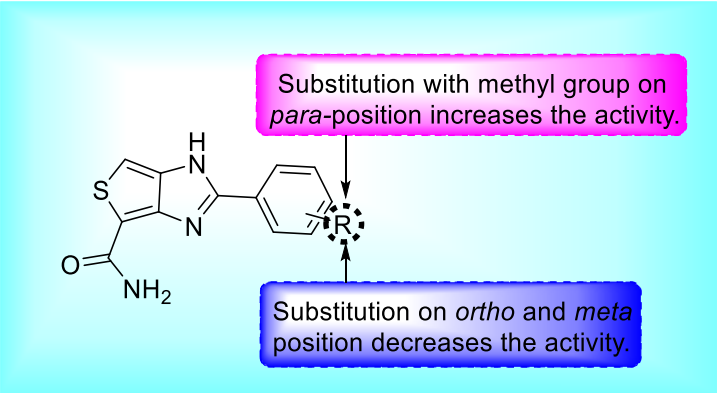

COMPOUND	R	IC_{50}(μM)
13	4-CH_3	0.151
14	3-CF_3	0.043
Olaparib	-	0.013
Veliparib	-	0.014

Figure 2.16: SAR studies of 1H-thieno[3,4-d]imidazole-4-carboxamide derivatives

Wang et al. designed and synthesized a series of novel 5-fluorine-benzimidazole-4-carboxamide analogs. The molecular docking studies were conducted on PDB ID: 2RCW and displayed that carbonyl oxygen group of **15** forms three hydrogen bonds with Ser243, Gly202 and His201. Meanwhile, the carboxamide hydrogen unveiled hydrogen bond interaction with the backbone carbonyl oxygen of Gly202. Fluorine atom at the 5-position of benzimidazole formed an additional hydrogen bond with the hydroxyl group of Ser243. In addition, the benzimidazole ring formed π-stacking interactions with Tyr246 and Tyr235 (Wang et al., 2016). The docking interaction of compound **15** as shown below **(Fig. 2.17).**

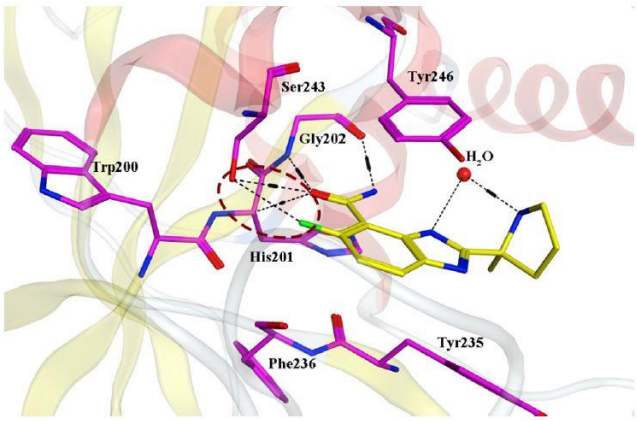

Figure 2.17: Docked conformation of compound **15** into the active binding site of PARP-1 (Wang et al., 2016)

The SAR study revealed that substitution with 2-methyl pyrrolidine group at R position increases the activity. Substitution with carbamide and fluorine group on benzene ring increases the activity. NH_2 group act as hydrogen bond donor and increases activity and oxygen atom increase activity by acting as hydrogen bond donor (Wang et al., 2016) **(Fig. 2.18)**.

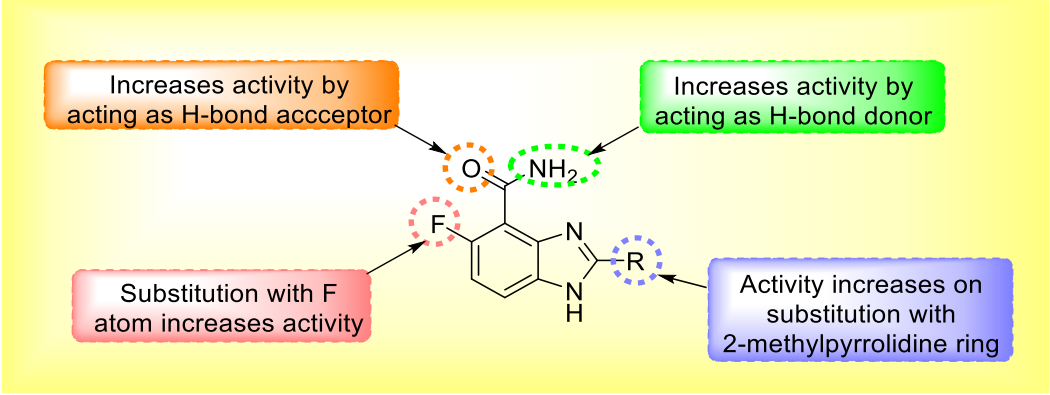

Compound	R	IC_{50} (nM)
15	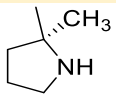	5.7
Veliparib	-	64µM

Figure 2.18: SAR of 5-fluorine-benzimidazole-4-carboxamide analogs

In 2016, El-Mongy et al. designed and synthesized cyclohepta[b]thiophene and substituted pentahydrocycloheptathieno[2,3-d]pyrimidine derivatives for their PARP-1 inhibitory activity. The modeling study with PDB Code:1UK1 declared that most of the docked compounds showed the same interactions as 3-aminobenzamide, where Gly 894, His 862, Tyr 896, Arg 878, and Ser 864 were the main residues involved in hydrogen bond formation. The molecular docking studies of the thienopyrimidine scaffold with PARP-1 crystal structure revealed that Gly 894 residue was involved in hydrogen bonding interactions with NH_2 and Tyr 896 residue was involved in hydrophobic interactions (Elmongy et al., 2017) as shown in **fig.2.19.**

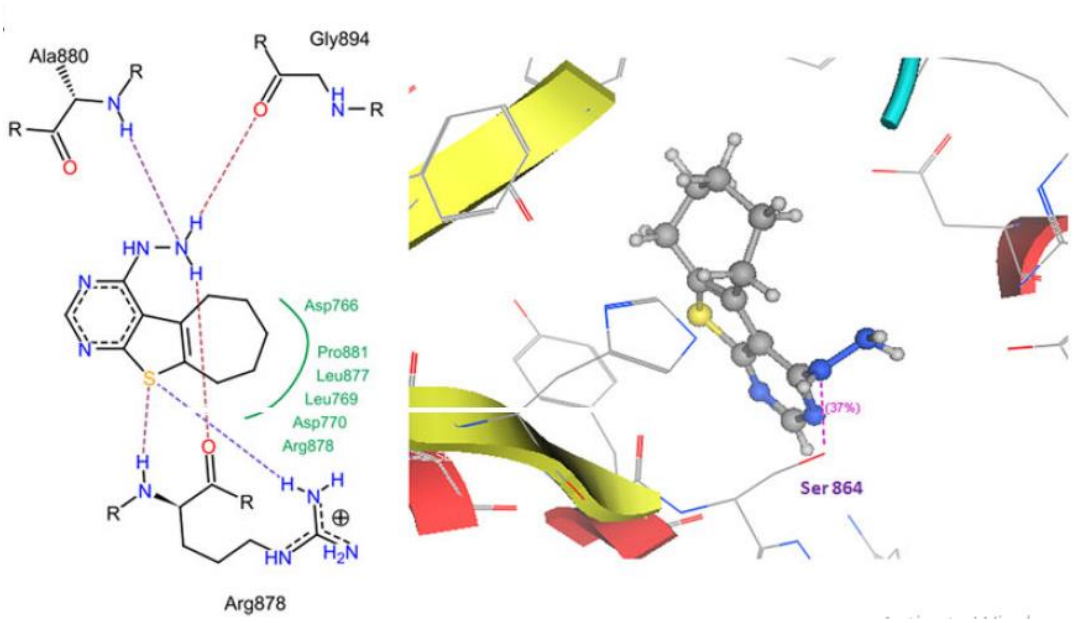

Figure 2.19: Molecular docking structure of compound **17** (Elmongy et al., 2017)

Out of various synthesized compounds, compound **16 and 17** exhibits best inhibitory activity against PARP-1. Compound **16** was more potent than compound **17** due to the presence of alkyl chain which increases the lipophilicity of the compound (Elmongy et al., 2017) as shown in **fig. 2.20.**

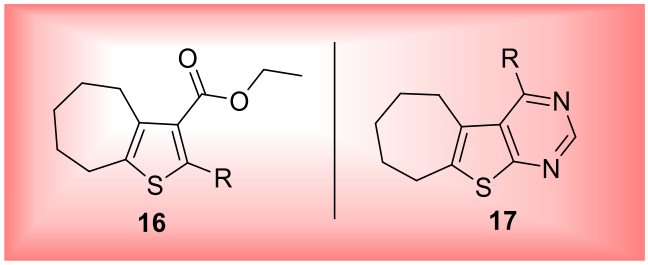

Compounds	Docking Score	IC_{50} Value
16	-21.91	50.392
17	-18.57	58.206
3-Amino benzamide	-15.86`	--

Figure 2.20: SAR of cycloheptathieno[2,3-d]pyrimidines

2.10.4. From 2017

Zhao et al. in 2017 designed and synthesized novel quinazoline-2,4(1H,3H)- dione derivatives to discover the selective PARP inhibition potential. The synthesized compounds have shown good PARP inhibition activity. They performed the SAR studies of the synthesized compounds for minimal structural requirements for better activity. Out of various synthesized molecules, compound **17 (Fig. 2.21)** exhibited best PARP-1 inhibition activity (Zhao et al., 2017).

The SAR studies revealed that substitution of ‘X’ with nitrogen atom decreases the activity whereas substitution with carbon increases PARP-1 inhibition activity. Substitution with electron withdrawing group at ‘Y’ also upsurges the PARP inhibition activity. From the SAR study authors concluded that substitution on nitrogen group will lead to more specific PARP-2 inhibitors rather than PARP1 inhibitors (Zhao et al., 2017).

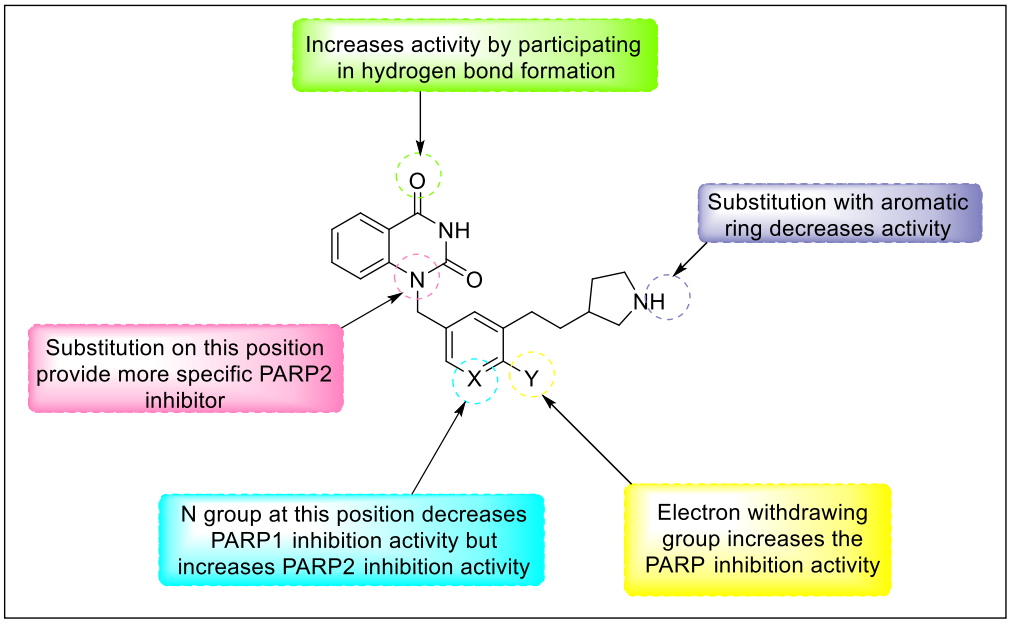

Compound	X	Y	PARP-1 [IC_{50}(nM)]	PARP-2 [IC_{50}(nM)]
16	N	F	39.8±11.6	8.6±1.7
17	C	Cl	6.2±0.1	9.1±2.1
Olaparib	-	-	8.1	1.2

Figure 2.21: SAR of quinazoline-2,4 (1H,3H)- dione derivatives

In 2017, Chadda et al. synthesized thiazolidine-2,4-dione analogs and evaluated their PARP-1 inhibition activity. They synthesized various analogs of thiazolidine-2,4-dione. Out of synthesized analogs, compound **18** emerged as a most potent PARP-1 inhibitor. They studied the molecular docking interactions of compound **18** which revealed that amide group shows hydrogen bonding interactions with Gly202 and Ser243 amino acid residue (Chadha et al., 2017). Thiazolidinedione ring condensed with indole nucleus shows π-π interactions with Tyr246 and Tyr235 as shown in **Fig. 2.22**.

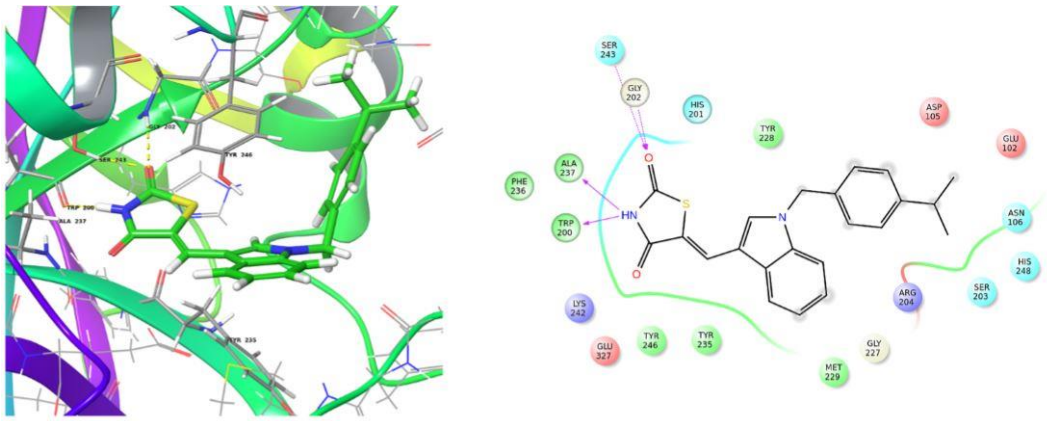

Figure 2.22: Molecular docking interactions of compound **18** (Chadha et al., 2017)

Further SAR study confirmed that substitution with long alkyl chain on para position of benzene ring intensifies the activity as shown in **Fig. 2.23**. Thiazolidinedione ring and indole ring showed a significant role in PARP-1 inhibition activity by participating in various interactions with a PARP-1 enzyme (Chadha et al., 2017).

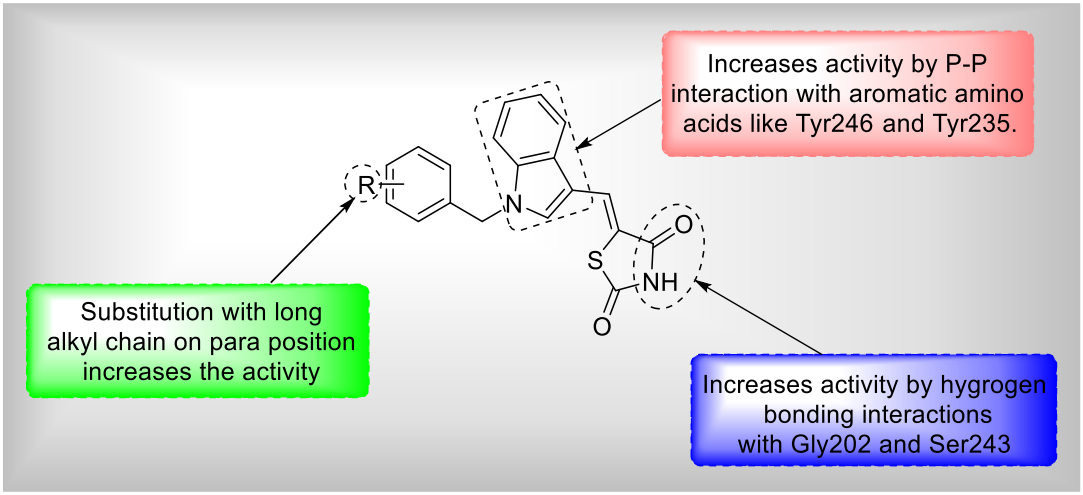

Compound	R	PARP-1 [IC_{50}(nM)]
1**8**	4-$CH(CH_3)_2$	0.74±0.25
1**9**	4-CH_3	13.95±6.59
3-Aminobenzamide	-	4.78

Figure 2.23: SAR of thiazolidine-2,4-dione analogs as PARP-1 inhibitors

In 2017, Upton et al. designed and synthesized a series of (Z)-4-(3-carbamoylphenylamino)-4-oxobut-2-enyl amides and tested their ability to inhibit the mono-(ADP-ribosyl) transferase. Initial SAR studies discovered that the primary amide on the A-ring formed three hydrogen-bonding interactions. Any derivatization around this amide or replacement of the amide will decrease potency. Out of various synthesized compounds, the compound **20** showed better inhibition against PARP-1. Molecular docking study demonstrated that oxygen group shows hydrogen bonding interactions with Ser1722 and Gly1683. Amide group also show hydrogen bonding interactions with the oxygen of Gly1683 (Upton et al., 2017). The hydroxy group attached to the moiety act as hydrogen bond donor as shown in **Fig. 2.24.**

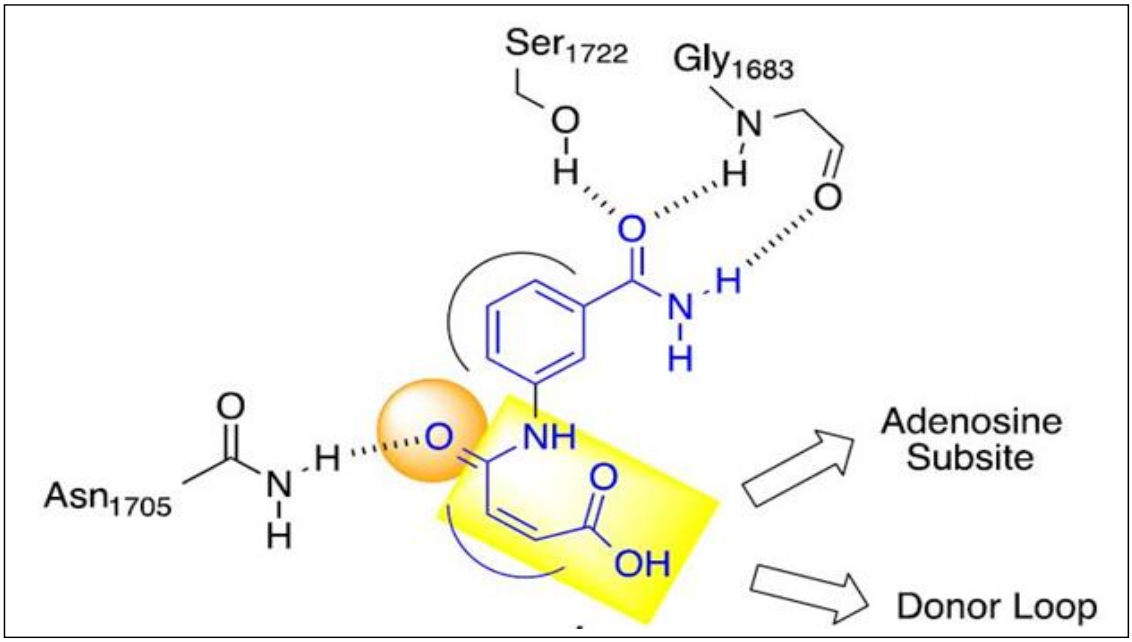

Figure 2.24: Molecular docking interactions of the general structure of (Z)-4-(3-carbamoylphenylamino)-4-oxobut-2-enyl amides (Upton et al., 2017)

SAR studies revealed that substitution with 1-(4-chlorophenyl)piperazine increases the activity than substitution with 3-phenoxypiperidine decreases the activity. The oxygen and amide groups present in moiety increases the activity by participating in hydrogen bonding interactions (Upton et al., 2017) as shown in **Fig.2.25.**

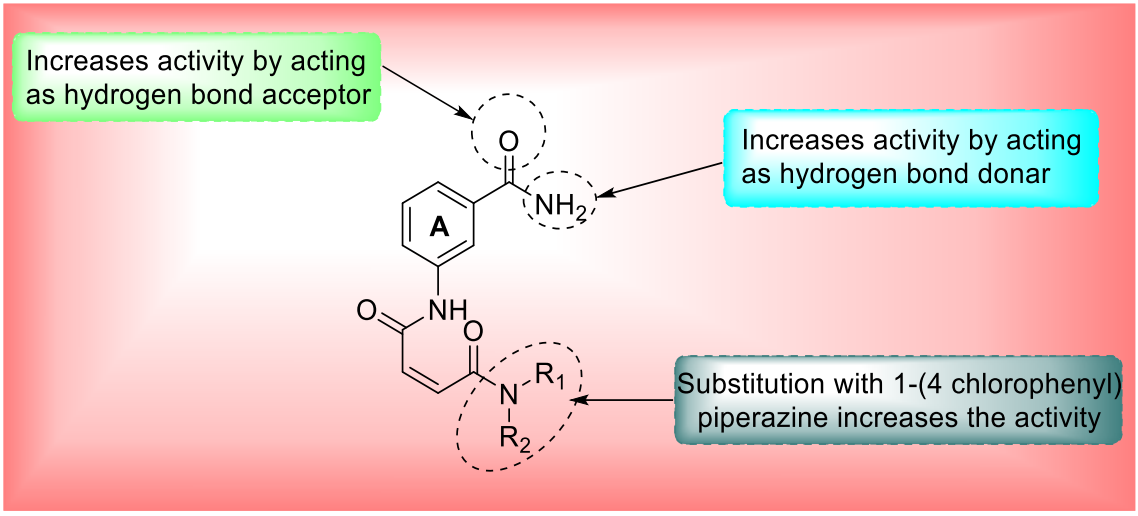

Compound	-NR1R2	PARP-1 IC50 µM
20	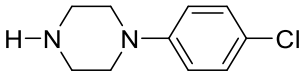	0.22 µM
21	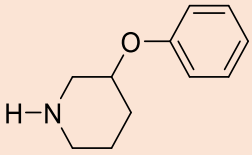	5 µM

Figure 2.25: SAR of (Z)-4-(3-carbamoylphenylamino)-4-oxobut-2-enyl amides

In 2017, Chadha et al. designed and synthesized a series of novel thiazolidine-2,4-dione (TZD) derivatives as dual inhibitors of ALR2 and PARP-1. They also evaluated in-vitro inhibitory activities against PARP-1. They synthesized various analogs of thiazolidine-2,4-dione. Out of these, compound **24** was a most potent PARP-1 inhibitor. They studied the molecular docking interactions of synthesized compounds which revealed that thiazolidine-2,4-dione shows hydrogen bonding interactions with PARP-1 residues (Chadha & Silakari, 2017). Indole nucleus and substation on R with benzyl group derivatives interact with hydrophobic pocket of PARP-1 as shown in **Fig. 2.26.**

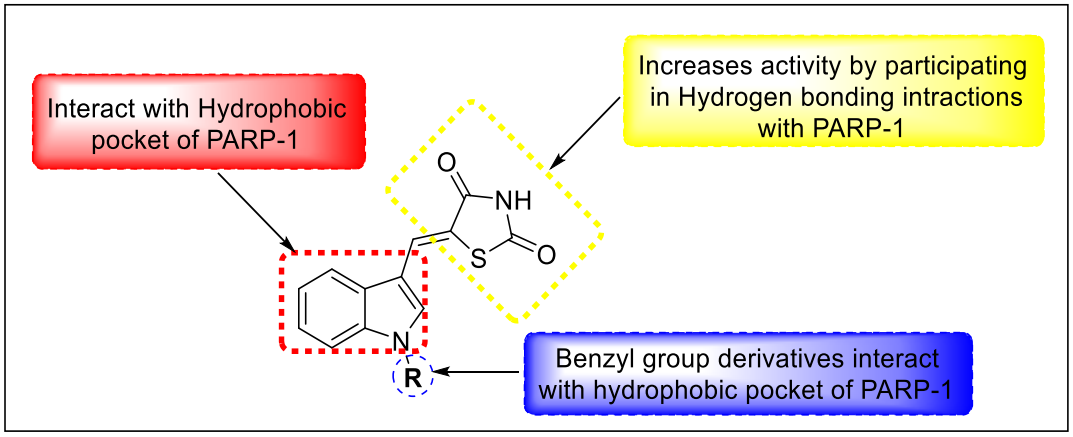

Figure 2.26: Molecular docking studies of thiazolidine-2,4-dione (TZD) derivatives

Further SAR study revealed that substitution with 4-isopropyl benzyl at **R** increased the activity and substitution with 4-methyl benzyl at **R** decreased the activity against PARP-1 (Chadha & Silakari, 2017)as shown in **Fig. 2.27**.

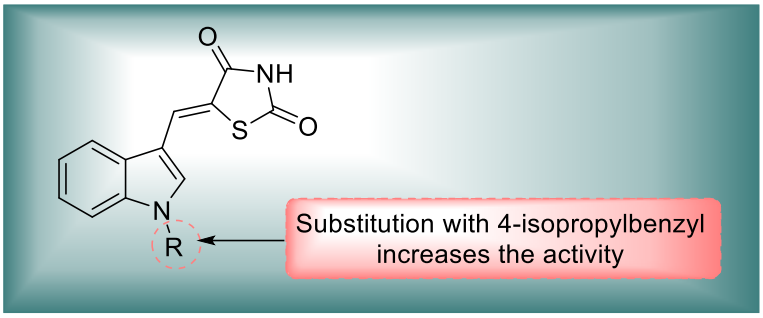

Compound	R	PARP-1 IC_{50} µM
22	2-chlorobenzyl	1.34 ± 1.67
23	4-methylbenzene	13.95 ± 6.59
24	4-isopropylbenzyl	0.74 ± 0.25
3-Aminobenzamide	-	4.78

Figure 2.27: SAR studies of thiazolidine-2,4-dione (TZD) derivatives

2.11. Quinazolinones

Heterocycles are defined as cyclic compounds in which one or more atoms of the ring are heteroatoms i.e. O, N, S, P, etc. They are present in many biologically important molecules such as amino acids, nucleic acids, and hormones. Quinazolinone is a heterocyclic aromatic organic compound with the chemical formula $C_8H_6N_2O$. It has two structural isomers, 2-quinazolinone and 4-quinazolinone **(Fig. 2.28)**.

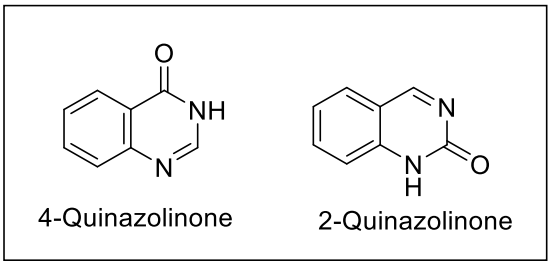

Figure 2.28: Isomers of quinazolinone

The chemical name of 4-quinazolinone is found to be quinazolin-4(3H)-one or 4-oxo-3, 4-dihydroquinazoline or 4-oxoquinazolinol or (3H) quinazoline or 3, 4-dihydroquinazolin-4-one or 4-quinazolinone. Two nitrogen atoms are incorporated in chemicals with two conjoined aromatic rings, one of the carbon which is oxidized with keto oxygen. Quinazolin-4-(3H)-one is synthesized when keto group is introduced in the pyrimidine ring of quinazoline.

2.11.1. The biological importance of Quinazolinones:

Quinazolinone and its derivatives possess a wide range of its biological activities such as anti-HIV, anticancer (Gawad et al., 2010), antimicrobial (Rana et al., 2013), anti-inflammatory (Kumar et al., 2003), antimalarial , antioxidant (Kavitha et al., 2018), antiviral (Z. Wang et al., 2012), antiulcer, analgesic (Hemalatha et al., 2011), antituberculosis, anti-proliferative activities (Rajput et al., 2012) (Fig. 2.29) and inhibitory effects for thymidylate synthase enzyme and poly (ADP-ribose) polymerase (PARP) (Darwish et al., 2017). Recently, quinazolinone derivatives have attracted strong interest in organic and medicinal chemistry due to their potent biological and pharmacological activities (Kavitha et al., 2018).

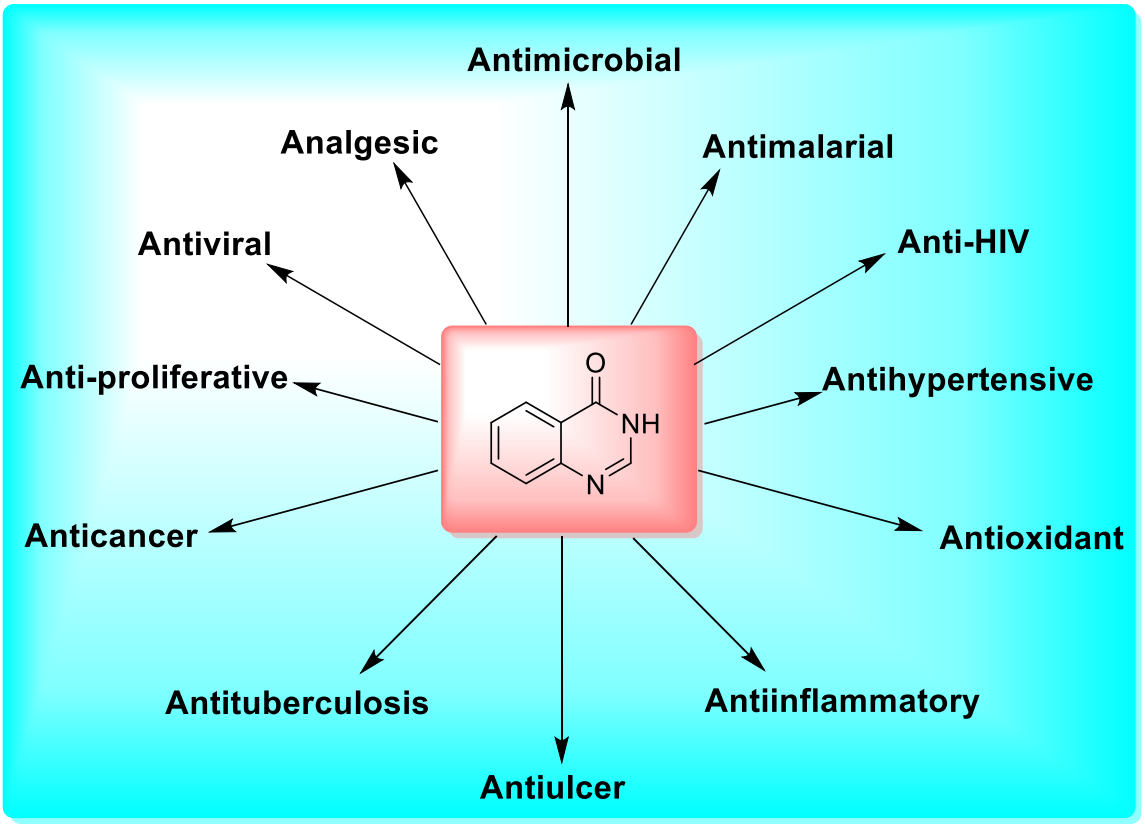

Figure 2.29: Biological activities of Quinazolinones

2.11.2. Quinazolinone derivatives as anticancer agents

Quinazolinone moiety containing drugs have been considered as a very important class of therapeutic agents, hence a number of quinazolinone compounds have been synthesized and evaluated for their different biological activities. The first quinazolinone marketed drug is Methaqualone which is used as sedative-hypnotic since 1951. Presently, a number of quinazolinone derivatives are available in the market as potential drugs for various diseases (Tiwary et al., 2015). The quinazolinone containing anticancer drugs which are available in the market are given in **Fig. 2.30.**

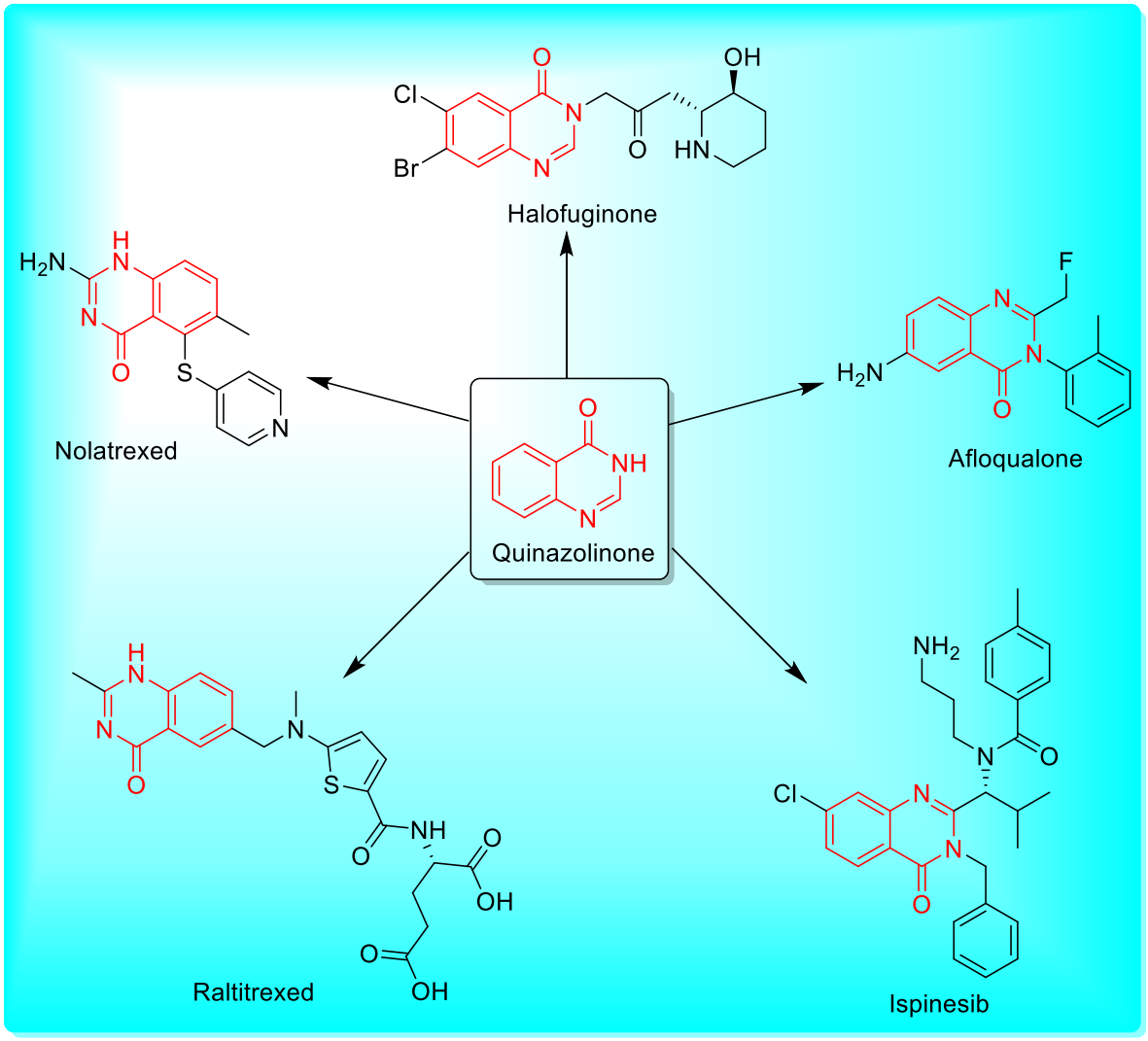

Figure 2.30: Quinazolinone containing anticancer drugs available in the market

2.11.3. Quinazolinone derivatives as PARP-1 inhibitors

Poly (ADP-ribose) polymerase-1 (PARP-1) is involved in many fundamental processes including DNA repair and transcriptional regulations (Jafari et al., 2016). Many quinazolinone derivatives are reported to have as PARP-1 inhibitory activity. Some of the quinazolinone derivatives as PARP-1 inhibitors are given in Table **Table 2.4.**

Table 2.4: Quinazolinone derivatives as PARP-1 inhibitors

Sr. No.	Structure	IC_{50} Value	References
1.	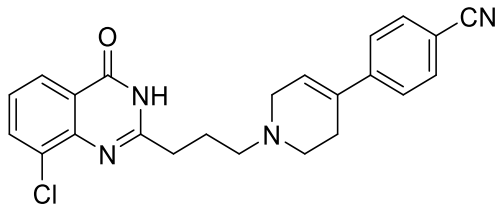	3.0 ± 0.6 nM	(Iwashita et al., 2005)
2.	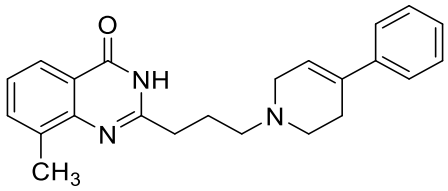	16 nM	(Hattori et al., 2004)
3.	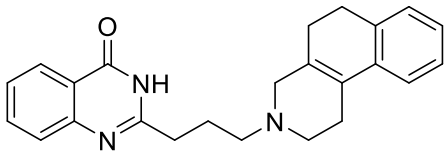	12 nM	(Hattori et al., 2004)
4.	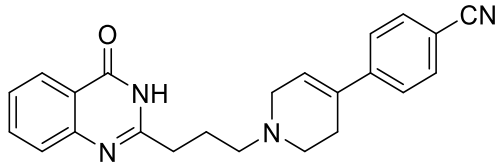	6 nM	(Hattori et al., 2004)
5.	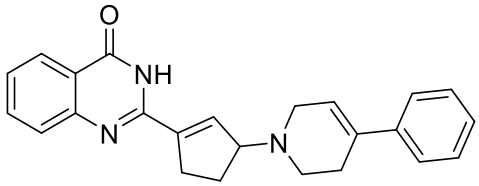	16 nM	(Hattori et al., 2007)
6.	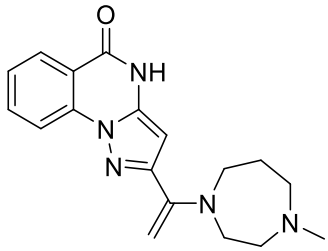	0.01 µM	(Orvieto et al., 2009)

7.	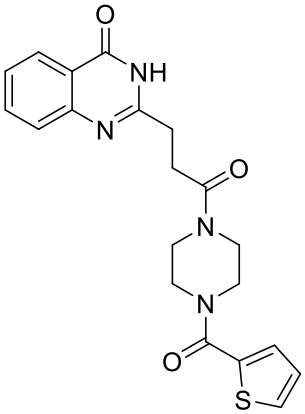	9.8 ± 2.5 nM	(Giannini et al., 2014)
8.	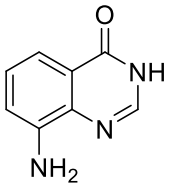	0.76 ± 0.05 µM	(Kulkarni et al., 2012)
9.	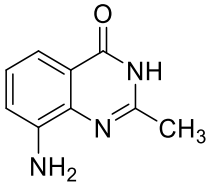	0.40±0.05 µM	(Kulkarni et al., 2012)

CHAPTER - 3

RATIONALE

3. Rationale

3.1 Design of proposed molecules

From the review of the literature, we found that quinazolinone derivatives have good anticancer potential. The present compounds were designed based on the following observations:

- As we know that over-activation of PARP-1 cause cellular mutations and lead to uncontrolled growth of cancer cells. By inhibiting PARP-1, we can inhibit the growth of cancer cells.
- From the review of the literature, we found that quinazolinones show good PARP-1 inhibition activity. The literature study revealed that hydrogen bonding and π-π interactions play an important role in PARP-1 inhibition activity.
- Veliparib and Olaparib are available in the market as PARP inhibitors. So we have designed the pharmacophore keeping in view the primary structural requirements.
- The proposed pharmacophore was designed by replacing Phthalazine-1-one moiety of olaparib with quinazolinone and pyrrolidine moiety of veliparib with the benzene ring. The designed pharmacophore is shown in **Fig. 3.1**.

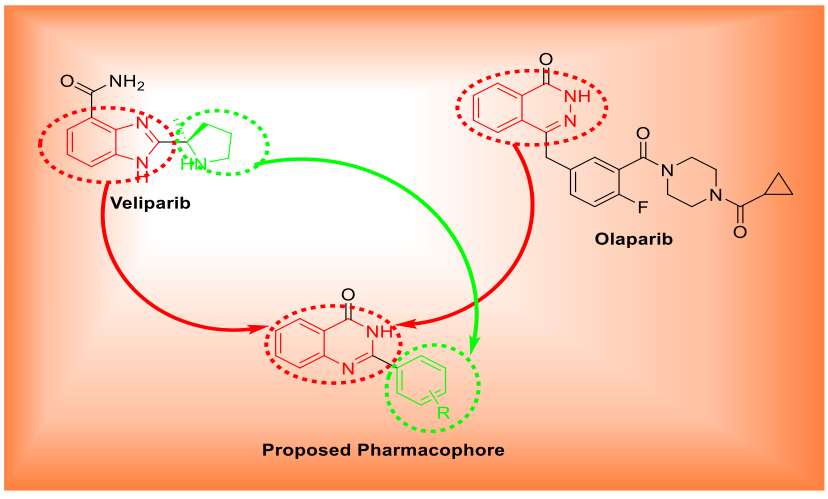

Figure 3.1: Rationale of quinazolinone derivatives as anticancer agents

3.2 Design of proposed molecules by docking

The docking studies of proposed pharmacophore and standard inhibitor revealed that the proposed pharmacophore binds at the same cavity where the standard inhibitor was bound. The overlapping of the proposed compound and standard inhibitor Veliparib shows that the benzene ring of Quinazolinone moiety overlaps with the benzene ring of Benzimidazole moiety of standard inhibitor. The ring expansion by substitution with aromatic ring results in better activity as it occupies the empty cavity of the protein. Overlapping of linkage of both compounds revealed that both the compounds interact with the protein in the same pattern and same site. The interaction pattern is shown in **Fig. 3.2.**

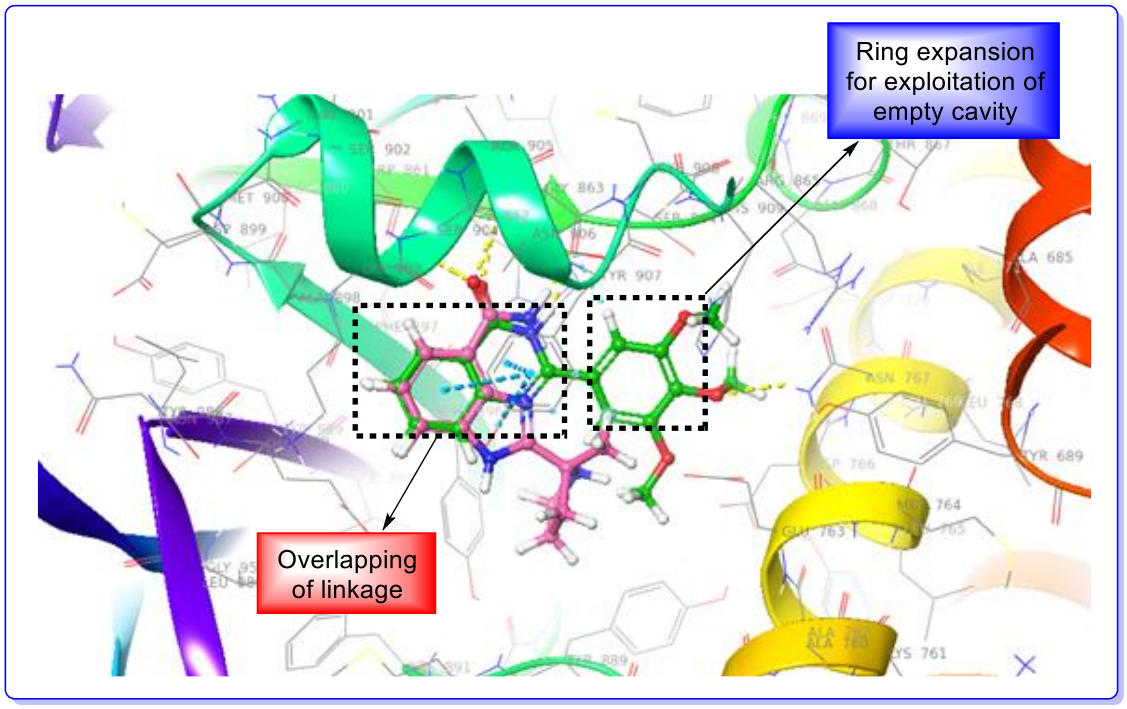

Figure 3.2: Docking interaction of proposed molecule and standard inhibitor (Veliparib); Green – Proposed molecule and Pink – Standard inhibitor

CHAPTER - 4

AIM & OBJECTIVES

3. Aim and Objectives

A. To design and synthesize proposed compounds pertaining to the structure **1 (Fig. 4.1)**.

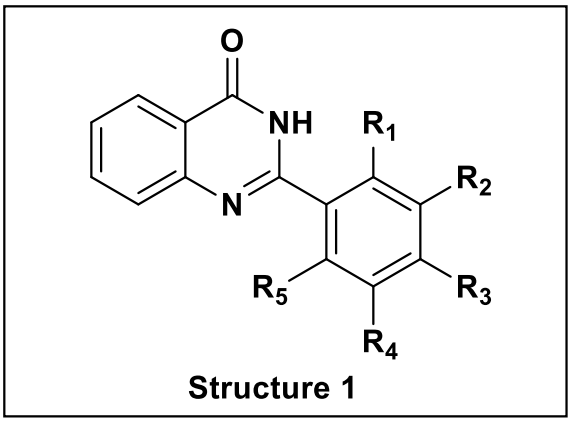

Figure 4.1: Quinazolinone-based designed compounds

B. To perform the in silico studies of synthesized compounds with the target protein (PDB ID: 5WTC).

CHAPTER – 5

MATERIALS AND METHODS

5.1. Synthesis

5.1.1. General

All the reagents were purchased from Sigma - Aldrich, Loba - Chemie Pvt. Ltd., S.D.F.C.L. and Avra Synthesis Ltd, which were used without any additional purification. For the weighing of the chemicals, Mettler Toledo and Sartorius Analytical Balance (BSA224S-CW) were used. Pre-coated Merck TLC were utilized for monitoring the progress of the reaction. The JSGW UV/fluorescent cabinet and iodine chamber was used for the visualization of the TLC spot on the pre-coated TLC plate. IKA RCT basic magnetic stirrer, Tarson spinot digital was used for the heating and stirring of the reactants. ILMVAC dist digital rotavapor was used for the removal of the solvents. The oven of Oven Universal (NSW-143) was used for the drying the glassware and silica. Melting point was measured by Stuart melting point apparatus (SMP-11) with open glass capillary tube. Celfrost and Samsung RT 35/2009 refrigerator were used for the storage of chemicals, final products and the recrystallization of final compounds. Citizen Ultrasonic Cleaner is used for the cleaning of some glassware and, plasticware. Infrared (IR) spectra of compounds were recorded on a Bruker FT-IR spectrophotometer. Mass spectra were recorded on Shimadzu GCMS-QP2010 with EI mode available at Central Instrumentation Laboratory (CIL), Central University of Punjab. ^{1}H NMR (Proton Nuclear Magnetic Resonance), and ^{13}C NMR (Carbon Nuclear Magnetic Resonance) spectra were recorded with the help of Brucker Avance II (400 MHz) NMR spectrometer, and $CDCl_3$ was used as a solvent. TMS (Tetramethylsilane) was used as an internal reference standard ($\delta = 0$).

5.2. *In silico* screening of compounds

The docking interactions were studied with the help of Maestro 11.0 (Schrodinger 2016) on Mac workstations. The study was done to identify the possible binding interactions of selected ligands with the active site receptor.

5.2.1. Selection and preparation of ligands

Ligand preparation was performed by using Ligprep wizard of Maestro 11.0 (Schrodinger 2016). In this step ligand structures were converted into a 3D form,

from 2D, hydrogen atoms were added, discrepancies between bond lengths and angle were resolved, low energy structure and ring conformation followed by minimization and OPLS 2005 force field were conducted. Consecutively, the rest of the factors such as ionization state were not altered, and specified chirality was retained.

5.2.2. Preparation of the Protein Molecule

For the X-ray crystallographic structure of PDB of PARP1 (PDB ID: 5WTC) was retrieved from protein data bank (RSCB) and prepared by Maestro 11.0 protein preparation wizard. Preprocessing, refinement, and minimization were main components of protein preparation wizard. Hydrogen atoms were added, zero-order bonds created for the metal, charges were fixed, missing disulfide bonds rectified, bond orders were assigned, and side chains which were not closed to binding cavity were neutralized. Any other problems like overlapping or alternate position or missing atoms were solved by adding hydrogen atoms, reorienting hydroxyl groups, water molecules, and amino acids. Then selected protein was reviewed and modified. Finally, refinement of the structure was done by restrained minimization.

5.2.3. Receptor grid generation

Ligand-bound within the X-ray crystal structure of the protein was utilized by Glide molecular docking for the identification of active site receptor grid. Thus, the ligands were assisted by grid-based molecular docking to bind in more than one possible conformation. 0.25 Å, scaling factor, and 1.0 Å, partial charge cutoff of Van der Waals radius were applied. Further, sites, constraints, rotatable groups, and excluded volumes were also implemented.

5.2.4. Glide molecular docking

Docking was carried out using XP (Extra Precision) after ligand preparation, a protein preparation, and grid generation on the active site of the target protein. Glide molecular docking was utilized for the evaluation of binding interactions and ligand flexibility. Glide molecular docking is a systemic approach for rapid and accurate molecular docking. The binding energy which includes ligand-protein interaction energies were calculated in kcal/mol. Determination of H-bonding, lipophilic

interactions, π-π stacking interactions, internal energy, RMSD (Root Mean Square Deviation) and desolvation energy were carried out. XP Visualizer was used for the analysis of the specific ligand-protein interactions. All of the selective ligands with the X-ray crystal structure were docked including reference compound using Glide.

5.2.5. Evaluation of docking study

On the basis of obtained dock score and ligand-protein interaction results, docking studies were evaluated. The compounds with highest dock score in negative and having good interaction profile are most active compounds against the target receptor protein.

5.2.6. Assessment of ADME properties of the compounds

QikProp tool of Schrodinger 2016 was used to assess ADME (Absorption, Distribution, Metabolism, and Excretion) properties of the selected ligands. QikProp tool accomplished rapid ADME prediction for the drug candidates. It helped to predict the essential principle and physiological descriptors of possible drug compounds. Properties such as QP log 62 HERG, QP log Po/w, QPP MDCK, QPP Caco, log Khsa and the % of human oral absorption were determined.

5.3. General procedure for the synthesis of compounds

A mixture of 2-aminobenzamide (1 eq.) and benzaldehyde (1.1 eq.) and dimethyl sulfoxide (DMSO) (5 eq.) was added to the 10 ml RBF (Round Bottom Flask). The reaction mixture was stirred on the magnetic stirrer. The progress of the reaction monitored by the TLC (Thin Layer Chromatography). After completion of the reaction, water was added to the reaction mixture to obtain precipitates of the desired compound. After that water workup was performed with ethyl acetate (10 mL × 3), washed with water and brine solution. The organic layer was dried over anhydrous Na_2SO_4 and purified via column chromatography (EtOAc: Pet ether). The compounds were recrystallized in the mixture of methanol/ethanol and dichloromethane (DCM).

5.3.1. Synthesis of 2-(2-chloro-6-fluorophenyl)quinazolin-4(3*H*)-one (SVA-1)

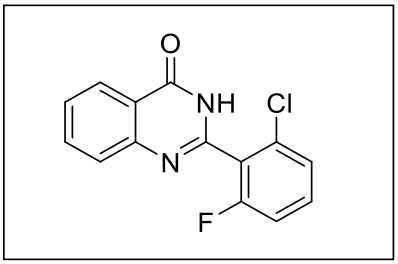

2-Aminobenzamide (0.00367 mmol) and 2-chloro-6-fluorobenzaldehyde (0.00440 mmol) were allowed to react in the solvent DMSO for 24h at 90-100℃. The completion of the reaction was monitored by TLC. After completion of the reaction, water was added to the reaction mixture to obtain precipitates of desired compound. After that water workup was performed with ethyl acetate (10 mL × 3), washed with water and brine solution. The organic layer was dried over anhydrous Na_2SO_4 and purified via column chromatography (EtOAc:Pet ether; 2:8). The product obtained was dried and recrystallized in methanol and DCM.

Yield = 77 %, Creamish white solid, **MP** = 206 - 208 ℃,

EI (m/z): M^+ = 274, [M+2] = 276

IR (DCM, cm^{-1}): 3696 (N-H), 3006 (C-H), 1543 (C=O), 1442 (C=C), 1219 (C-N), 1036 (C-F), 772 (C-Cl).

^{1}H NMR (400 MHz, $CDCl_3$, TMS = 0) δ: 11.21 (1H, s), 8.31 - 8.18 (1H, m), 7.84 - 7.81 (2H, m), 7.56 - 7.51 (1H, m), 7.47 - 7.43 (1H, m), 7.36 - 7.33 (1H, m), 7.19 - 7.15 (1H, m).

^{13}C NMR (100 MHz, $CDCl_3$, TMS = 0) δ: 163.33, 162.00, 159.47, 148.89, 146.61, 135.06, 132.39, 132.30, 128.12, 127.72, 126.52, 125.99, 125.95, 115.00.

5.3.2. Synthesis of 2-(2-methoxyphenyl)quinazolin-4(3*H*)-one (SVA-2)

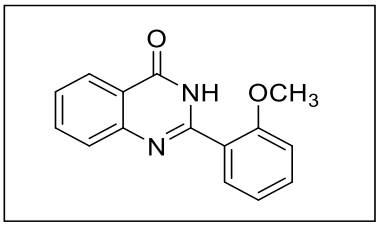

2-Aminobenzamide (0.00146 mmol) and 2-methoxybenzaldehyde (0.00160 mmol) were allowed to react in the solvent DMSO for 24h at 90-100℃. The completion of the reaction was monitored by TLC. After completion of the reaction, water was added to the reaction mixture to obtain precipitates of the desired compound. After that water workup was performed with ethyl acetate (10 mL × 3), washed with water and brine solution. The organic layer was dried over anhydrous Na_2SO_4 and purified via column chromatography (EtOAc: Pet ether; 2:8). The product obtained was dried and recrystallized in methanol and DCM.

Yield = 65 %, Creamish white, **MP** = 200 - 202 ℃,

EI (m/z): 252

IR (DCM, cm^{-1}): 3325 (N-H), 3040 (C-H), 2922 (C-H), 1678 (C=O), 1601 (C=C), 1298 (C-N), 1194 (C-O).

^{1}H NMR (400 MHz, $CDCl_3$, TMS = 0) δ: 10.91 (1H, s), 8.54 - 8.52 (1H, m), 8.30 - 8.28 (1H, d, J = 8 Hz), 7.79 - 7.73 (2H, m), 7.52 - 7.49 (1H, m), 7.47 - 7.43 (1H, m), 7.18 - 7.14 (1H, t, J = 8 Hz), 7.08 - 7.06 (1H, d, J = 8 Hz), 4.05 (3H, s).

^{13}C NMR (100 MHz, $CDCl_3$, TMS = 0) δ: 161.98, 157.84, 150.83, 149.46, 134.56, 133.28, 131.60, 127.92, 126.55, 126.48, 121.94, 121.25, 119.95, 111.89, 56.23.

5.3.3. Synthesis of 2-(2,3-dichlorophenyl)quinazolin-4(3*H*)-one (SVA-3)

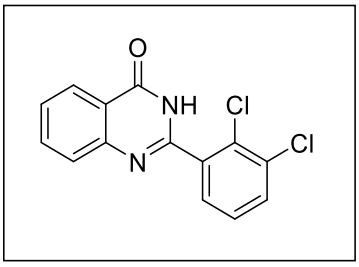

2-Aminobenzamide (0.00146 mmol) and 2,3-dichlorobenzaldehyde (0.00160 mmol) were allowed to react in the solvent DMSO for 24h at 90-100℃. The completion of the reaction was monitored by TLC. After completion of the reaction, water was added to the reaction mixture to obtain precipitates of the desired compound. After that water workup was performed with ethyl acetate (10 mL × 3), washed with water and brine solution. The organic layer was dried over anhydrous Na_2SO_4 and purified

via column chromatography (EtOAc: Pet ether; 2:8). The product obtained was dried and recrystallized in methanol and DCM.

Yield = 69 %, Creamish white, **MP** = 212 - 214 ℃,

EI (m/z): M^+ = 290, [M+2] = 292

IR (DCM, cm^{-1}): 2922 (C-H), 1676 (C=O), 1610 (C=C), 1341 (C-N), 760 (C-Cl).

^{1}H NMR (400 MHz, $CDCl_3$, TMS = 0) δ: 10.05 (1H, s), 8.29 - 8.27 (1H, d, J = 8 Hz), 7.83 - 7.78 (2H, m), 7.67 - 7.64 (2H, m), 7.56 - 7.52 (1H, m), 7.40 - 7.36 (1H, t, J = 8 Hz).

^{13}C NMR (100 MHz, $CDCl_3$, TMS = 0) δ: 162.32, 159.82, 150.61, 148.85, 135.14, 134.44, 132.77, 130.85, 129.49, 128.12, 127.77, 126.63, 121.21.

5.3.4. Synthesis of 2-(4-chlorophenyl)quinazolin-4(3H)-one (SV*A*-4)

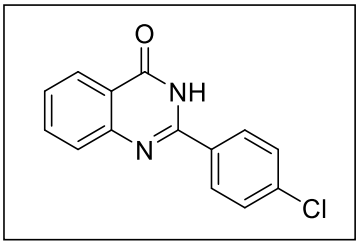

2-Aminobenzamide (0.00146 mmol) and 4-chlorobenzaldehyde (0.00160 mmol) were allowed to react in the solvent DMSO for 24h at 90-100℃. The completion of the reaction was monitored by TLC. After completion of the reaction, water was added to the reaction mixture to obtain precipitates of the desired compound. After that water workup was performed with ethyl acetate (10 mL × 3), washed with water and brine solution. The organic layer was dried over anhydrous Na_2SO_4 and purified via column chromatography (EtOAc: Pet ether; 2:8). The product obtained was dried and recrystallized in methanol and DCM.

Yield = 70 %, White, **MP** = 218 - 220 ℃,

EI (m/z): M^+ = 256, [M+2] = 258

IR (DCM, cm^{-1}): 2922 (C-H), 1729 (C=O), 1550 (C=C), 1343 (C-N), 760 (C-Cl).

^{1}H NMR (400 MHz, $CDCl_3$, TMS = 0) δ: 9.92 (1H, s), 8.31 – 8.29 (1H, d, J = 8 Hz), 8.04 - 8.02 (2H, m), 7.81 - 7.80 (2H, m), 7.55 - 7.51 (3H, m).

^{13}C NMR (100 MHz, $CDCl_3$, TMS = 0) δ: 162.14, 150.83, 148.41, 136.35, 133.93, 131.14, 129.03, 128.18, 127.17, 126.05, 125.49, 120.78.

5.3.5. Synthesis of 2-(p-tolyl)quinazolin-4(3H)-one (SV*A*-5)

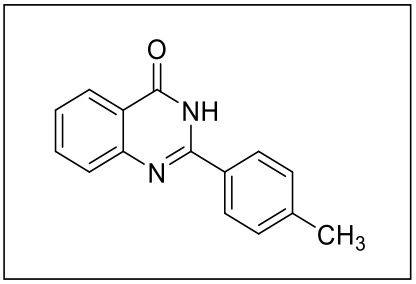

2-Aminobenzamide (0.00146 mmol) and p-tolubenzaldehyde (0.00160 mmol) were allowed to react in the solvent DMSO for 24h at 90-100℃. The completion of the reaction was monitored by TLC. After completion of the reaction, water was added to the reaction mixture to obtain precipitates of the desired compound. After that water workup was performed with ethyl acetate (10 mL × 3), washed with water and brine solution. The organic layer was dried over anhydrous Na_2SO_4 and purified via column chromatography (EtOAc: Pet ether; 2:8). The product obtained was dried and recrystallized in methanol and DCM.

Yield = 73 %, Creamish white, **MP** = 232 - 234 ℃,

EI (m/z): 236

IR (DCM, cm^{-1}): 3023 (C-H), 1665 (C=O), 1604 (C=C), 1298 (C-N).

^{1}H NMR (400 MHz, $CDCl_3$, TMS = 0) δ: 11.25 (1H, s), 8.32 - 8.30 (1H, d, J = 8 Hz), 8.12 - 8.09 (2H, t, J = 8 Hz), 7.82 - 7.76 (2H, m), 7.50 - 7.47 (1H, m), 7.38 - 7.36 (2H, d, J = 8 Hz), 2.45 (3H, s).

^{13}C NMR (100 MHz, $CDCl_3$, TMS = 0) δ: 164.07, 151.92, 149.72, 142.25, 134.90, 130.07, 129.82, 127.98, 127.45, 126.62, 126.43, 120.86, 21.63.

5.3.6. Synthesis of 2-(2-fluorophenyl)quinazolin-4(3*H*)-one (SVA-6)

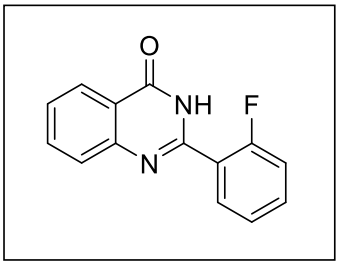

2-Aminobenzamide (0.00146 mmol) and 2-fluorobenzaldehyde (0.00160 mmol) were allowed to react in the solvent DMSO for 24h at 90-100℃. The completion of the reaction was monitored by TLC. After completion of the reaction, water was added to the reaction mixture to obtain precipitates of the desired compound. After that water workup was performed with ethyl acetate (10 mL × 3), washed with water and brine solution. The organic layer was dried over anhydrous Na_2SO_4 and purified via column chromatography (EtOAc: Pet ether; 2:8). The product obtained was dried and recrystallized in DCM and methanol.

Yield = 72 %, Creamish white, **MP** = 160 - 162 ℃,

EI (m/z): 240

IR (DCM, cm^{-1}): 3406 (N-H), 3020 (C-H), 1680 (C=O), 1608 (C=C), 1217 (C-N), 1306 (C-F).

^{1}H NMR (400 MHz, $CDCl_3$, TMS = 0) δ: 9.96 (1H, s), 8.38 - 8.34 (1H, m), 8.31 - 8.28 (1H, m), 7.80 - 7.76 (2H, m), 7.56 - 7.48 (2H, m), 7.37 - 7.32 (1H, m), 7.25 - 7.20 (1H, m).

^{13}C NMR (100 MHz, $CDCl_3$, TMS = 0) δ: 162.19, 162.05, 159.56, 149.05, 134.88, 133.58, 131.38, 128.07, 127.27, 126.60, 125.24, 121.26, 120.41, 116.81.

5.3.7. Synthesis of 2-(4-isopropylphenyl)quinazolin-4(3*H*)-one (SVA-7)

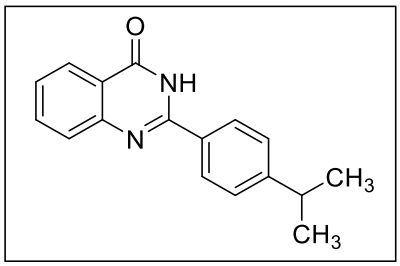

2-Aminobenzamide (0.00146 mmol) and 4-isopropyl benzaldehyde (0.00160mmol) were allowed to react in the solvent DMSO for 24h at 90-100℃. The completion of the reaction was monitored by TLC. After completion of the reaction, water was added to the reaction mixture to obtain precipitates of the desired compound. After that water workup was performed with ethyl acetate (10 mL × 3), washed with water and brine solution. The organic layer was dried over anhydrous Na_2SO_4 and purified via column chromatography (EtOAc: Pet ether; 2:8). The product obtained was dried and recrystallized in DCM and ethanol.

Yield = 73 %, White, **MP** = 204 - 206 ℃,

EI (m/z): 264

IR (DCM, cm^{-1}): 3022 (C-H), 1669 (C=O), 1530 (C=C), 1216 (C-N).

^{1}H NMR (400 MHz, $CDCl_3$, TMS = 0) δ: 10.71 (1H, s), 8.32 - 8.30 (1H, d, J = 8 Hz), 8.09 - 8.07 (2H, d, J = 8 Hz), 7.82 - 7.76 (2H, m), 7.50 - 7.46 (1H, m), 7.43 - 7.41 (2H, d, J = 8 Hz), 3.04 - 2.97 (1H, m), 1.31 - 1.29 (6H, d, J = 8 Hz).

^{13}C NMR (100 MHz, $CDCl_3$, TMS = 0) δ: 164.32, 153.00, 152.03, 149.78, 134.88, 130.44, 128.00, 127.67, 127.20, 126.58, 126.42, 120.84, 34.25, 23.88.

5.3.8. Synthesis of 2-(2-chlorophenyl)quinazolin-4(3*H*)-one (SVA-8)

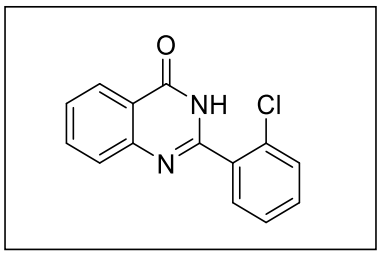

2-Aminobenzamide (0.00146 mmol) and 2-chlorobenzaldehyde (0.00160 mmol) were allowed to react in the solvent DMSO for 24h at 90-100℃. The completion of

the reaction was monitored by TLC. After completion of the reaction, water was added to the reaction mixture to obtain precipitates of the desired compound. After that water workup was performed with ethyl acetate (10 mL × 3), washed with water and brine solution. The organic layer was dried over anhydrous Na_2SO_4 and purified via column chromatography (EtOAc: Pet ether; 2:8). The product obtained was dried and recrystallized in ethanol.

Yield = 78 %, Creamish white solid, **MP** = 184 - 186 ℃,

EI (m/z): M^+ = 256, [M+2] = 258

IR (DCM, cm^{-1}): 3022 (C-H), 1679 (C=O), 1607 (C=C), 1218 (C-N), 746 (C-Cl).

^{1}H NMR (400 MHz, $CDCl_3$, TMS = 0) δ: 10.16 (1H, s), 8.29 - 8.27 (1H, d, J = 8 Hz), 7.80 - 7.79 (3H, m), 7.52 - 7.45 (4H, m).

^{13}C NMR (100 MHz, $CDCl_3$, TMS = 0) δ: 162.09, 151.03, 149.04, 134.98, 132.75, 132.14, 131.97, 131.57, 130.70, 128.09, 127.63, 127.48, 126.61, 121.21.

5.3.9. Synthesis of 2-(4-methoxyphenyl)quinazolin-4(3*H*)-one (SVA-9)

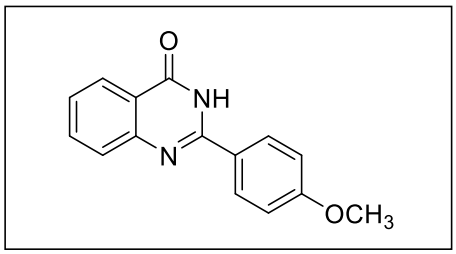

2-Aminobenzamide (0.00146 mmol) and 4-methoxybenzaldehyde (0.00160 mmol) were allowed to react in the solvent DMSO for 24h at 90-100℃. The completion of the reaction was monitored by TLC. After completion of the reaction, water was added to the reaction mixture to obtain precipitates of the desired compound. After that water workup was performed with ethyl acetate (10 mL × 3), washed with water and brine solution. The organic layer was dried over anhydrous Na_2SO_4 and purified via column chromatography (EtOAc: Pet ether; 2:8). The product obtained was dried and recrystallized in ethanol and DCM.

Yield = 64 %, White, **MP** = 240 - 242 ℃,

EI (m/z): M^+ = 252

IR (DCM, cm^{-1}): 2922 (C-H), 1673 (C=O), 1603 (C=C), 1340 (C-N), 1194 (C-O).
^{1}H NMR (400 MHz, $CDCl_3$, TMS = 0) δ: 10.65 (1H, s), 8.31 - 8.29 (1H, d, J = 8Hz), 8.14 - 8.12 (2H, m), 7.80 - 7.77 (2H, m), 7.47 - 7.44 (1H, m), 7.07 - 7.05 (2H, m).

^{13}C NMR (100 MHz, $CDCl_3$, TMS = 0) δ: 163.32, 162.59, 151.23, 149.71, 134.92, 128.86, 127.87, 126.47, 125.13, 122.03, 120.74, 114.59, 55.62.

5.3.10 Synthesis of 2-(2,5-difluorophenyl)quinazolin-4(3*H*)-one (SVA-10)

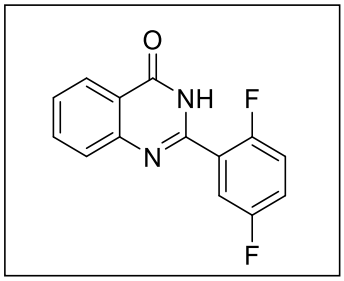

2-Aminobenzamide (0.00146 mmol) and 2,5-difluoro benzaldehyde (0.00160 mmol) were allowed to react in the solvent DMSO for 24h at 90-100℃. The completion of the reaction was monitored by TLC. After completion of the reaction, water was added to the reaction mixture to obtain precipitates of the desired compound. After that water workup was performed with ethyl acetate (10 mL × 3), washed with water and brine solution. The organic layer was dried over anhydrous Na_2SO_4 and purified via column chromatography (EtOAc: Pet ether; 2:8). The product obtained was dried and recrystallized in ethanol.

Yield = 67 %, White, **MP** = 204 - 206 ℃,

EI (m/z): M^+ = 258
IR (DCM, cm^{-1}): 3023 (C-H), 1685 (C=O), 1603 (C=C), 1217 (C-N), 1020 (C-F).
^{1}H NMR (400 MHz, $CDCl_3$, TMS = 0) δ: 9.85 (1H, s), 8.31 - 8.29 (1H, m), 8.14 - 8.11 (1H, m), 7.81 - 7.79 (2H, m), 7.53 - 7.52 (1H, m), 7.25 - 7.22 (2H, m).

^{13}C NMR (100 MHz, $CDCl_3$, TMS = 0) δ: 161.81, 160.30, 158.14, 157.86, 148.72, 147.17, 135.04, 128.19, 127.65, 126.66, 121.40, 120.44, 118.31, 117.67.

5.3.11. Synthesis of 2-(3,4,5-trimethoxyphenyl)quinazolin-4(3*H*)-one (SVA-11)

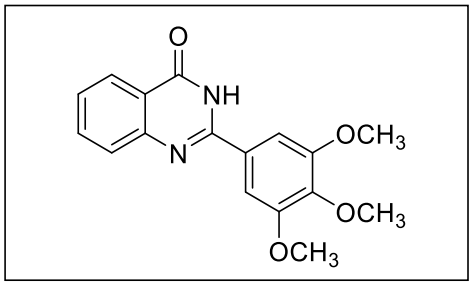

2-Aminobenzamide (0.00146 mmol) and 3,4,5-trimethoxy benzaldehyde (0.00160 mmol) were allowed to react in the solvent DMSO for 24h at 90-100℃. The completion of the reaction was monitored by TLC. After completion of the reaction, water was added to the reaction mixture to obtain precipitates of the desired compound. After that water workup was performed with ethyl acetate (10 mL × 3), washed with water and brine solution. The organic layer was dried over anhydrous Na_2SO_4 and purified via column chromatography (EtOAc: Pet ether; 2:8). The product obtained was dried and recrystallized in n-hexane and ethyl acetate.

Yield = 58 %, Creamish white, **MP** = 248 - 250 ℃,

EI (m/z): M^+ = 312

IR (DCM, cm^{-1}): 3698 (N-H), 3024 (C-H), 2979 (C-H), 1542 (C=O), 1441 (C=C), 1218 (C-N), 1036 (C-O).

^{1}H NMR (400 MHz, $CDCl_3$, TMS = 0) δ: 11.37 (1H, s), 8.30 - 8.28 (1H, d, J = 8Hz), 7.88 - 7.81 (2H, m), 7.54 - 7.52 (1H, m), 7.49 (2H, s), 4.07 (6H, s), 3.98 (3H, s).

^{13}C NMR (100 MHz, $CDCl_3$, TMS = 0) δ: 163.76, 153.69, 151.46, 149.47, 141.29, 134.95, 128.01, 126.81, 126.76, 126.19, 120.69, 104.79, 61.02, 56.48.

CHAPTER – 6

RESULTS AND DISCUSSION

6. Results and Discussion

6.1. Synthesis of designed compounds

Quinazolinone pharmacophore is widely encountered in nature, and their biological activities have prompted considerable interest in the development of new methods for their synthesis. The designed compounds were synthesized by taking 2-aminobenzamide and differently substituted benzaldehydes **(Fig. 6.1)**.

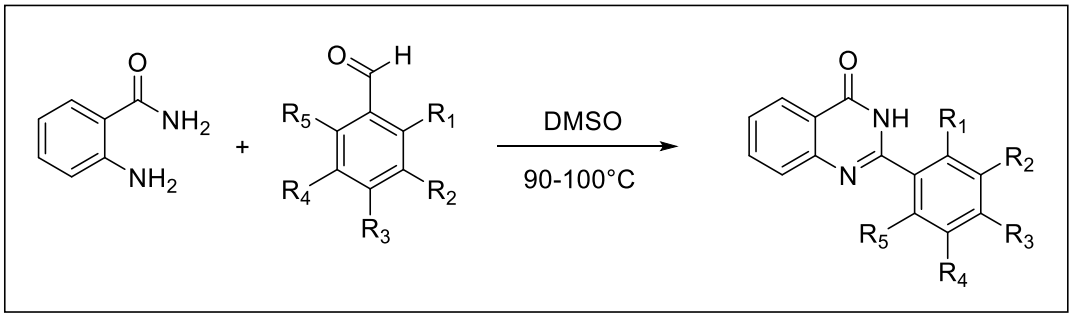

Figure 6.1: General scheme for the synthesis of designed compounds

Mechanistically, the reaction initiates by the nucleophilic attack of amine N-atom lone pair of 2-aminobenzamide on electrophilic carbonyl carbon atom substituted benzaldehyde. Further dehydration takes place which results in the formation of iminium ion. Without an acid catalyst, Iminium ion formation is very slow. Iminium ion behaves as an electrophile which is further attached by amide N-atom lone pair and cyclization takes place. At last, the loss of a water molecule in the presence of atmospheric oxygen leads to the formation of the final product (**Fig. 6.2).** The percentage yield of the compounds varies with different substitution on benzaldehyde ring. The benzaldehyde rings containing electron donating groups give lower percentage yield in comparison to the benzaldehyde rings which contain electron withdrawing groups. For example, the percentage yield of **SVA-11** was 58% and percentage yield of **SVA-8** was 78%. Electron donating groups increases the electron density on the positively charged carbon atom and lower the percentage yield and rate of reaction. Whereas electron donating groups increases the positive character of carbon atom and give good percentage yields with a faster rate of reaction.

6.1.1. The proposed mechanism of the designed scheme

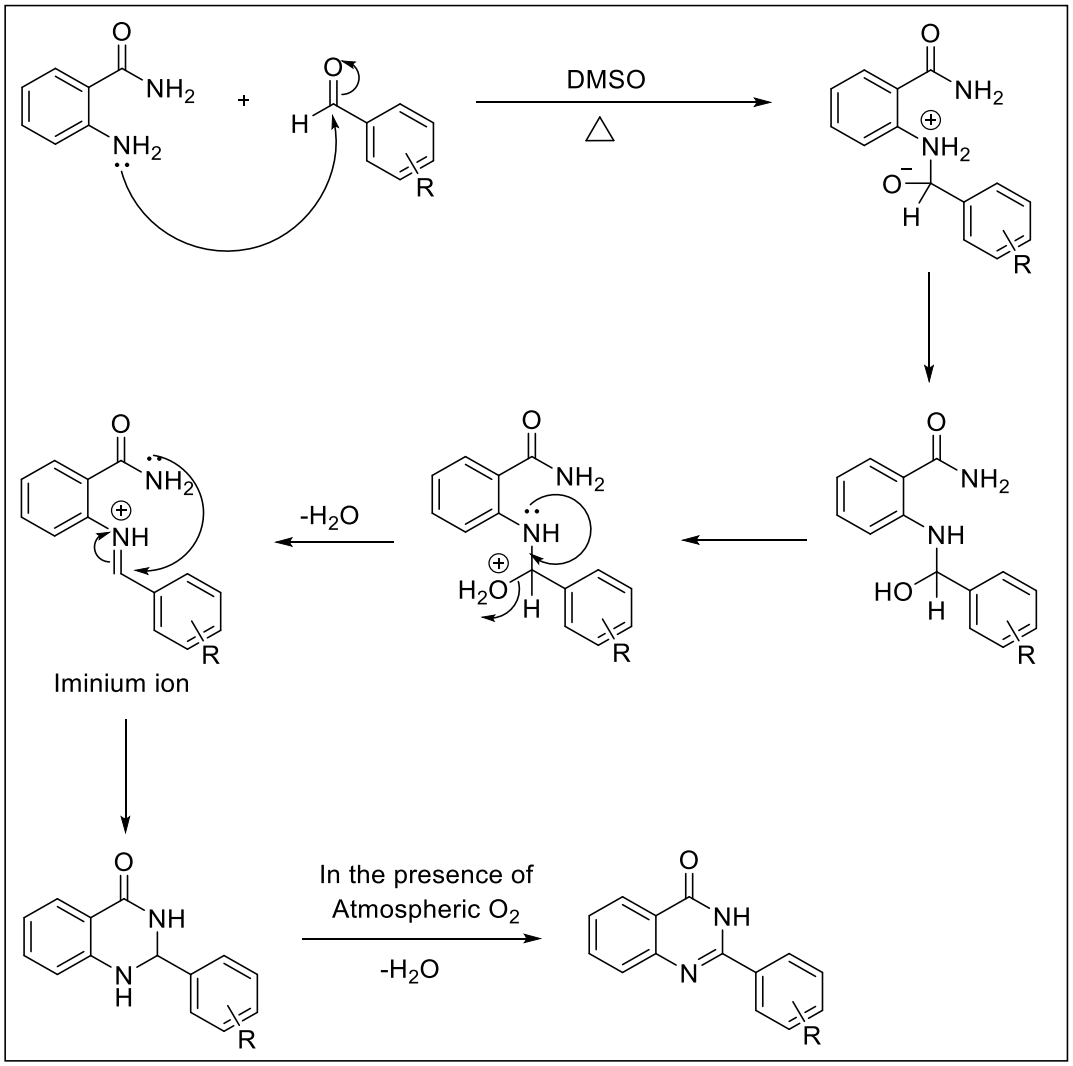

Figure 6.2: Proposed mechanism of the designed scheme

The structure of synthesized compounds was confirmed by IR spectroscopy, ^{1}H NMR, ^{13}C NMR, and Mass Spectroscopy. In ^{1}H NMR we found that the significant and characteristic peak near 10 ppm was for 'NH' present on the 3rd position of synthesized compounds. Further peaks of C-5, C-6, C-7, and C-8 were around 7-8 ppm. The protons of methoxy group show a singlet around 4 ppm. In ^{13}C NMR the characteristic peaks near 160 - 162 ppm for carbonyl group were identified in the spectra. The characteristic peak of 2nd carbon lies near 157-159 due to the presence of nitrogen on both sides of the carbon. IR peaks of C=N, N-H, C=O, C-Cl, C-F and

C-O of quinazolinone derivatives were found in the spectra near 1438-1472 cm^{-1}, 3325-3696 cm^{-1}, 1669 - 1730 cm^{-1}, 746-760 cm^{-1},1217-1218 cm^{-1} and 1194-1195 cm^{-1} respectively.

For example, SVA-11 shows ^{1}H NMR value around 10 ppm which confirms the presence of –NH group and two singlets at around 4 ppm might be due to hydrogens of methoxy groups present at substituted phenyl ring of quinazolinone.

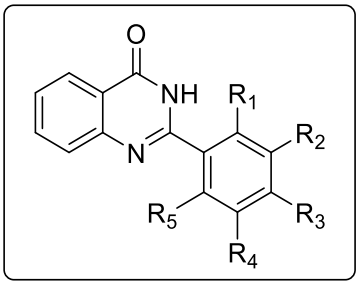

Table 6.1: List of synthesized compounds and their substitutions and percentage yield

Compound	R_1	R_2	R_3	R_4	R_5	% yield
SVA-1	Cl	H	H	H	F	77
SVA-2	OCH_3	H	H	H	H	65
SVA-3	Cl	Cl	H	H	H	69
SVA-4	H	H	Cl	H	H	70
SVA-5	H	H	CH_3	H	H	73
SVA-6	F	H	H	H	H	72
SVA-7	H	H	$CH_2(CH_3)_2$	H	H	73
SVA-8	Cl	H	H	H	H	78
SVA-9	H	H	OCH_3	H	H	64
SVA-10	F	H	H	F	H	67
SVA-11	H	OCH_3	OCH_3	OCH_3	H	58

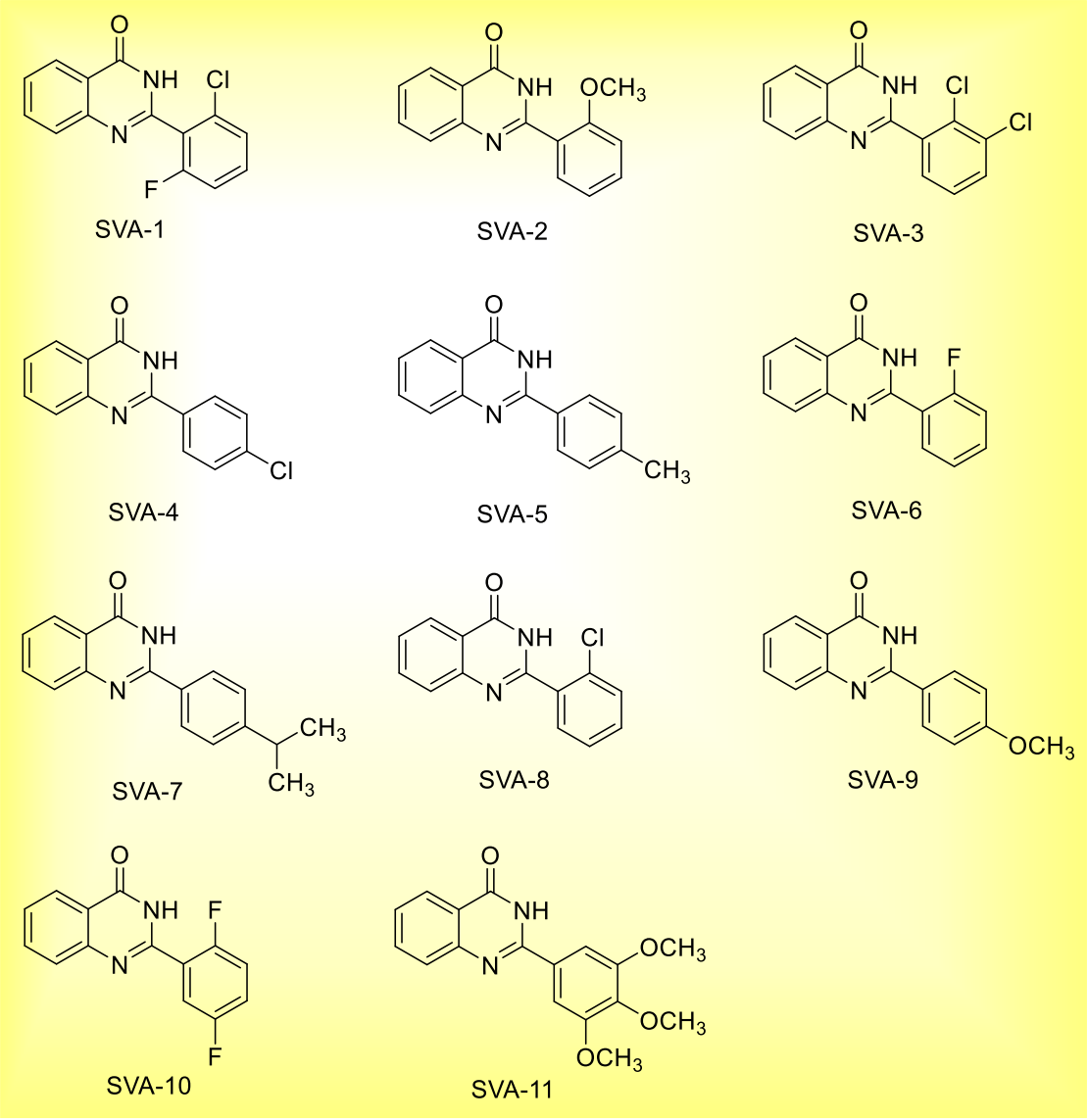

Figure 6.3: Synthesized Compounds

The percentage yield of synthesized compounds lies between 58-78%. The compound substituted with 'Cl' and 'F' give more percentage yield than other compounds substituted with 'OCH_3' groups. Compound SVA-11 (58%) give minimum percentage yield, and compound SVA-8 (78%) give maximum percentage yield (**Table 6.1**). And, the synthesized compounds are shown in **Fig. 6.3.**

6.2. *In-silico* study

The molecular docking studies of designed compounds were carried out using Maestro 11.0. Veliparib were taken as a standard inhibitor of human PARP-1 (PDB ID: 5WTC). The 2D interaction diagram of Veliparib is shown below **(Fig. 6.4).**

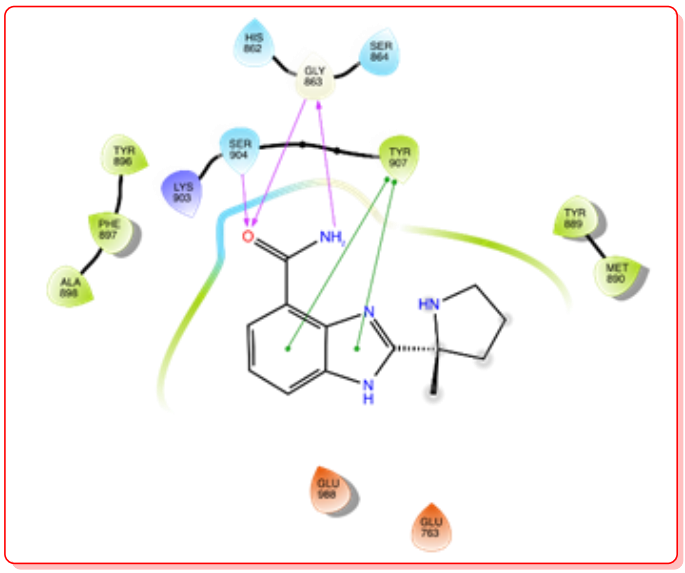

Figure 6.4: 2D interaction diagram of Veliparib

From 2D interaction diagram, it was found that standard inhibitor binds to the target site. It has shown hydrogen bonding interactions with Ser904, Gly863, and π – π interactions with Tyr 907. Molecular docking studies demonstrated that the designed compounds best fit in the active site showed π – π interactions with Tyr 907 and H – bonding interactions with Ser904, Gly863, Asn767 and pi-cation interactions with Tyr896. All of the compounds have shown better dock score results in comparison to standard drug (Veliparib). The docking interaction structures and dock score of designed compounds are given in **Table 6.2.**

Table 6.2: Docking pose of the synthesized compounds and their dock score.

S. No.	Compound	Docking Pose	Dock Score
1.	SVA-11	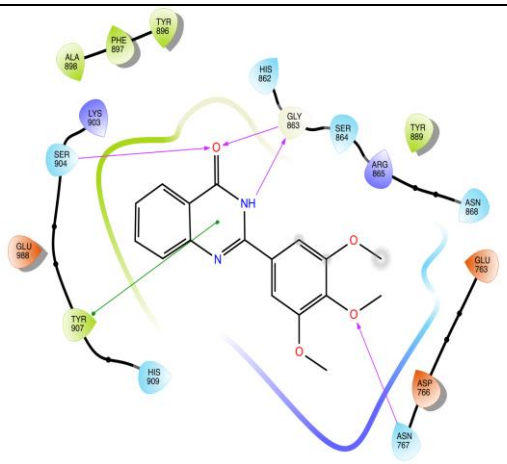	-10.421
2.	SVA-7	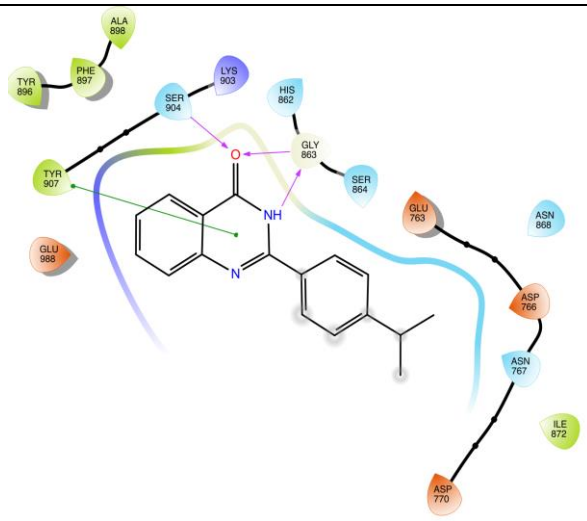	-10.182
3.	SVA-4	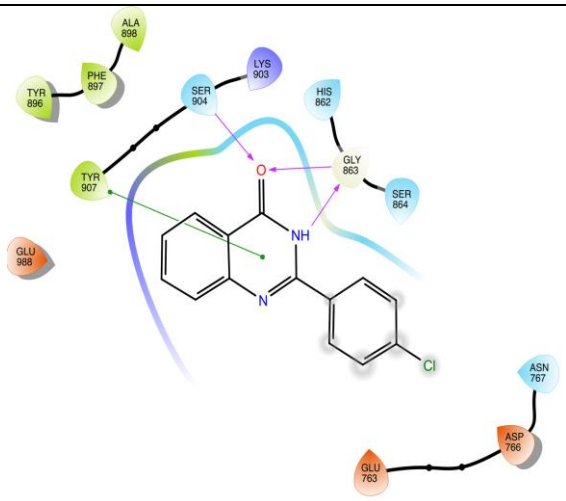	-10.038

4.	**SVA-2**	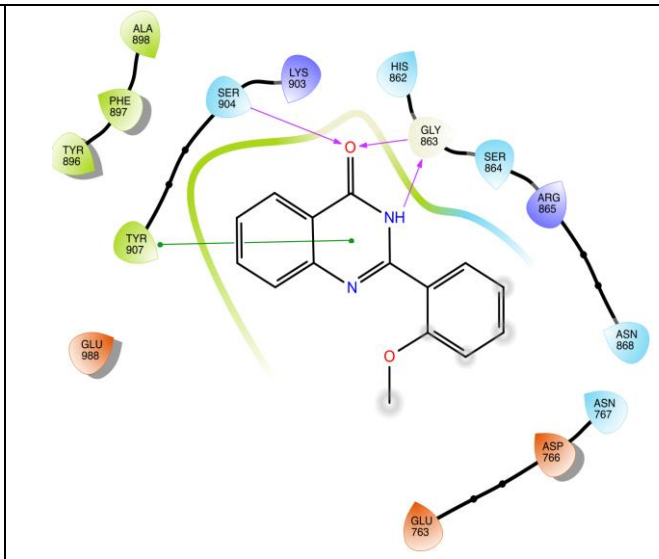	-9.787
5.	**SVA-6**	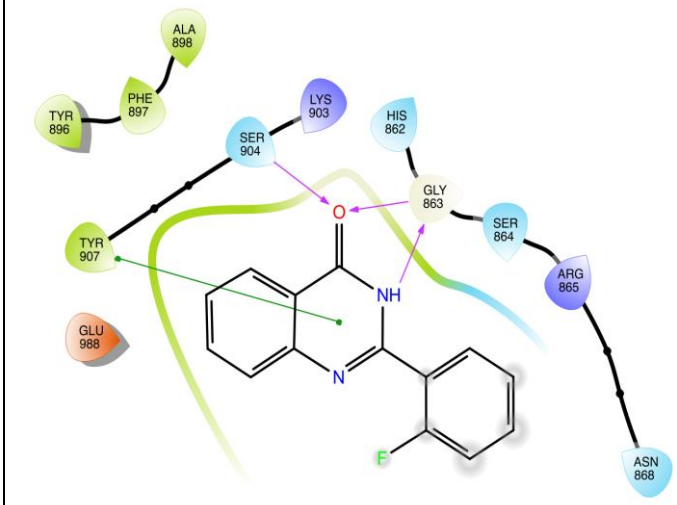	-9.731
6.	**SVA-5**	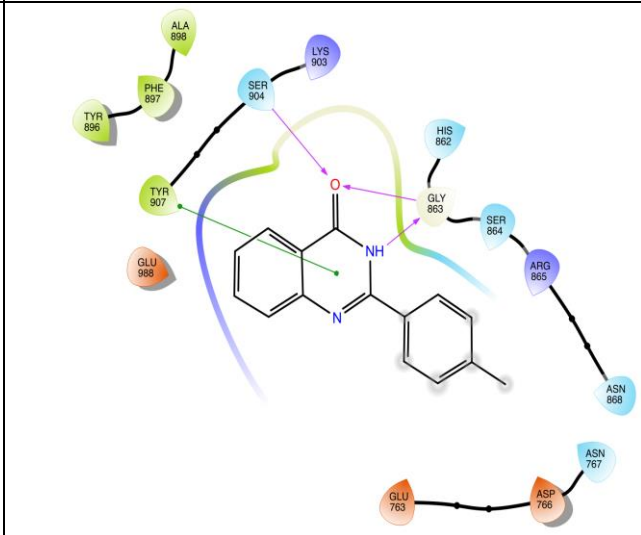	-9.723

7.	**SVA-8**	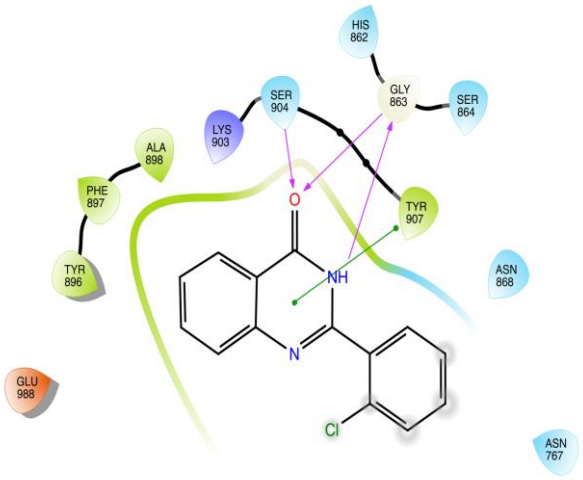	-9.701
8.	**SVA-3**	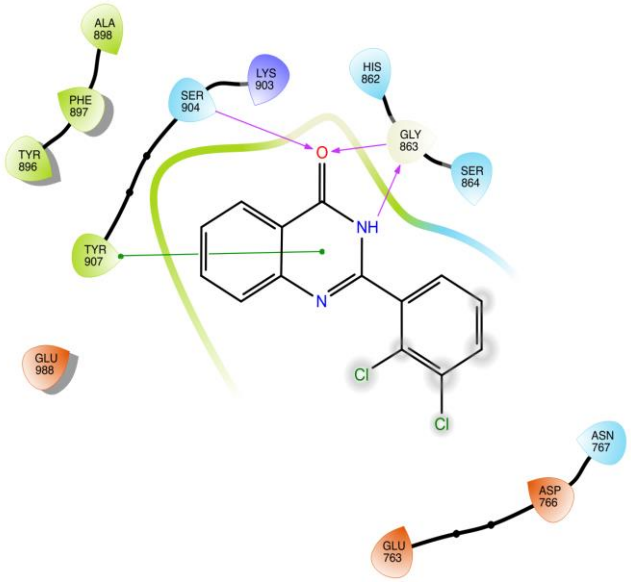	-9.547
9.	**SVA-10**	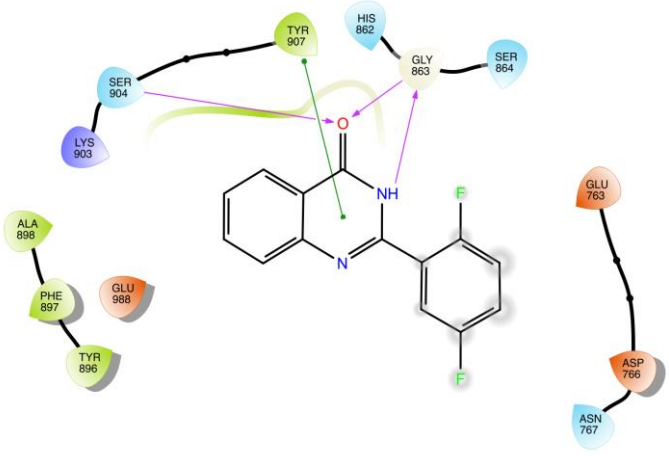	-9.447

10.	**SVA-1**	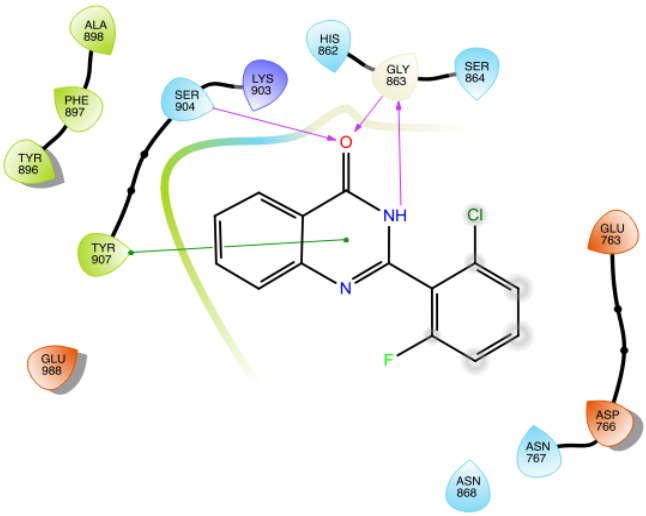	-9.257
11.	**SVA-9**	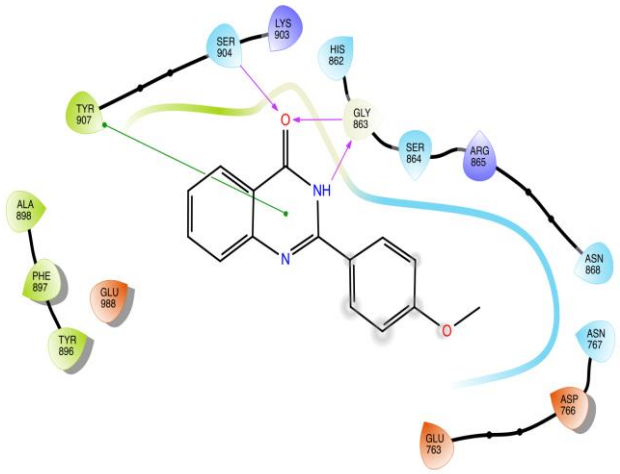	-8.842
12.	**Veliparib**	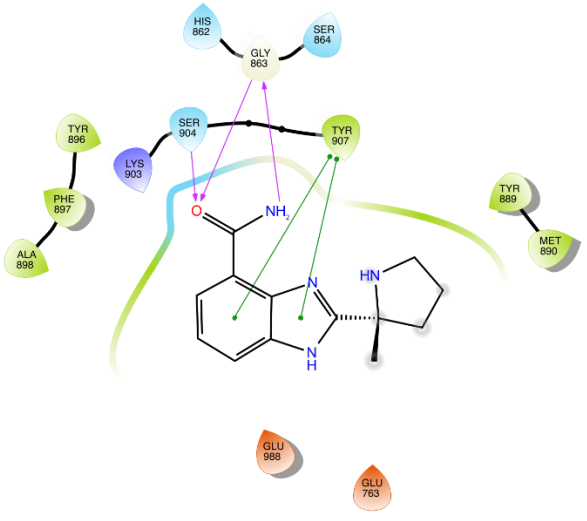	-7.337

Molecular docking study of designed compounds revealed that compound SVA-11 shows best docking interactions (dock score of SVA-11 = -10.421) than standard (dock score = -7.337) and other designed compounds. The 3D interaction diagrams of standards and the compounds possessing good dock score are discussed below.

a. Docking studies of Veliparib

The docking studies of standard molecule Veliparib revealed that the standard inhibitor was having various interactions with different amino acid residues of the selected protein. From 3D interaction diagram, it was found that standard inhibitor binds to the target site. It has shown hydrogen bonding interactions with Ser904, Gly863, and π – π interactions with Tyr 907 **(Fig. 6.5)**. Due to these interactions, the standard inhibitor shows dock score (-7.337).

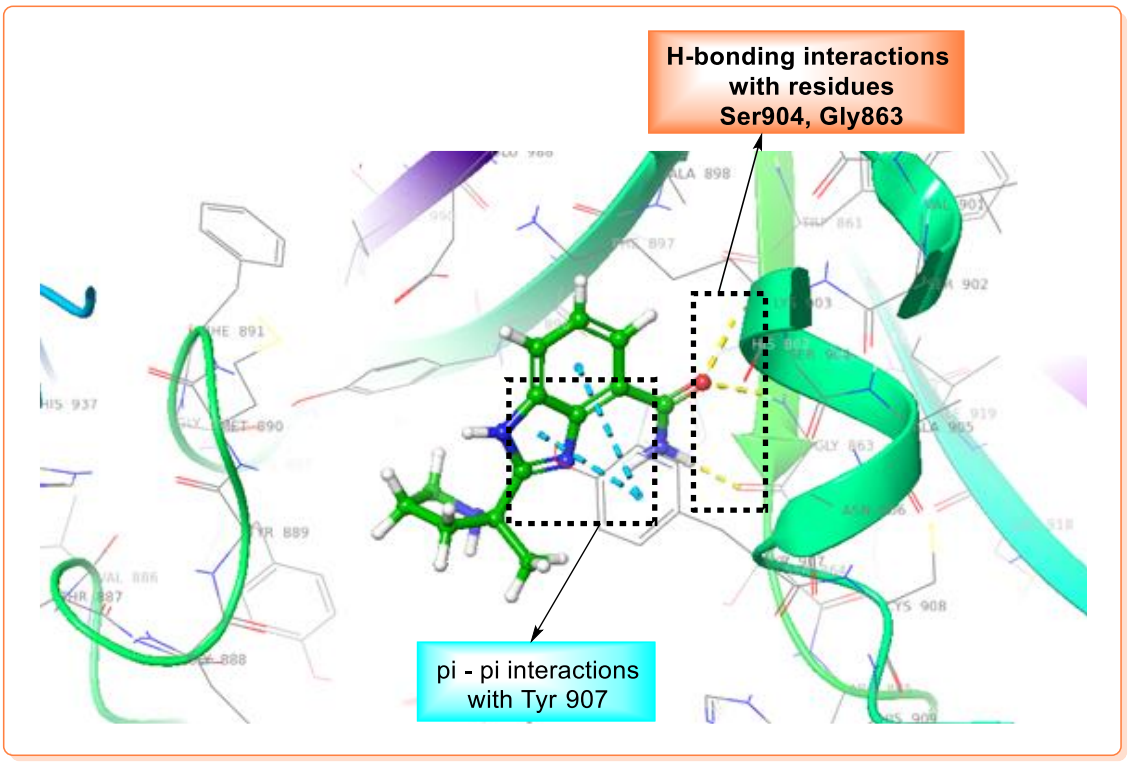

Figure 6.5: 3D interaction diagram of Veliparib

b. Docking studies of SVA-11

The 3D interaction diagram demonstrated that SVA-11 best fit in the receptor site and showed H-bonding interactions with active site residues like Ser904, Gly863, Asn767, and π- π interactions with Tyr907 **(Fig. 6.6)**. Due to these interactions, SVA-11 shows best dock score (-10.421) than other designed compounds.

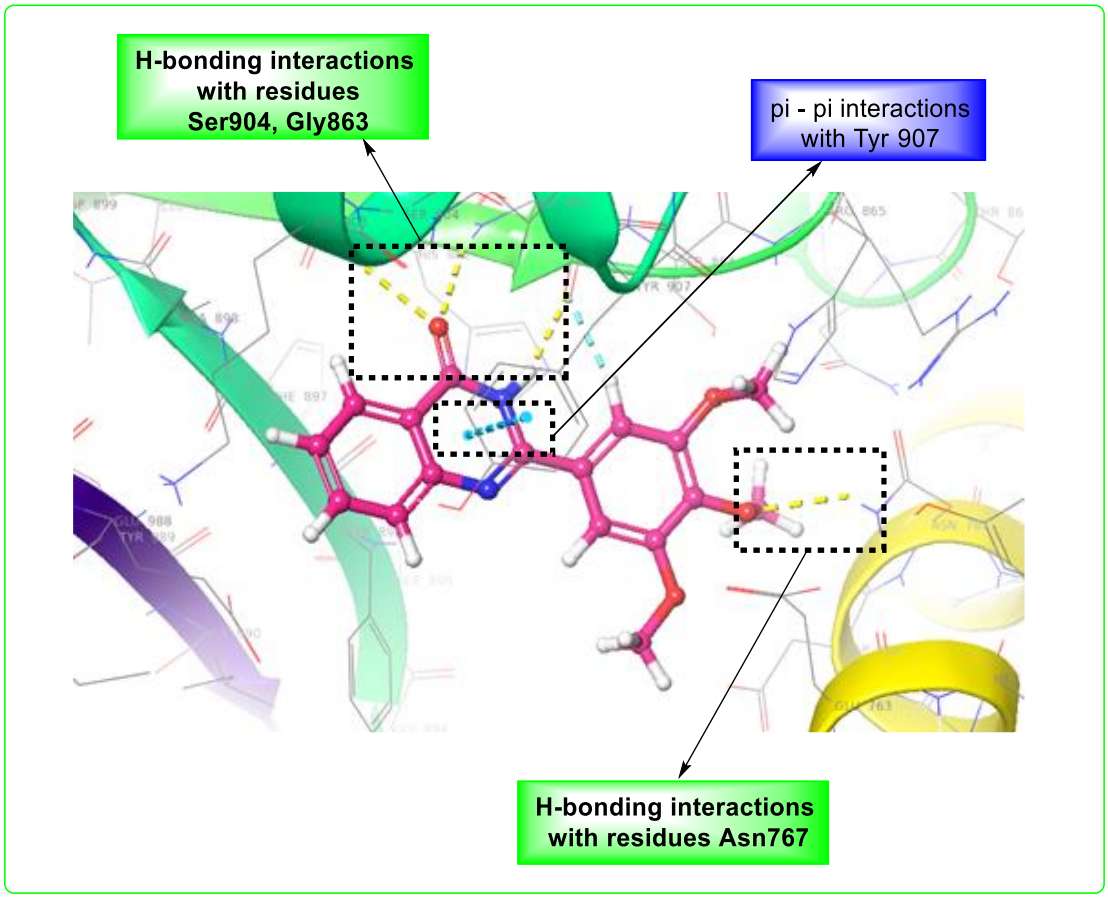

Figure 6.6: 3D interaction diagram of SVA-11

c. Docking studies of SVA-7

The 3D interaction diagram demonstrated that SVA-7 best fit in the receptor site and showed H-bonding interactions with active site residues like Ser904, Gly863, and π-π interactions with Tyr907 **(Fig. 6.7)**. Due to these interactions, SVA-7 shows dock score (-10.182) than other designed compounds.

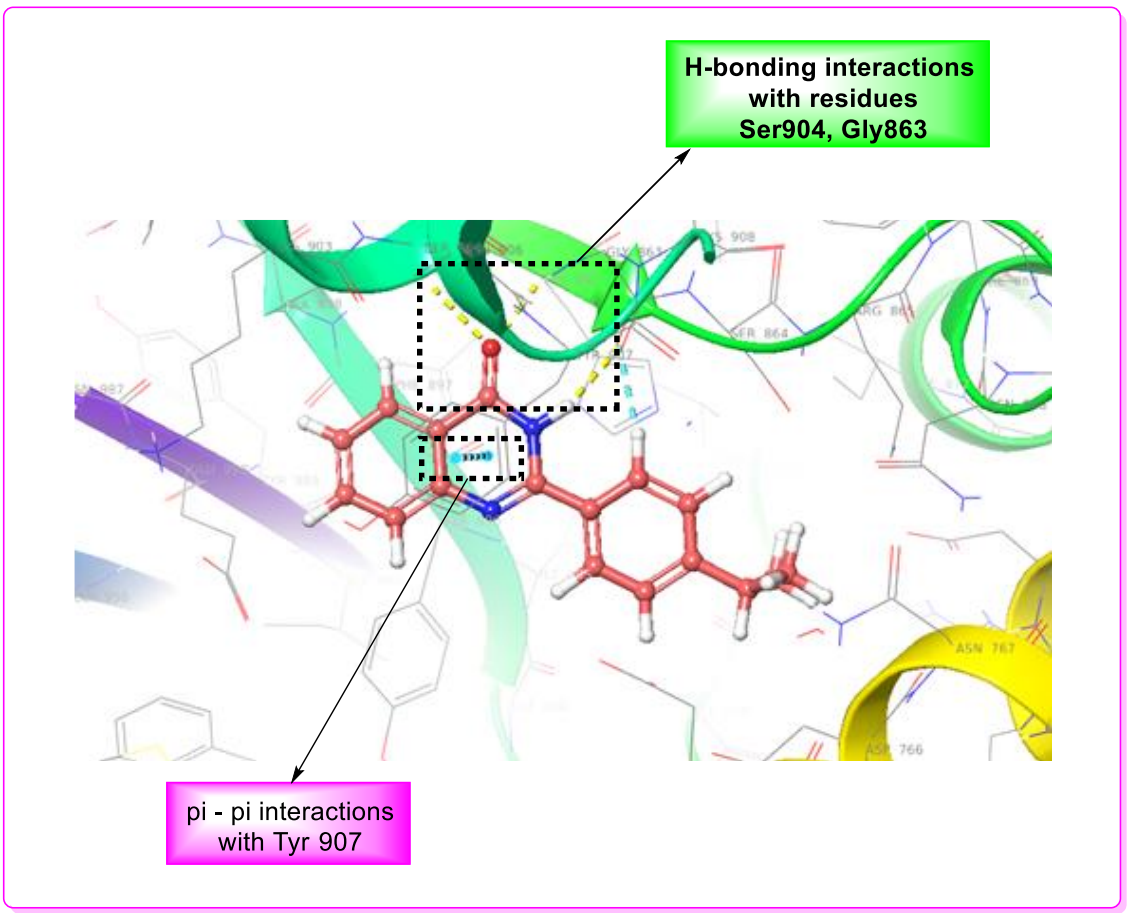

Figure 6.7: 3D interaction diagram of SVA-7

d. Docking studies of SVA-4

The 3D interaction diagram demonstrated that SVA-4 best fit in the receptor site and showed H-bonding interactions with active site residues like Ser904, Gly863, and π-π interactions with Tyr907 **(Fig. 6.8)**. Due to these interactions, SVA-7 shows dock score (-10.038) than other designed compounds.

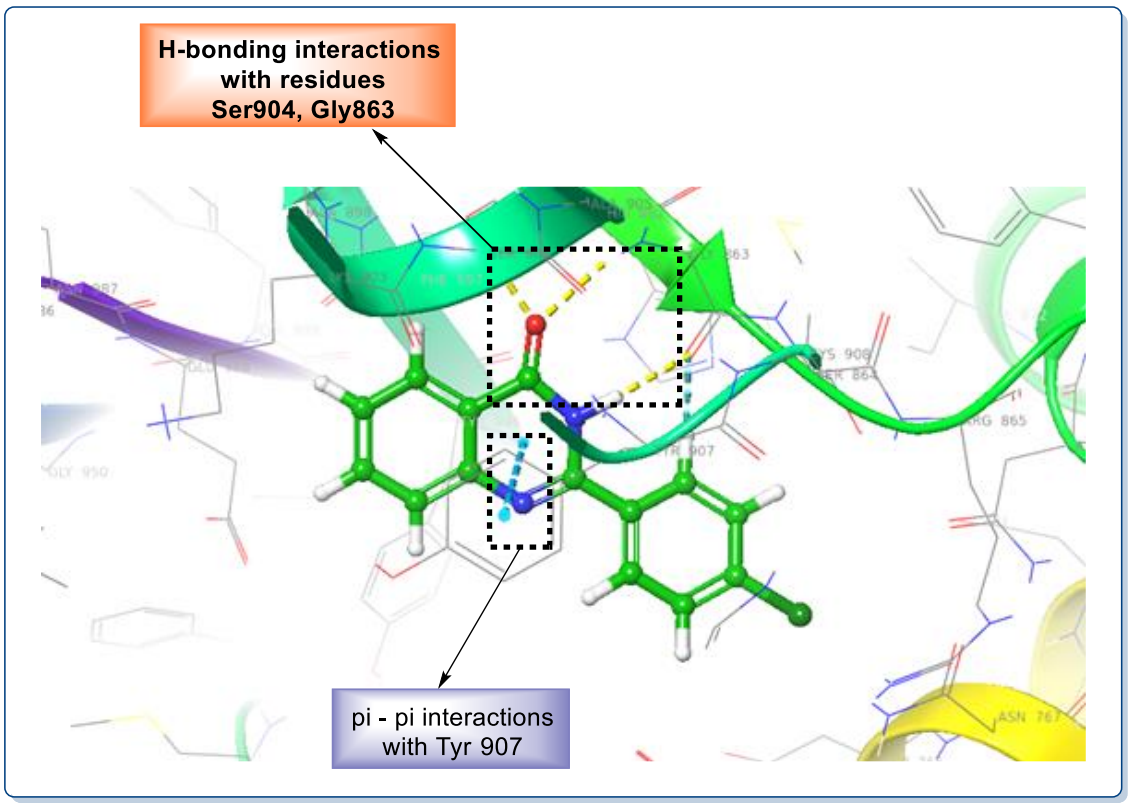

Figure 6.8: 3D interaction diagram of SVA-4

6.3 Structure-activity relationship (SAR) of synthesized compounds on the basis of docking studies

The synthesized compounds contain five substitutions i.e. R_1, R_2, R_3, R_4, and R_5, on the benzene ring of Quinazolinone derivatives as shown in **Fig. 6.9.** On the basis of docking studies, the following SAR may be established:

1. Substitution with halogens at R_1 decreases the activity.
2. Substitution with methoxy or electron donating groups at R_2, R_3, and R_4 increases the activity.
3. Substitution with the nitro group at R_5 increases the activity.
4. The benzamide moiety is required for an activity where oxygen atom of carbonyl group increases the activity by acting as hydrogen bond acceptor, -NH group increases the activity by acting as hydrogen bond donor, and benzene ring increases the activity by participating π-π interactions with PARP-1 receptor site **(Fig. 6.9).**

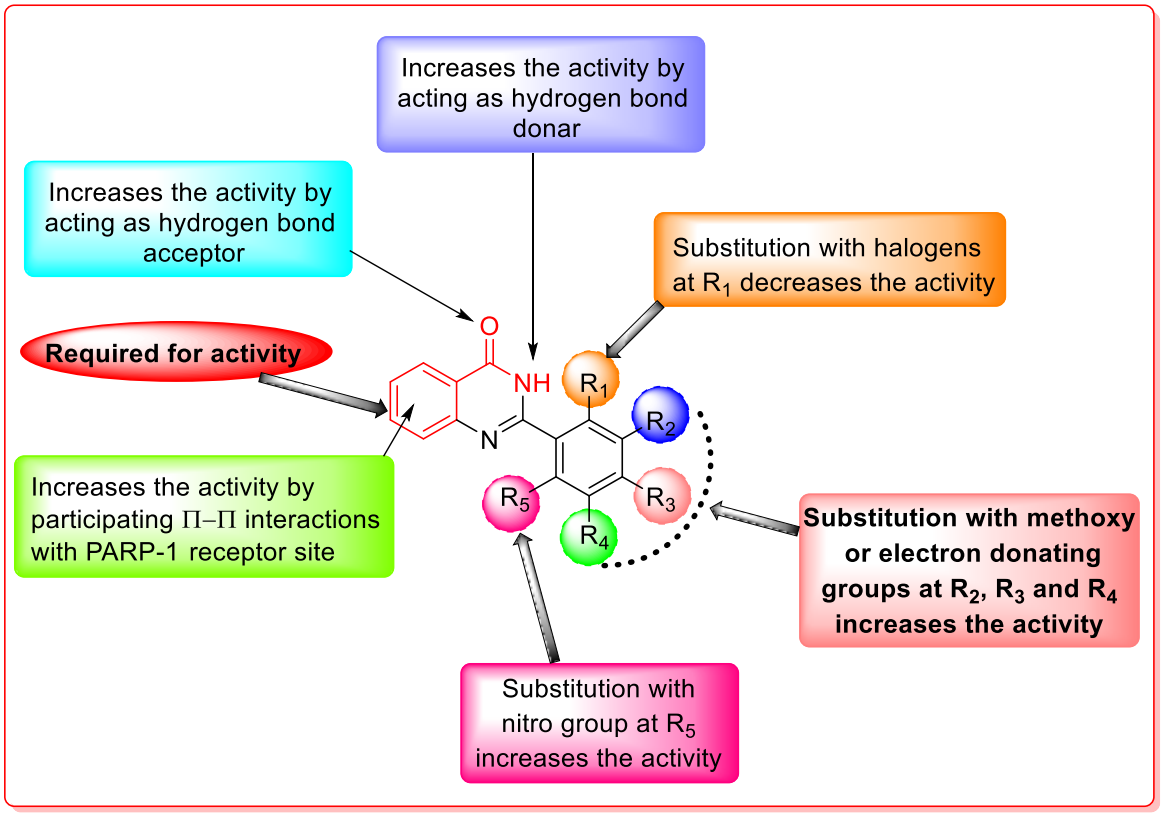

Figure 6.9: SAR of synthesized compounds on the basis of docking studies

6.4 ADME study

Furthermore, along with the docking study, we have calculated ADME properties of synthesized compounds. ADME is an important parameter for examining the bioavailability and pharmacokinetic properties of the drug. During ADME study diverse ‘parameters were calculated such as molecular weight, percentage human oral absorption, octanol/water partition coefficient (QPlogPo/w), IC_{50} value for blockage of HERG K^+ channels (QPlogHERG), brain/blood partition coefficient (QPlogBB), apparent MDCK cell permeability in nm/sec (QPPMDCK), and skin permeability (QPlogKp). ADME study revealed that all the synthesized compounds possessed percentage human oral absorption in between 82.02 to 100 whereas standard drug talazoparib/ niraparib showed only 91.391/76.695 percent human oral absorption. The predicted octanol/water partition coefficient of all compounds lies in the range of 1.8 to 3.5 (recommended range -2 to 6.5) that suggested that all compounds possessed balanced lipophilicity and hydrophilicity. The predicted IC_{50}

value for the blockage of HERG K^+ channels (QPlogHERG) of all compounds is in the range of -6 to -4 (recommended range is below -6). The brain/blood partition coefficient values also lie within the concerned range. The synthesized compounds demonstrated MDCK cell permeability greater than 500 nm/s. The most potent compound SVA-11 shows better oral absorption in comparison to a standard. The ADME results of synthesized compounds were shown in **Table 6.3**.

Table 6.3: ADME results of synthesized compounds

Title	mol MW	QPlog Po/w	QPlog HERG	QPlog BB	QPP MDCK	QPlog Kp	% Human Oral Absorp-tion
SVA-1	274.681	3.018	-5.104	0.1	3277.414	-1.576	100
SVA-2	252.272	2.608	-5.547	-0.337	800.401	-1.707	100
SVA-3	291.136	3.24	-5.505	-0.063	2838.775	-1.984	100
SVA-4	256.691	3.042	-5.812	-0.144	1888.904	-1.804	100
SVA-5	236.273	2.789	-5.815	-0.325	766.376	-1.833	100
SVA-6	240.236	2.699	-5.516	-0.183	1195.959	-1.724	100
SVA-7	264.326	3.452	-5.959	-0.417	766.095	-1.82	100
SVA-8	256.691	2.91	-5.448	-0.116	1619.453	-1.734	100
SVA-9	252.272	2.589	-5.798	-0.383	766.144	-1.735	100
SVA-10	258.227	2.862	-5.405	-0.076	2156.333	-1.857	100
SVA-11	312.324	2.833	-5.648	-0.543	766.12	-1.887	100
Veliparib	244.296	0.568	-4.989	-0.323	54.295	-5.582	67.351

CHAPTER - 7

CONCLUSION

7. Conclusion

Quinazolinone is class of heterocyclic chemical compound that has been reported to possess a various number of pharmacological activities. This skeleton was considered as an important pharmacophore for anticancer compounds and has also shown PARP-1 inhibition activity. From the literature survey, it was established that quinazolinone nucleus with benzene ring substitution on 2^{nd} position leads to the generation of potent PARP-1 inhibitors. The benzene ring increases the inhibition activity by participating in π- π interactions with the hydrophobic site of PARP-1. Proposed compounds were designed on the basis of structures of PARP-1 inhibitors (Veliparib and Olaparib). The designed compounds were synthesized and characterized by physico-chemical as well as spectral means and were docked on human PARP-1 (PDB: 5WTC) to study the interactions of compounds with target receptor. From in silico studies, we found that all the compounds fit in the active site and show various hydrophobic interactions, H-bond interactions, and π- π interactions. All of the designed compounds showed better docking score than standard (Veliparib) and compounds **SVA-11, SVA-7** and **SVA-4** were found to be most active compounds against PARP-1. ADME studies of the designed compounds revealed that all the compounds have good human oral absorption than standard (Veliparib). In future, there is a possibility of in vitro and in vivo studies of these synthesized compounds. The pharmacophore can be utilized for the generation of a library of compounds, and their biochemical, biophysical and computational analysis could lead to the potent PARP-1 inhibitors.

CHAPTER – 8

REFERENCES

8. References

Ali, A. A., Timinszky, G., Arribas-Bosacoma, R., Kozlowski, M., Hassa, P. O., Hassler, M., Ladurner, A. G., Pearl, L. H., & Oliver, A. W. (2012). The zinc-finger domains of PARP1 cooperate to recognize DNA strand breaks. Nature Structural and Molecular Biology, ***19***(7), 685.

Chadha, N., Jaggi, A. S., & Silakari, O. (2017). Structure-based design of new poly (ADP-ribose) polymerase (PARP-1) inhibitors. Molecular Diversity, ***21***(3), 655-660.

Chadha, N., & Silakari, O. (2017). Identification of low micromolar dual inhibitors for aldose reductase (ALR2) and poly (ADP-ribose) polymerase (PARP-1) using structure based design approach. Bioorganic & Medicinal Chemistry Letters, ***27***(11), 2324-2330.

Cotter, M. B., & Loda, M. (2017). Introduction to Pathology Pathology and Epidemiology of Cancer (pp. 27-42): Springer.

Darwish, K., & Dakhil, O. (2017). A Review on synthesis and biological profiles of some Quinazolines and (4H)-3, 1-Quinazolin-4-ones of active substituents and their uses as starting materials in reaction schemes. Libyan Journal of Science & Technology, ***6***(1), 8-13.

De Mas, I. M., Aguilar, E., Jayaraman, A., Polat, I. H., Martin-Bernabe, A., Bharat, R., Foguet, C., Milà, E., Papp, B., & Centelles, J. J. (2014). Cancer cell metabolism as new targets for novel designed therapies. Future, ***6***(16), 1791-1810.

Durkacz, B. W., Omidiji, O., Gray, D. A., & Shall, S. (1980). (ADP-ribose) n participates in DNA excision repair. Nature, ***283***(5747), 593-596.

Dziadkowiec, K. N., Gasiorowska, E., Nowak-Markwitz, E., & Jankowska, A. (2016). PARP inhibitors: review of mechanisms of action and BRCA1/2 mutation targeting. Przeglad Menopauzalny, ***15***(4), 215-219.

Elmongy, E. I., Khedr, M. A., Taleb, N. A., Awad, H. M., & Abbas, S. E. S. (2017). design, synthesis, and biological evaluation of some cyclohepta [b] thiophene and substituted pentahydrocycloheptathieno [2, 3-d] pyrimidine derivatives. Journal of Heterocyclic Chemistry, ***54***(2), 1084-1093.

Eustermann, S., Wu, W.-F., Langelier, M.-F., Yang, J.-C., Easton, L. E., Riccio, A. A., Pascal, J. M., & Neuhaus, D. (2015). Structural basis of detection and signaling of DNA single-strand breaks by human PARP-1. Molecular Cell, ***60***(5), 742-754.

Gawad, N. M. A., Georgey, H. H., Youssef, R. M., & El-Sayed, N. A. (2010). Synthesis and antitumor activity of some 2, 3-disubstituted quinazolin-4 (3H)-ones and 4, 6-disubstituted-1, 2, 3, 4-tetrahydroquinazolin-2H-ones. European Journal of Medicinal Chemistry, ***45***(12), 6058-6067.

Giannini, G., Battistuzzi, G., Vesci, L., Milazzo, F. M., De Paolis, F., Barbarino, M., Guglielmi, M. B., Carollo, V., Gallo, G., & Artali, R. (2014). Novel PARP-1 inhibitors based on a 2-propanoyl-3H-quinazolin-4-one scaffold. Bioorganic & Medicinal Chemistry Letters, ***24***(2), 462-466.

Gibson, B. A., & Kraus, W. L. (2012). New insights into the molecular and cellular functions of poly (ADP-ribose) and PARPs. Nature Reviews Molecular Cell Biology, ***13***(7), 411-424.

Hanahan, D., & Weinberg, R. A. (2011). Hallmarks of cancer: The next generation. Cell, ***144***(5), 646-674.

Hattori, K., Kido, Y., Yamamoto, H., Ishida, J., Iwashita, A., & Mihara, K. (2007). Rational design of conformationally restricted quinazolinone inhibitors of poly (ADP-ribose) polymerase. Bioorganic & Medicinal Chemistry Letters, ***17***(20), 5577-5581.

Hattori, K., Kido, Y., Yamamoto, H., Ishida, J., Kamijo, K., Murano, K., Ohkubo, M., Kinoshita, T., Iwashita, A., & Mihara, K. (2004). Rational approaches to discovery of orally active and brain-penetrable quinazolinone inhibitors of poly (ADP-ribose) polymerase. Journal of Medicinal Chemistry, ***47***(17), 4151-4154.

Hemalatha, K., & Girija, K. (2011). Synthesis of some novel 2, 3-disubstituted quinazolinone derivatives as analgesic and anti-inflammatory agents. International Journal of Pharmacy and Pharmaceutical Sciences, ***3***(2), 103-106.

Iwashita, A., Hattori, K., Yamamoto, H., Ishida, J., Kido, Y., Kamijo, K., Murano, K., Miyake, H., Kinoshita, T., & Warizaya, M. (2005). Discovery of quinazolinone and quinoxaline derivatives as potent and selective poly (ADP-ribose) polymerase-1/2 inhibitors. FEBS Letters, ***579***(6), 1389-1393.

Jafari, E., Khajouei, M. R., Hassanzadeh, F., Hakimelahi, G. H., & Khodarahmi, G. A. (2016). Quinazolinone and quinazoline derivatives: recent structures with potent antimicrobial and cytotoxic activities. Research in Pharmaceutical Sciences, ***11***(1), 1-14.

Jagtap, P., & Szabó, C. (2005). Poly (ADP-ribose) polymerase and the therapeutic effects of its inhibitors. Nature Reviews Drug Discovery, ***4***(5), 421-440.

Jagtap, P. G., Baloglu, E., Southan, G. J., Mabley, J. G., Li, H., Zhou, J., van Duzer, J., Salzman, A. L., & Szabo, C. (2005). Discovery of potent poly (ADP-ribose) polymerase-1 inhibitors from the modification of indeno [1, 2-c] isoquinolinone. Journal of Medicinal Chemistry, ***48***(16), 5100-5103.

Kavitha, K., Srinivasan, N., & Haribabu, Y. (2018). A Review on Quinazolinone andIts Derivatives with Diverse Biological Activities. World Journal Of Pharmacy And Pharmaceutical Sciences, ***7***(4), 628-649.

Kim, M. Y., Zhang, T., & Kraus, W. L. (2005). Poly (ADP-ribosyl) ation by PARP-1:PAR-laying'NAD^+ into a nuclear signal. Genes & Development, ***19***(17), 1951-1967.

Kulkarni, S. S., Singh, S., Shah, J. R., Low, W.-K., & Talele, T. T. (2012). Synthesis and SAR optimization of quinazolin-4 (3H)-ones as poly (ADP-ribose) polymerase-1 inhibitors. European Journal of Medicinal Chemistry, ***50***, 264-273.

Kumar, A., Sharma, S., Bajaj, K., Sharma, S., Panwar, H., Singh, T., & Srivastava, V. (2003). Some new 2, 3, 6-trisubstituted quinazolinones as potent anti-inflammatory, analgesic and COX-II inhibitors. Bioorganic & Medicinal Chemistry, ***11***(23), 5293-5299.

Laird, P. W. (2005). Cancer epigenetics. Human Molecular Genetics, ***14***(suppl 1), R65-R76.

Langelier, M.-F., Planck, J. L., Roy, S., & Pascal, J. M. (2012). Structural basis for DNA damage–dependent poly (ADP-ribosyl) ation by human PARP-1. Science, ***336***(6082), 728-732.

Loeffler, P. A., Cuneo, M. J., Mueller, G. A., DeRose, E. F., Gabel, S. A., & London, R. E. (2011). Structural studies of the PARP-1 BRCT domain. BMC Structural Biology, ***11***(1), 37.

Malyuchenko, N., Kotova, E. Y., Kulaeva, O., Kirpichnikov, M., & Studitskiy, V. (2015). PARP1 Inhibitors: Antitumor drug design. Acta Naturae, ***7***(3 (26)), 27-37.

Murtaugh, M. P., Steer, C. J., Sreevatsan, S., Patterson, N., Kennedy, S., & Sriramarao, P. (2017). The science behind One health: At the interface of humans, animals, and the environment. Annals of the New York Academy of Sciences, ***1395***(1), 12-32.

Orvieto, F., Branca, D., Giomini, C., Jones, P., Koch, U., Ontoria, J. M., Palumbi, M. C., Rowley, M., Toniatti, C., & Muraglia, E. (2009). Identification of substituted pyrazolo [1, 5-a] quinazolin-5 (4H)-one as potent poly (ADP-ribose) polymerase-1 (PARP-1) inhibitors. Bioorganic & Medicinal Chemistry Letters, ***19***(15), 4196-4200.

Purnell, M. R., & Whish, W. (1980). Novel inhibitors of poly (ADP-ribose) synthetase. Biochemical Journal, ***185***(3), 775-777.

Rajput, R., & Mishra, A. P. (2012). A review on biological activity of quinazolinones. International Journal of Pharmacy and Pharmaceutical Sciences, ***4***(2), 66-70.

Rana, A. M., Desai, K. R., & Jauhari, S. (2013). Synthesis, characterization, and pharmacological evaluation of 1-[2-(6-nitro-4-oxo-2-phenyl-4H-quinazolin-3-yl)-ethyl]-3-phenyl ureas. Medicinal Chemistry Research, ***22***(1), 225-233.

Rojo, F., Garcia-Parra, J., Zazo, S., Tusquets, I., Ferrer-Lozano, J., Menendez, S., Eroles, P., Chamizo, C., Servitja, S., & Ramirez-Merino, N. (2011). Nuclear PARP-1 protein overexpression is associated with poor overall survival in early breast cancer. Annals Of Oncology, ***23***(5), 1156-1164.

Rouleau, M., Patel, A., Hendzel, M. J., Kaufmann, S. H., & Poirier, G. G. (2010). PARP inhibition: PARP1 and beyond. Nature Reviews Cancer, ***10***(4), 293-301.

Schiewer, M. J., Goodwin, J. F., Han, S., Brenner, J. C., Augello, M. A., Dean, J. L., Liu, F., Planck, J. L., Ravindranathan, P., & Chinnaiyan, A. M. (2012). Dual roles of PARP-1 promote cancer growth and progression. Cancer Discovery, ***2***(12), 1134-1149.

Schiewer, M. J., & Knudsen, K. E. (2014). Transcriptional roles of PARP1 in cancer. Molecular Cancer Research, ***12***(8), 1069-1080.

Schiewer, M. J., Mandigo, A. C., Gordon, N., Han, S., Zhao, S., Evans, J., Parsons, T., Birbe, R., McCue, P., & Visakorpi, T. (2017). Abstract A08: PARP1-mediated E2F1 regulation of DNA repair capacity. Molecular Cancer Research, ***336***, 728-732.

Scott, C. L., Swisher, E. M., & Kaufmann, S. H. (2015). Poly (ADP-ribose) polymerase inhibitors: recent advances and future development. Journal of Clinical Oncology, ***33***(12), 1397-1406.

Swindall, A. F., Stanley, J. A., & Yang, E. S. (2013). PARP-1: Friend or foe of dna damage and repair in tumorigenesis? Cancers, ***5***(3), 943-958.

Tiwary, B. K., Pradhan, K., Nanda, A. K., & Chakraborty, R. (2015). Implication of quinazoline-4(3h)-ones in medicinal chemistry: A brief review. Journal of Chemical Biology & Therapeutics, ***1***(1), 1000104.

Upton, K., Meyers, M., Thorsell, A.-G., Karlberg, T., Holechek, J., Lease, R., Schey, G., Wolf, E., Lucente, A., & Schuler, H. (2017). Design and synthesis of potent inhibitors of the mono (ADP-ribosyl) transferase, PARP14. Bioorganic & Medicinal Chemistry Letters, ***27***(13), 2907-2911.

Wang, J., Tan, H., Sun, Q., Ge, Z., Wang, X., Wang, Y., & Li, R. (2015). Design, synthesis and biological evaluation of pyridazino [3, 4, 5-de] quinazolin-3 (2H)-one as a new class of PARP-1 inhibitors. Bioorganic & Medicinal Chemistry Letters, ***25***(11), 2340-2344.

Wang, J., Wang, X., Li, H., Ji, D., Li, Y., Xu, Y., & Zhu, Q. (2016). Design, synthesis and biological evaluation of novel 5-fluoro-1H-benzimidazole-4-carboxamide

derivatives as potent PARP-1 inhibitors. Bioorganic & Medicinal Chemistry Letters, ***26***(16), 4127-4132.

Wang, L., Liang, C., Li, F., Guan, D., Wu, X., Fu, X., Lu, A., & Zhang, G. (2017). PARP1 in carcinomas and PARP1 inhibitors as antineoplastic drugs. International Journal of Molecular Sciences, ***18***(10), 2111.

Wang, L., Liu, F., Jiang, N., Zhou, W., Zhou, X., & Zheng, Z. (2016). Design, Synthesis, and Biological Evaluation of Novel PARP-1 Inhibitors Based on a 1H-Thieno [3, 4-d] Imidazole-4-Carboxamide Scaffold. Molecules, ***21***(6), 772.

Wang, Z., Wang, M., Yao, X., Li, Y., Tan, J., Wang, L., Qiao, W., Geng, Y., Liu, Y., & Wang, Q. (2012). Design, synthesis and antiviral activity of novel quinazolinones. European Journal of Medicinal Chemistry, ***53***, 275-282.

Xie, Z., Zhou, Y., Zhao, W., Jiao, H., Chen, Y., Yang, Y., & Li, Z. (2015). Identification of novel PARP-1 inhibitors: Drug design, synthesis and biological evaluation. Bioorganic & Medicinal Chemistry Letters, ***25***(20), 4557-4561.

Yuan, Z., Chen, S., Sun, Q., Wang, N., Li, D., Miao, S., Gao, C., Chen, Y., Tan, C., & Jiang, Y. (2017). Olaparib hydroxamic acid derivatives as dual PARP and HDAC inhibitors for cancer therapy. Bioorganic & Medicinal Chemistry, ***25***(15), 4100-4109.

Zhao, H., Ji, M., Cui, G., Zhou, J., Lai, F., Chen, X., & Xu, B. (2017). Discovery of novel quinazoline-2, 4 (1H, 3H)-dione derivatives as potent PARP-2 selective inhibitors. Bioorganic & Medicinal Chemistry, ***25***(15), 4045-4054.

APPENDICES

Spectral data of synthesized compound

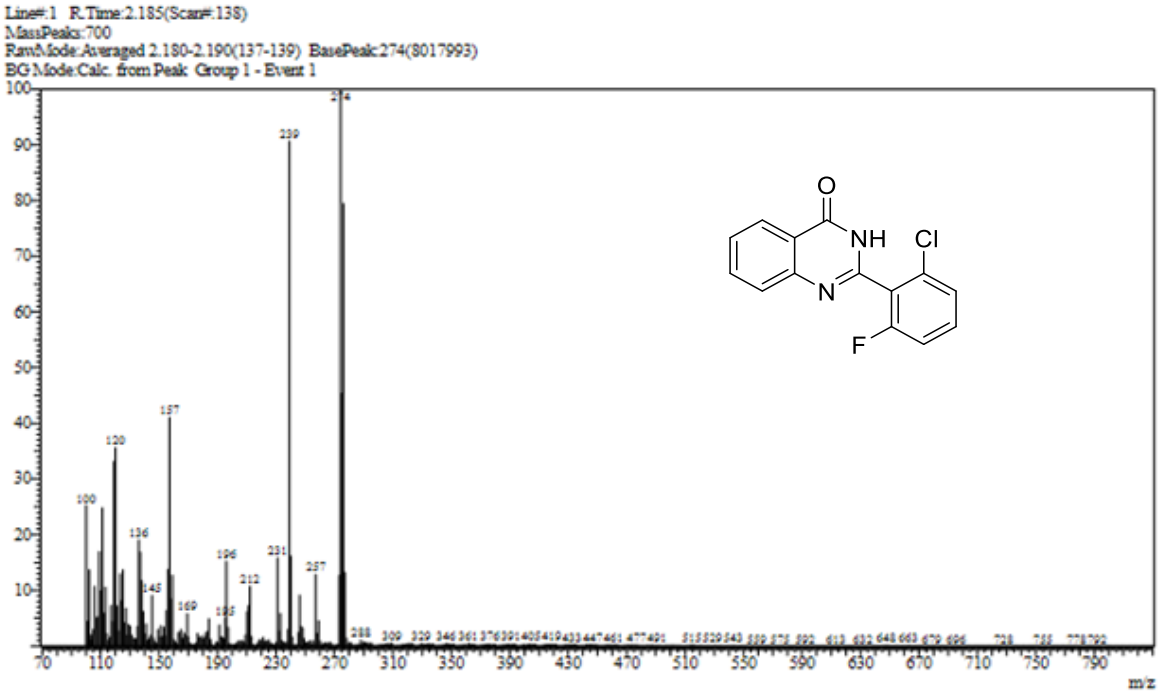

Figure 1: Mass spectrum of compound SVA-1

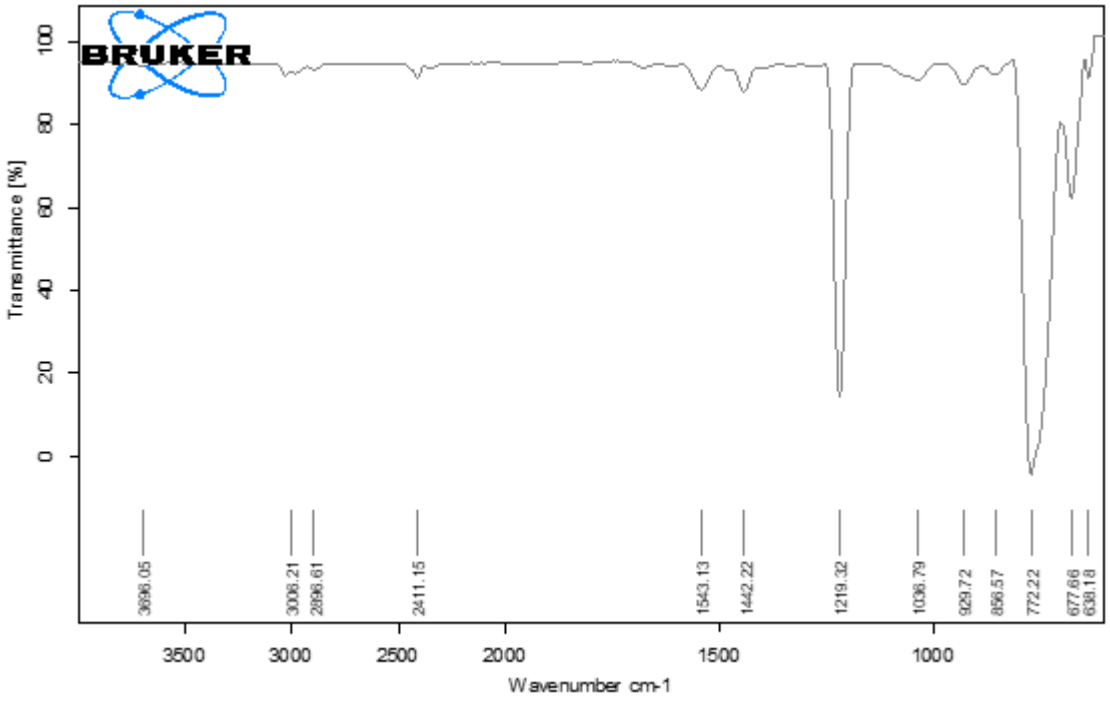

Figure 2: I.R. spectrum of compound SVA-1

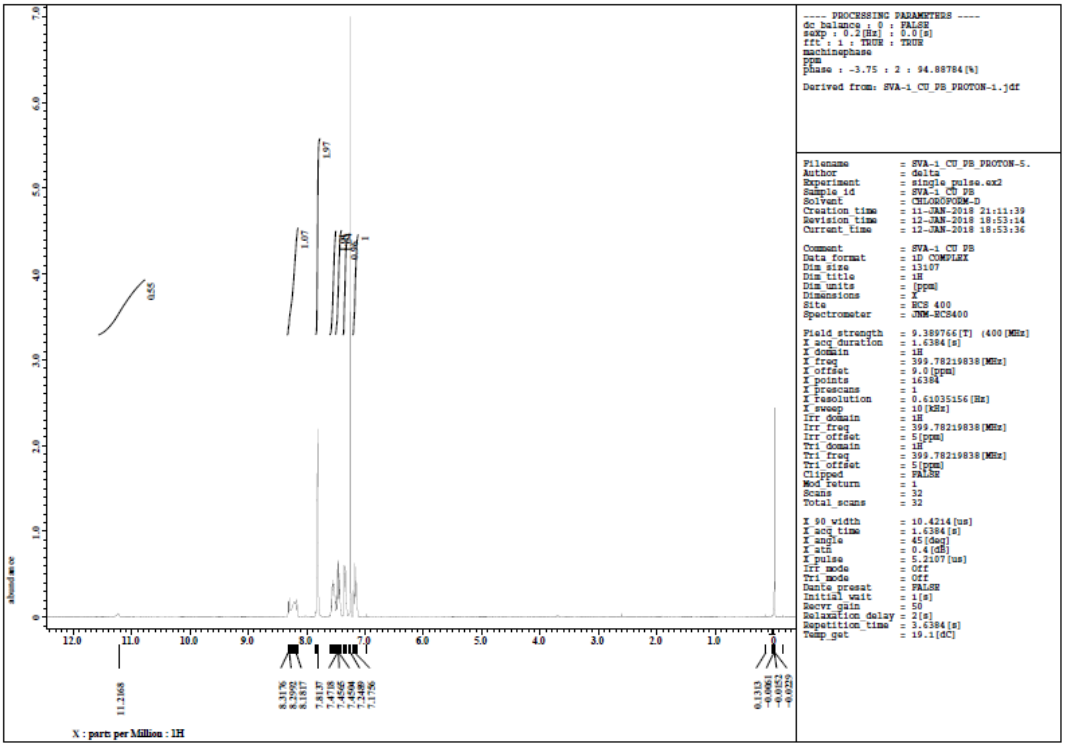

Figure 3: ^{1}H Spectrum of compound SVA-1

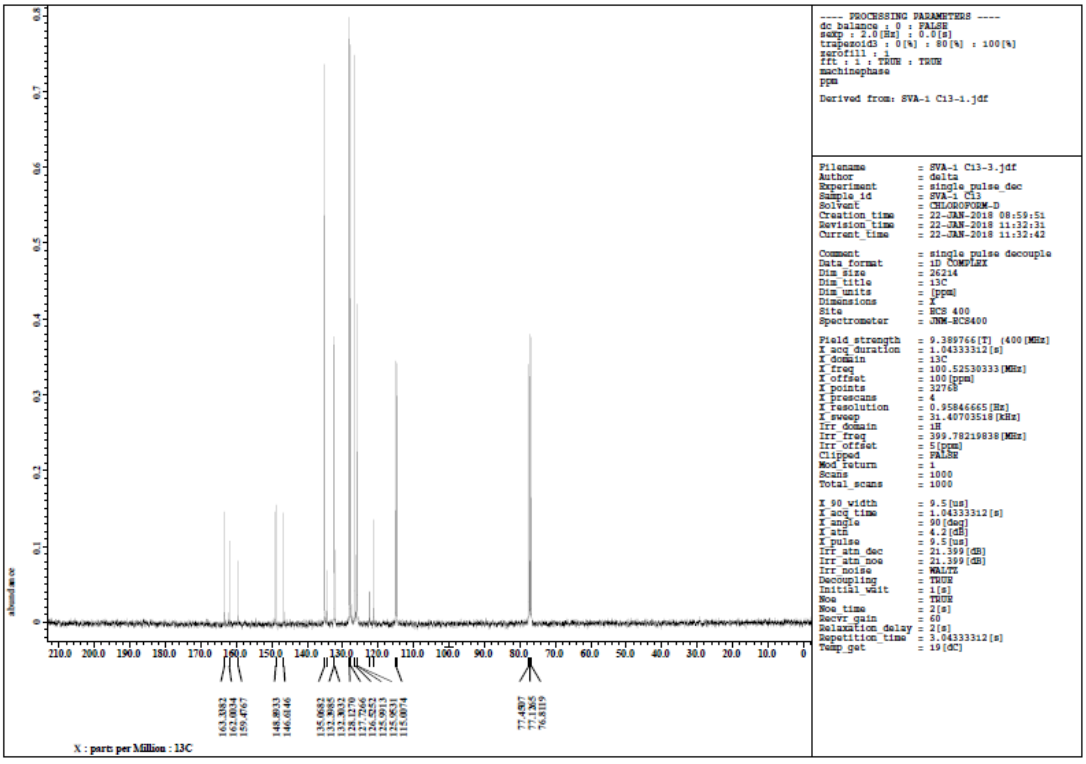

Figure 4: ^{13}C Spectrum of compound SVA-1

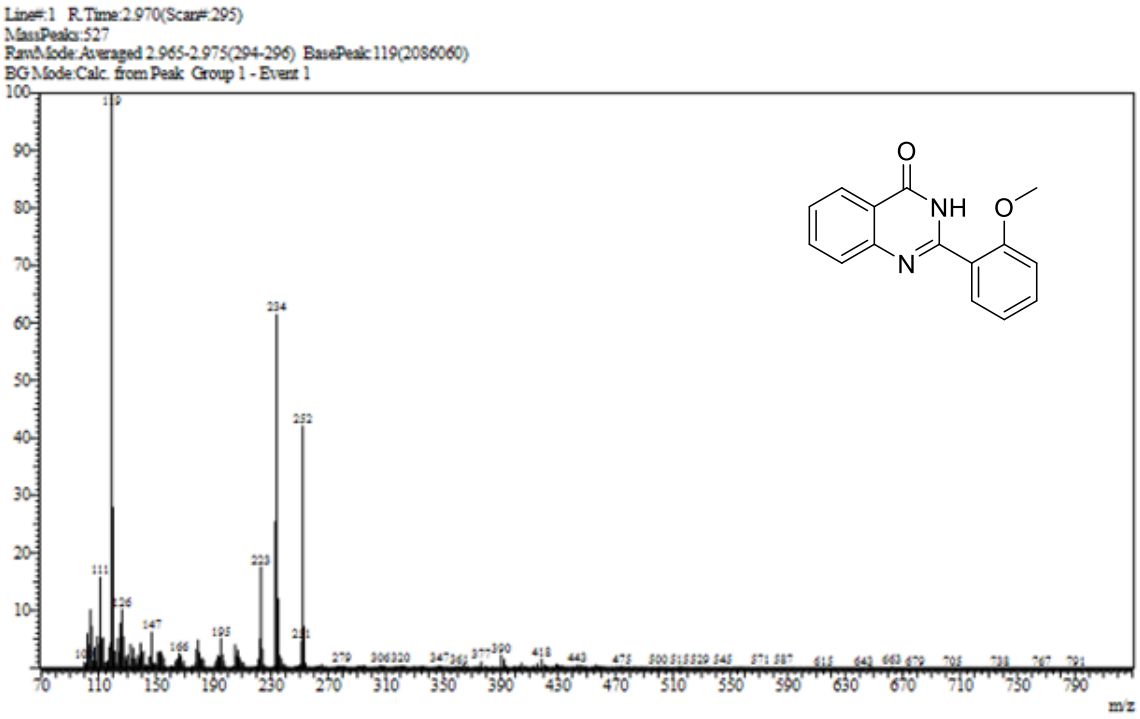

Figure 5: Mass spectrum of compound SVA-2

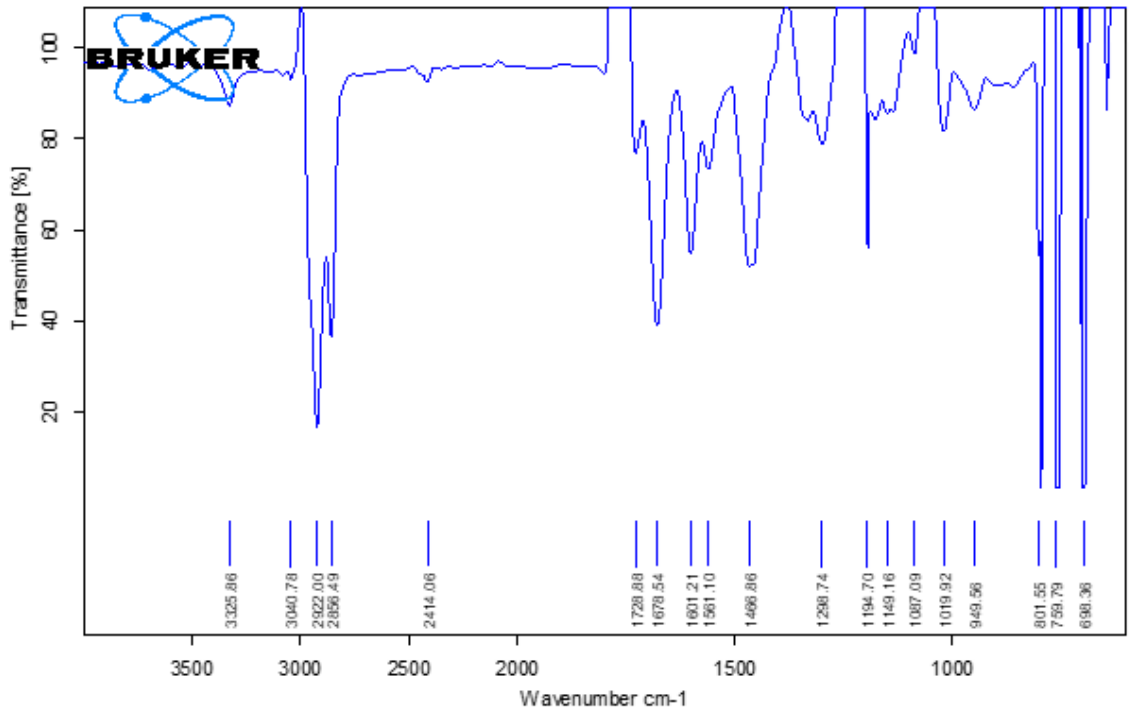

Figure 6: I.R. spectrum of compound SVA-2

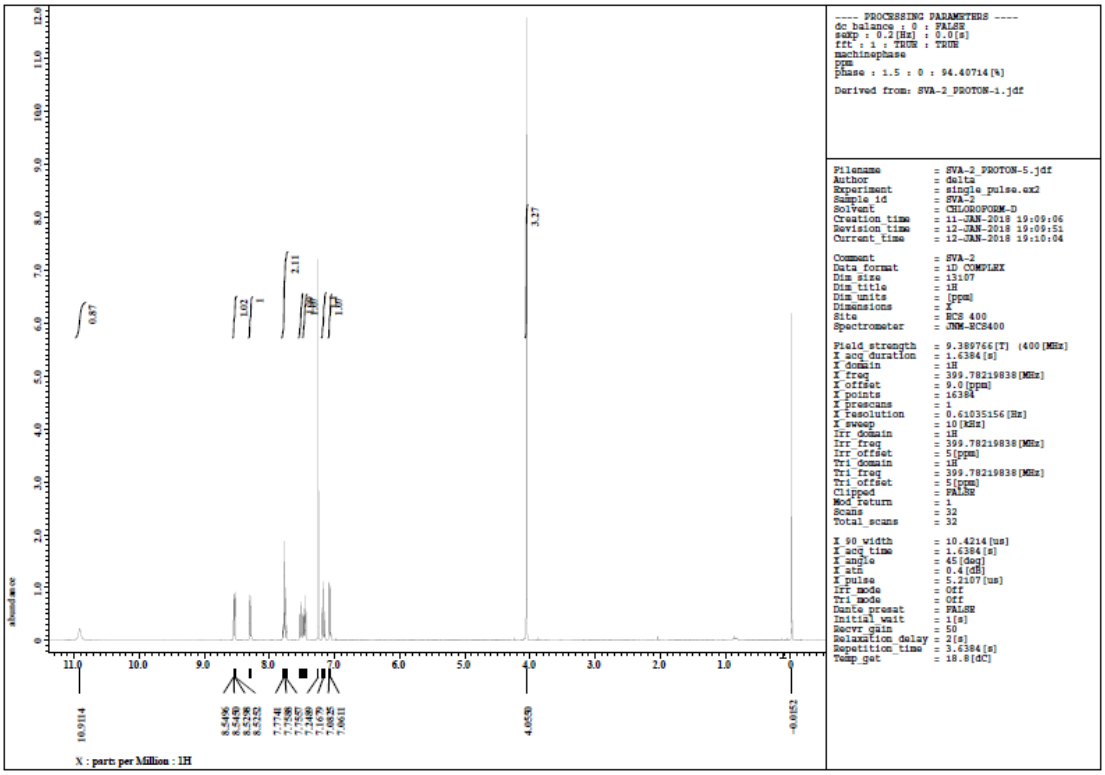

Figure 7: ^{1}H Spectrum of compound SVA-2

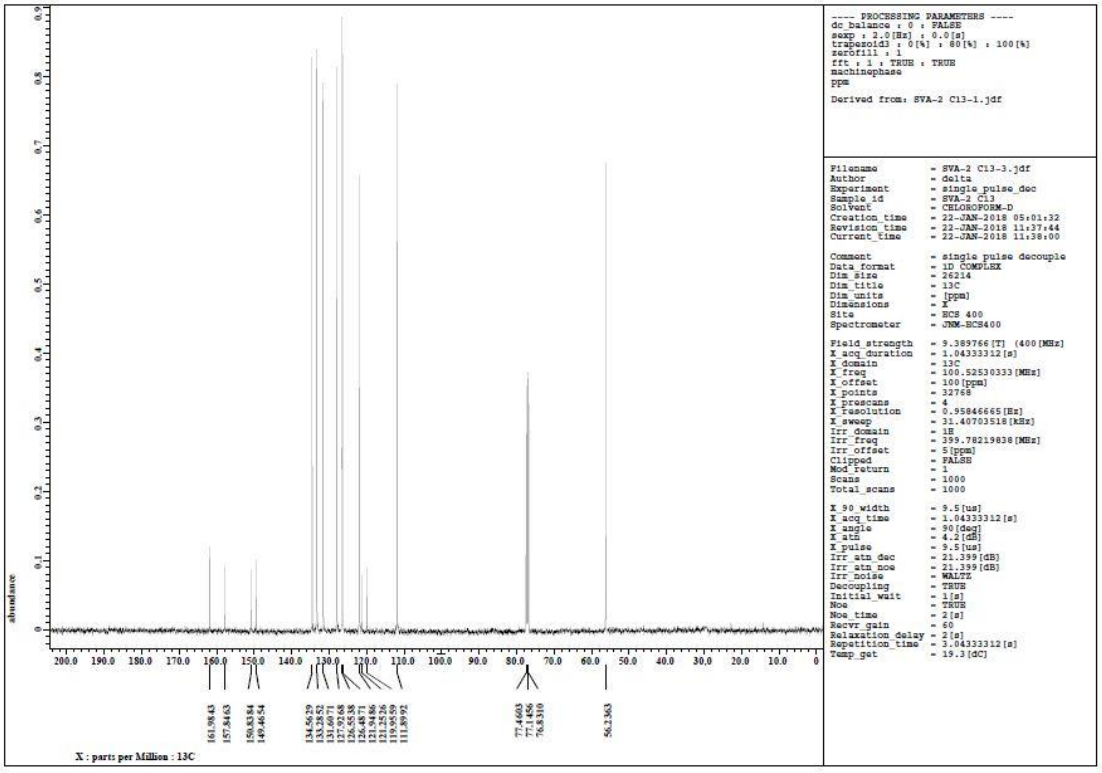

Figure 8: ^{13}C Spectrum of compound SVA-2

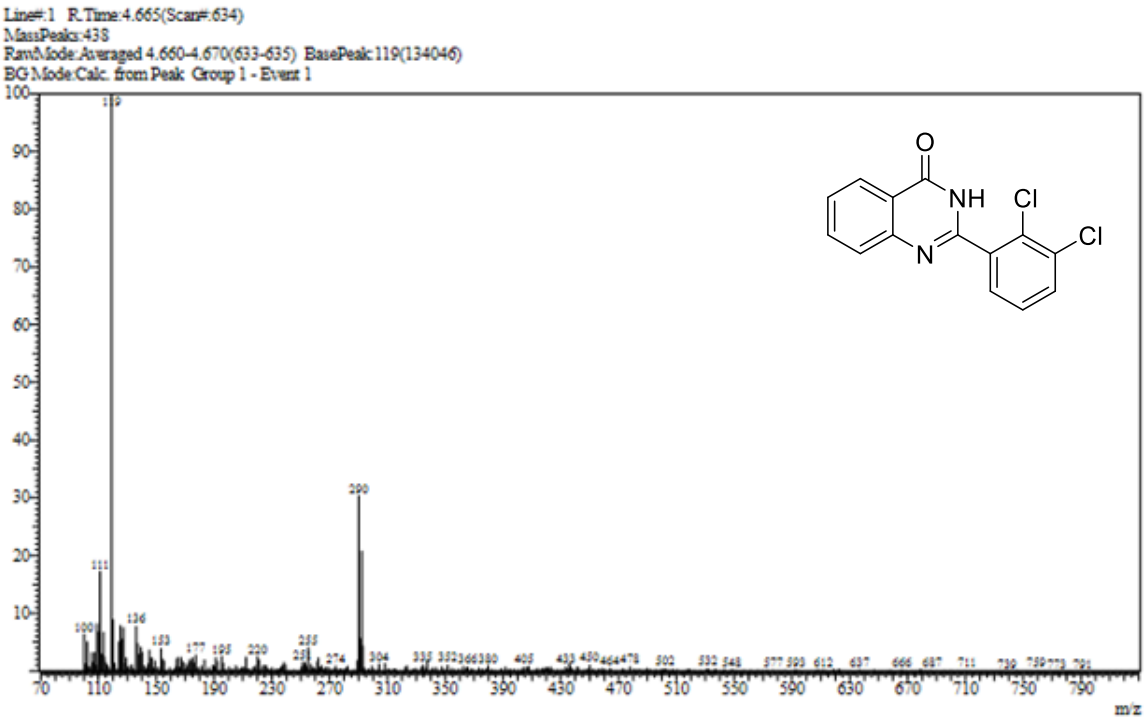

Figure 9: Mass spectrum of compound SVA-3

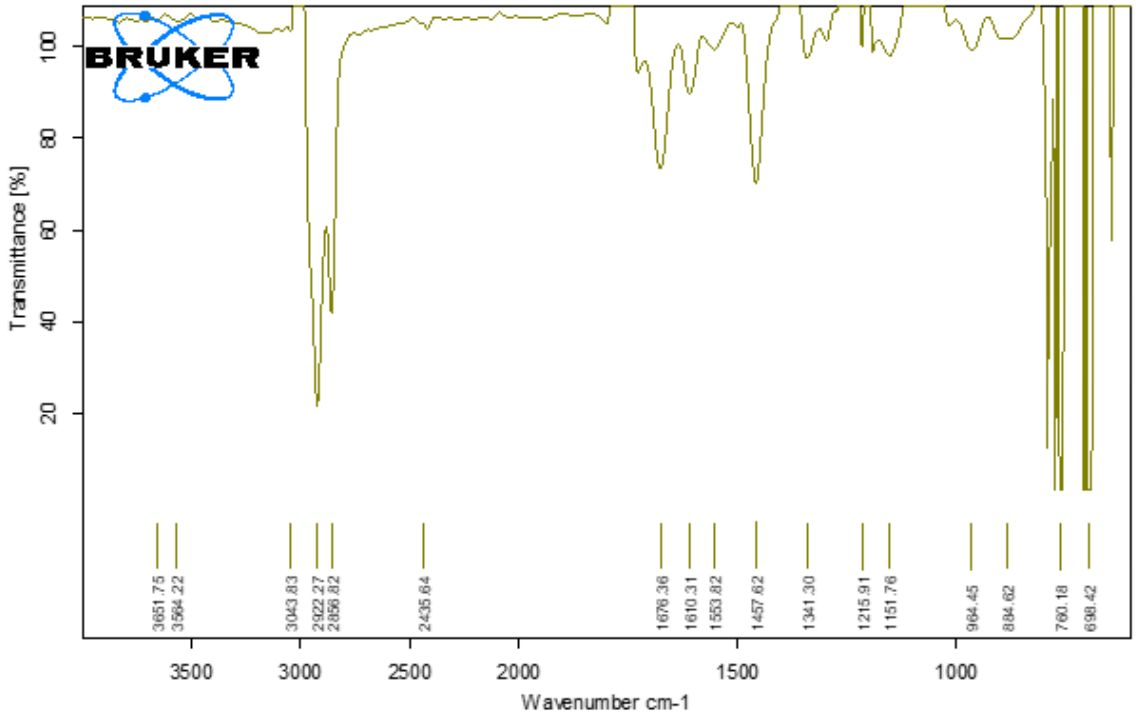

Figure 10: I.R. spectrum of compound SVA-3

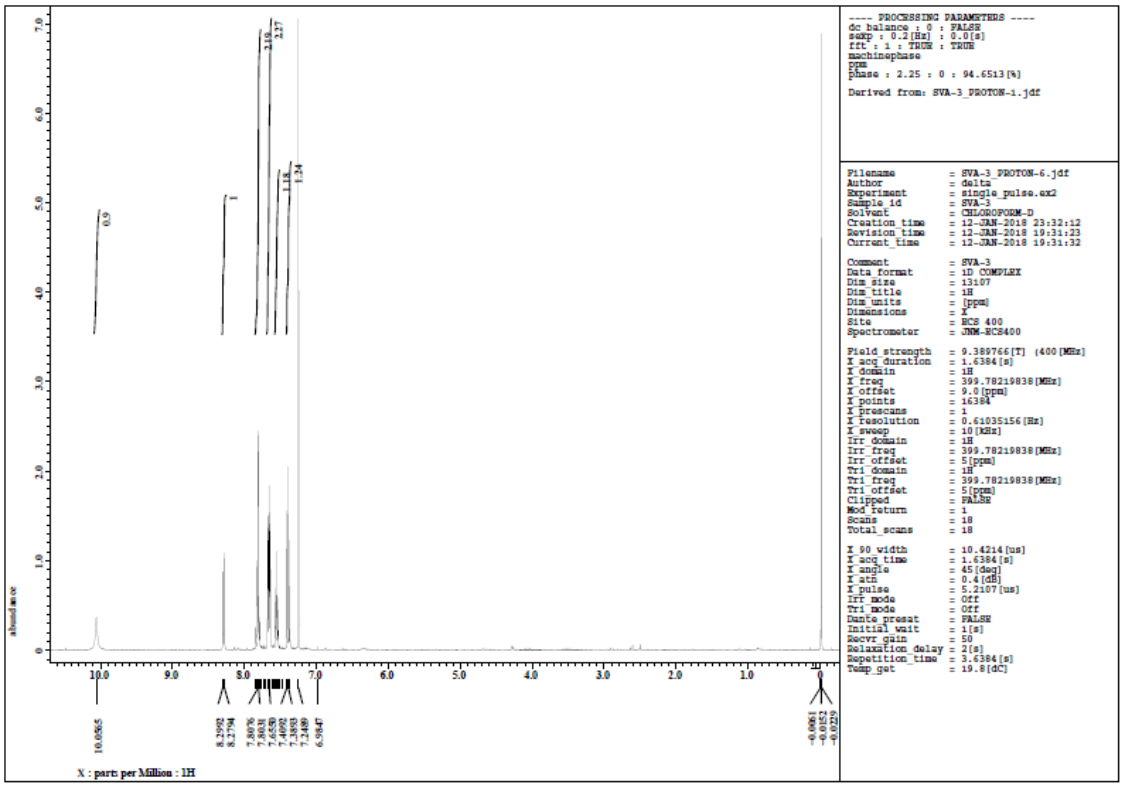

Figure 11: ^{1}H Spectrum of compound SVA-3

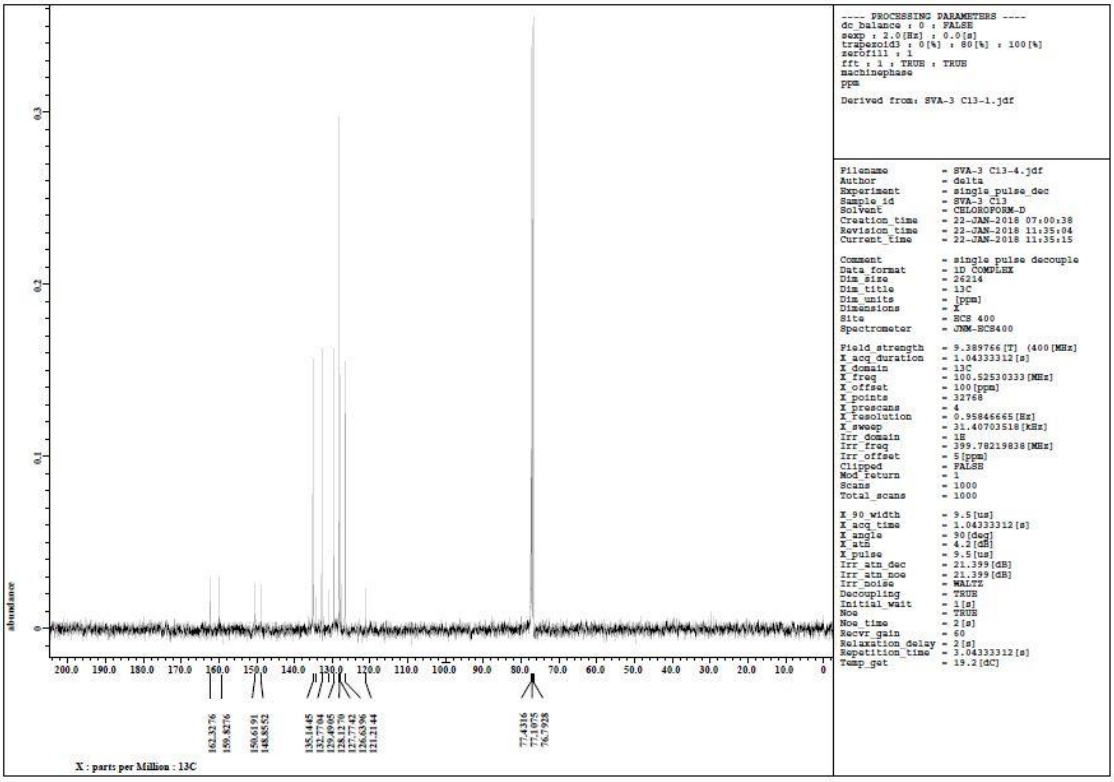

Figure 12: ^{13}C Spectrum of compound SVA-3

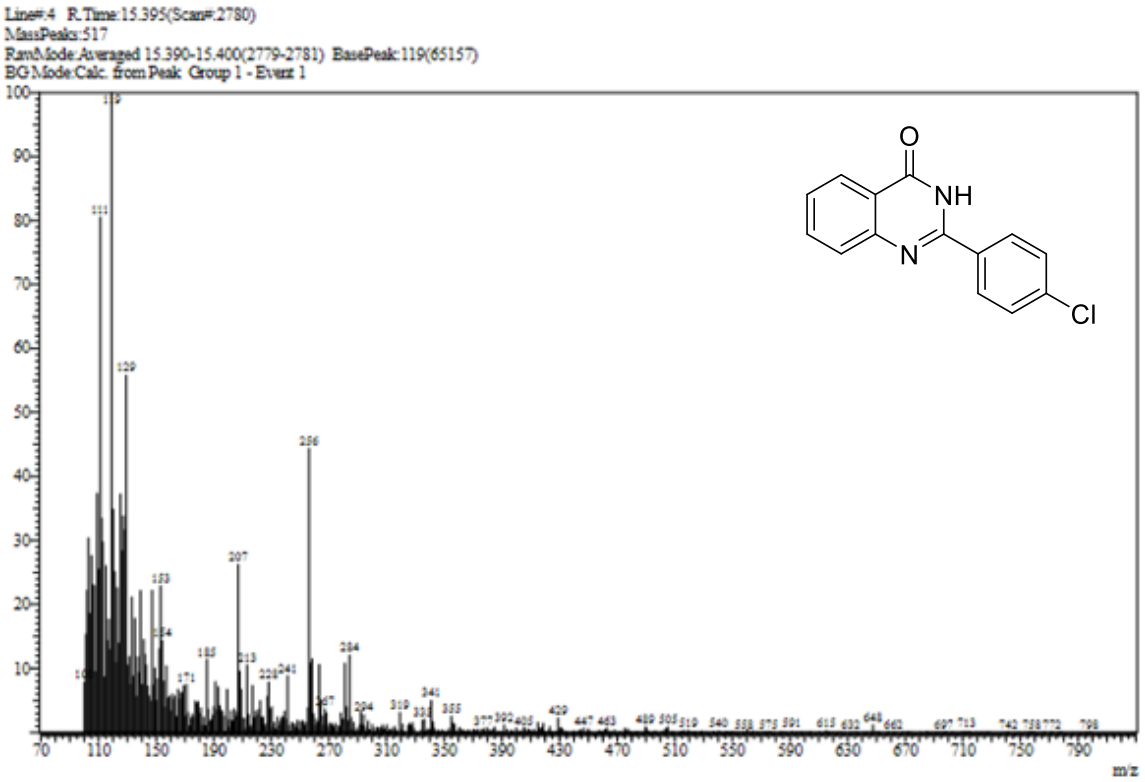

Figure 13: Mass spectrum of compound SVA-4

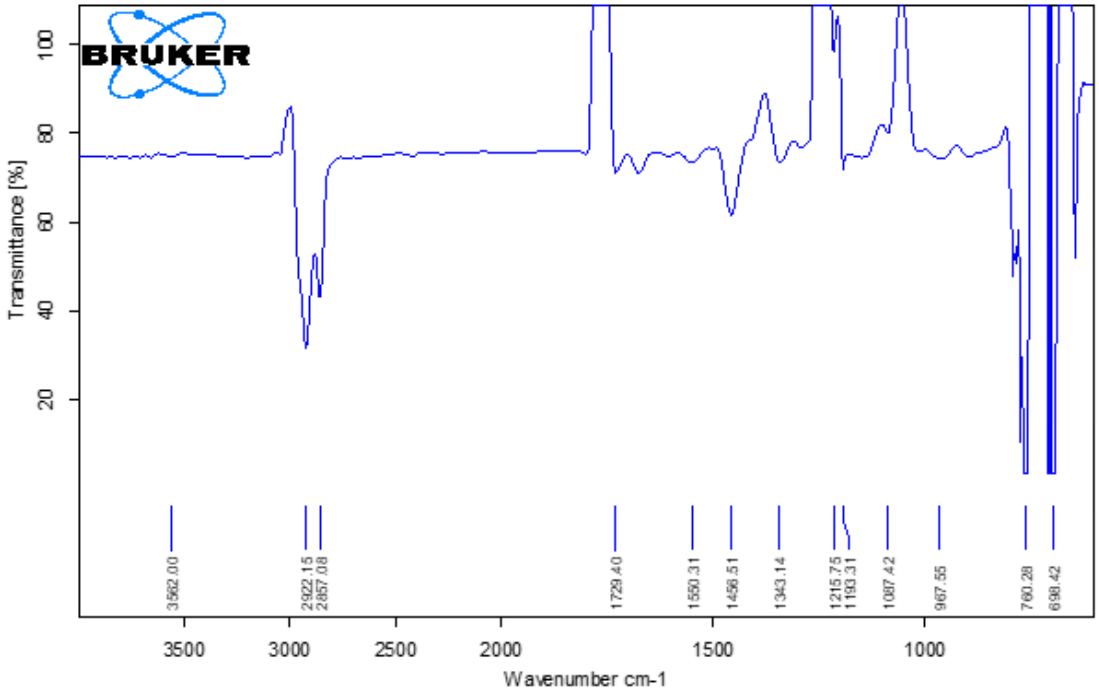

Figure 14: I.R. spectrum of compound SVA-4

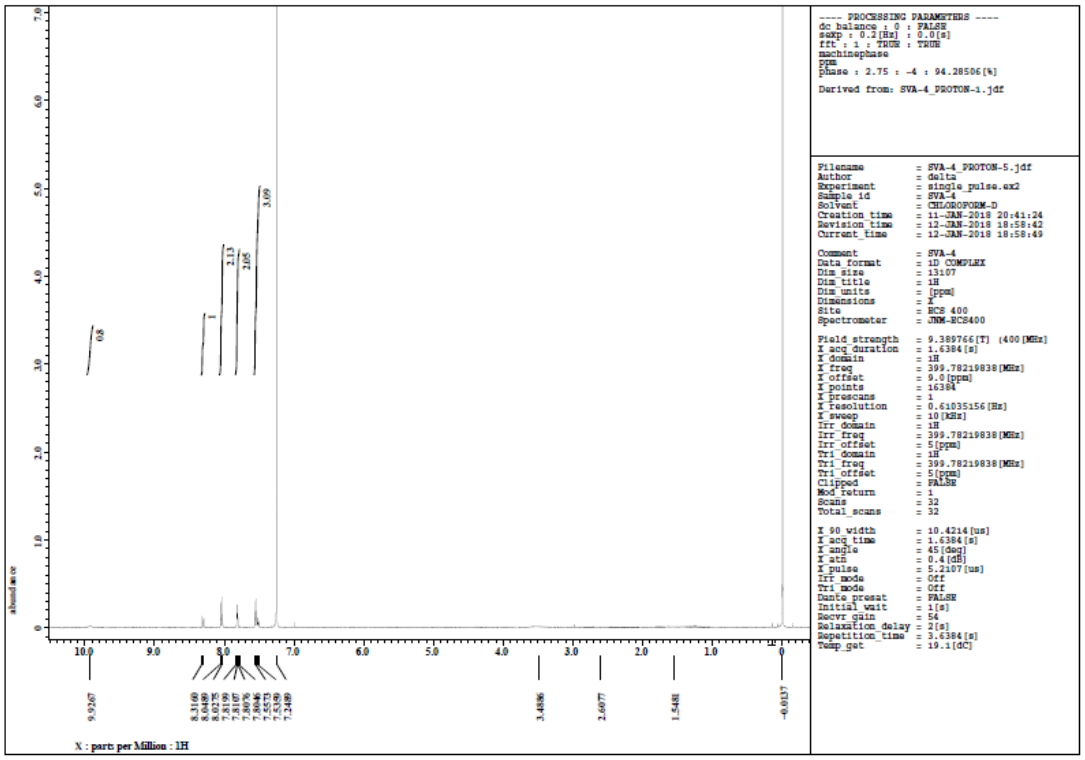

Figure 15: ^{1}H Spectrum of compound SVA-4

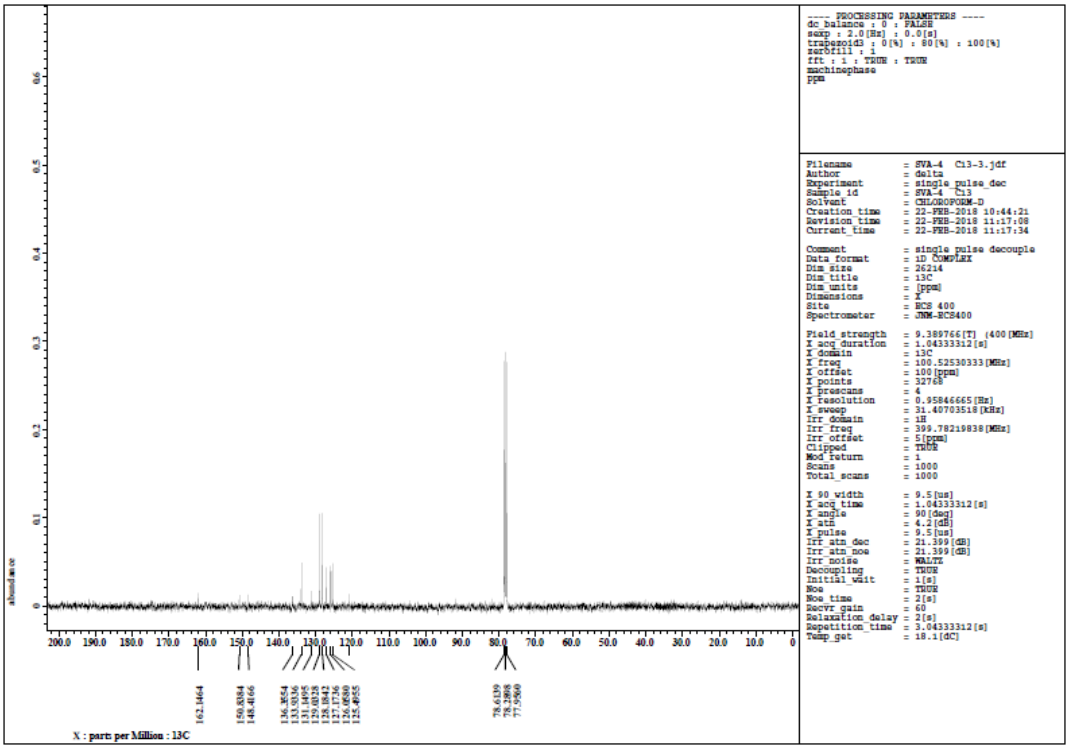

Figure 16: ^{13}C Spectrum of compound SVA-4

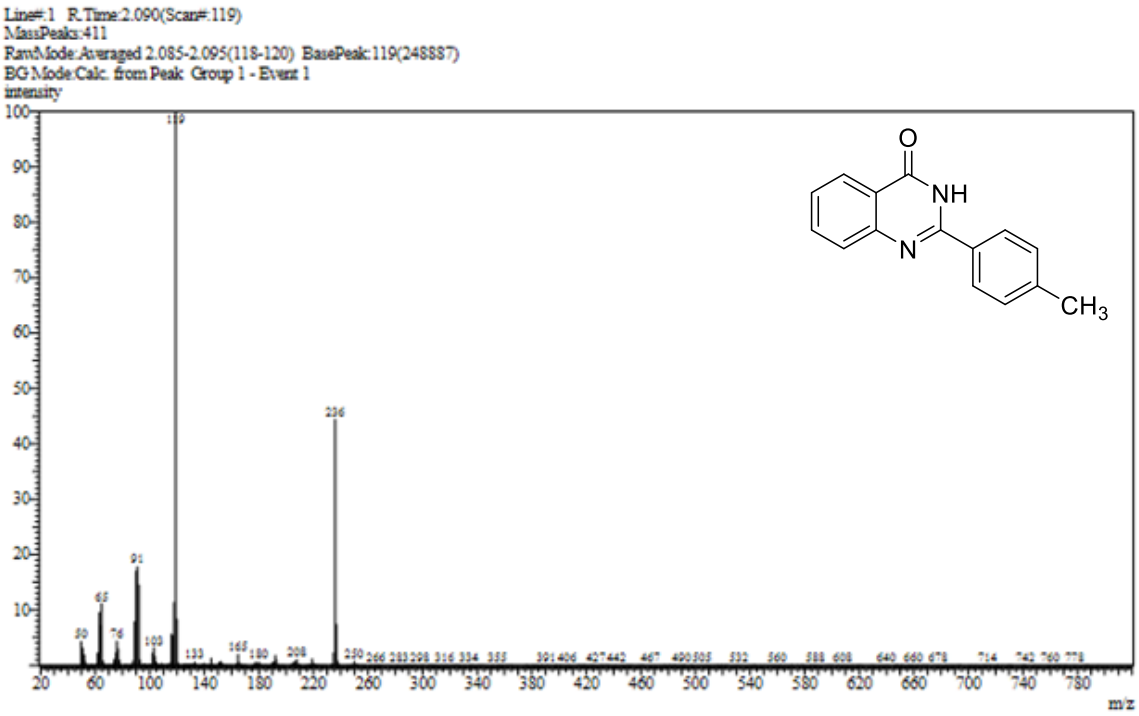

Figure 17: Mass spectrum of compound SVA-5

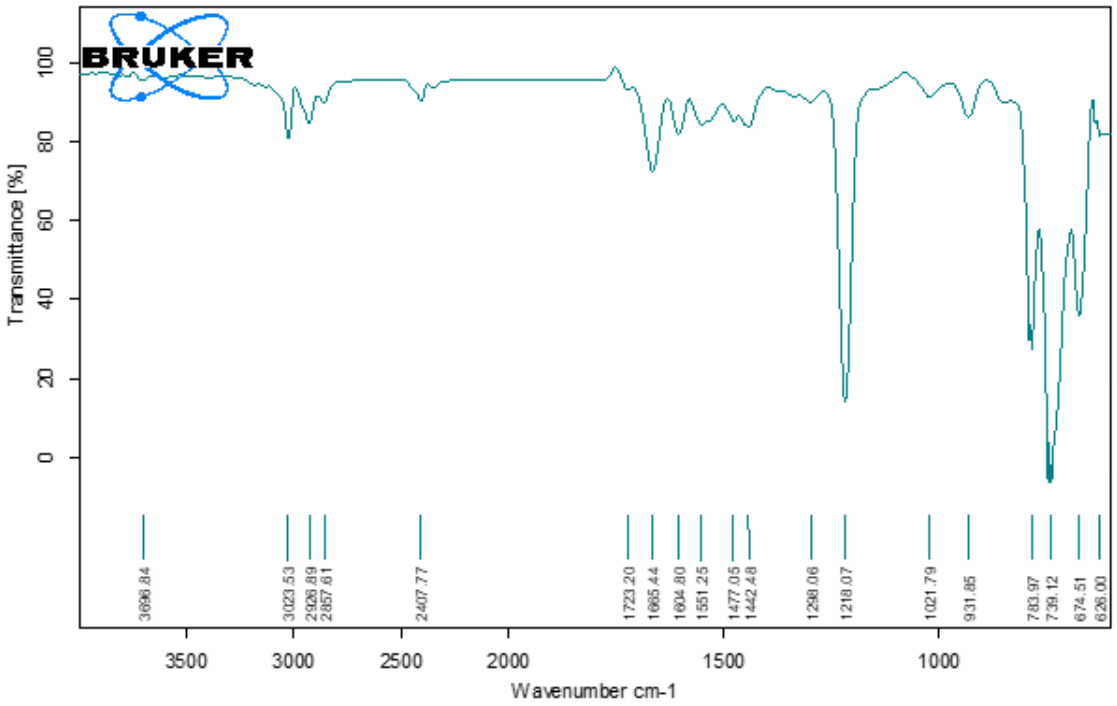

Figure 18: I.R. spectrum of compound SVA-5

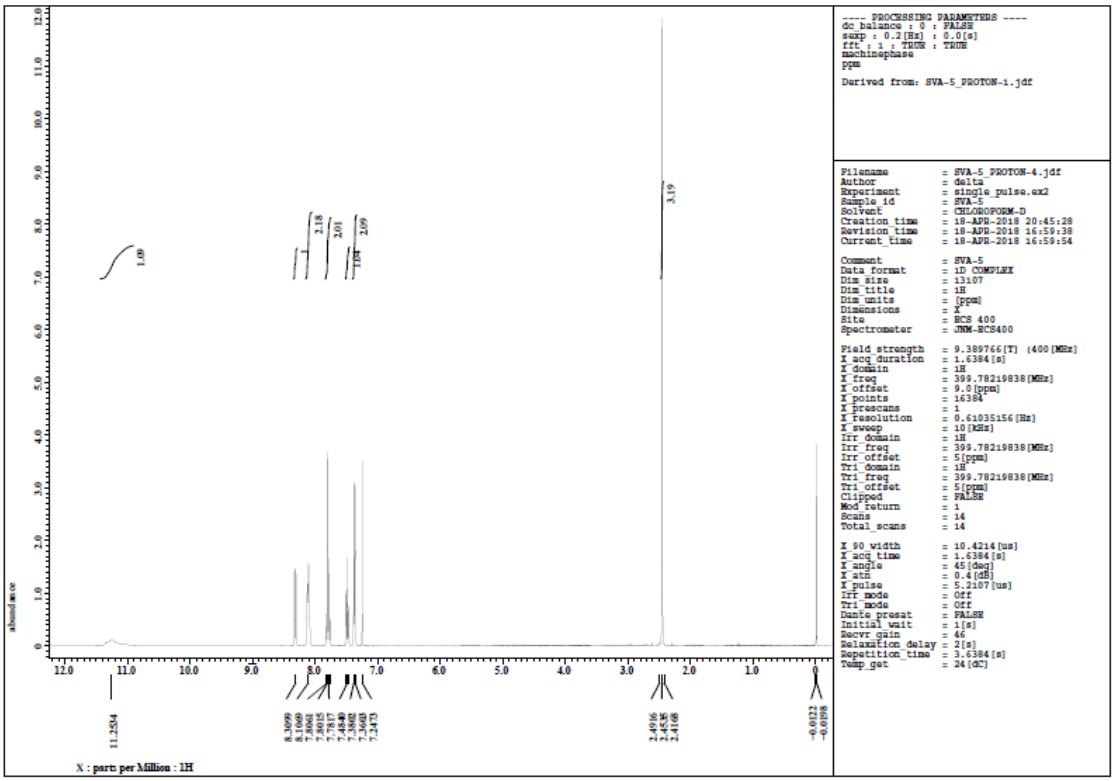

Figure 19: ^{1}H Spectrum of compound SVA-5

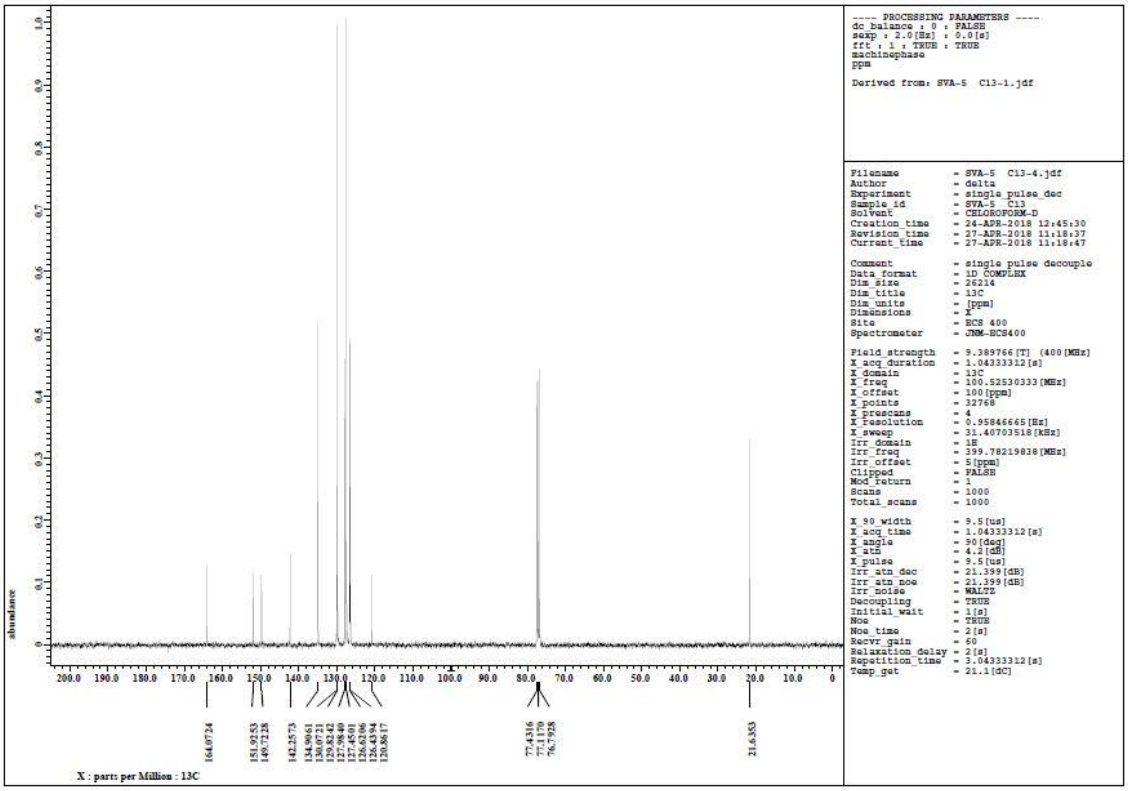

Figure 20: ^{13}C Spectrum of compound SVA-5

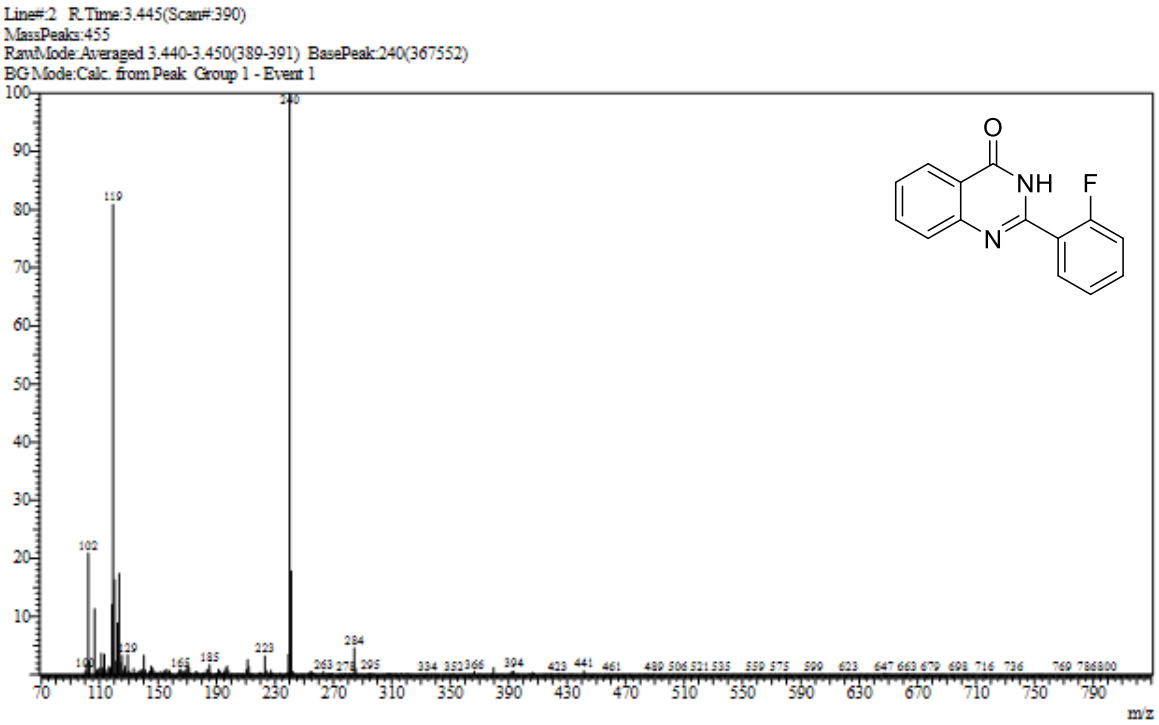

Figure 21: Mass spectrum of compound SVA-6

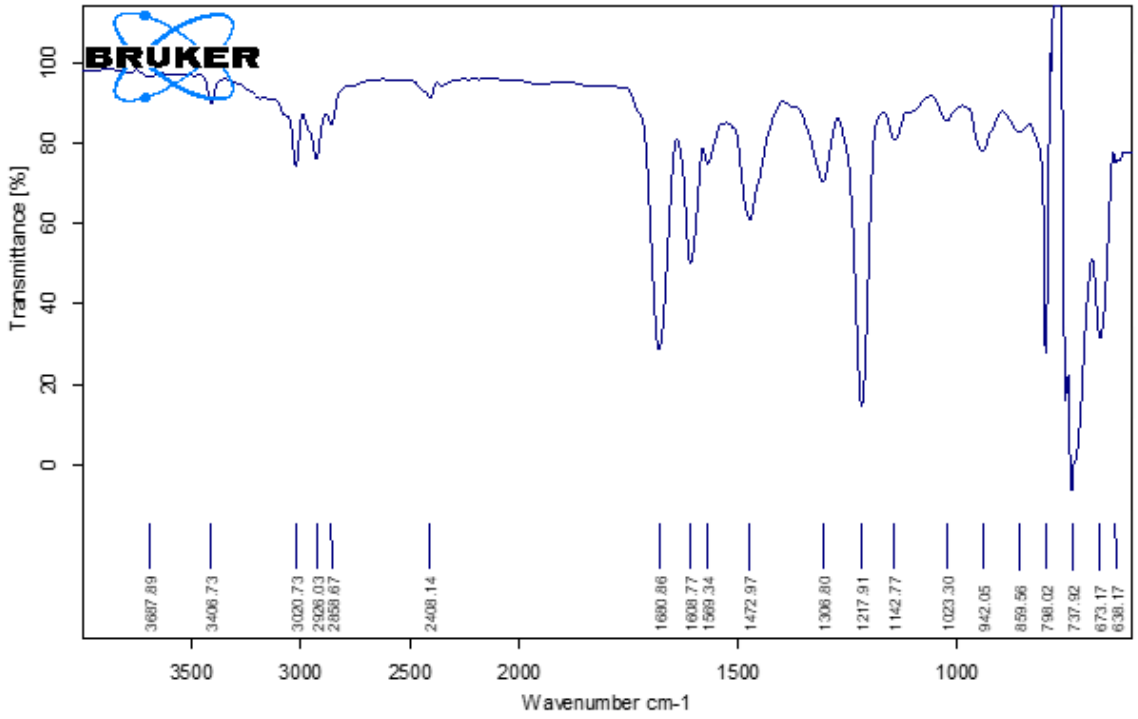

Figure 22: I.R. spectrum of compound SVA-6

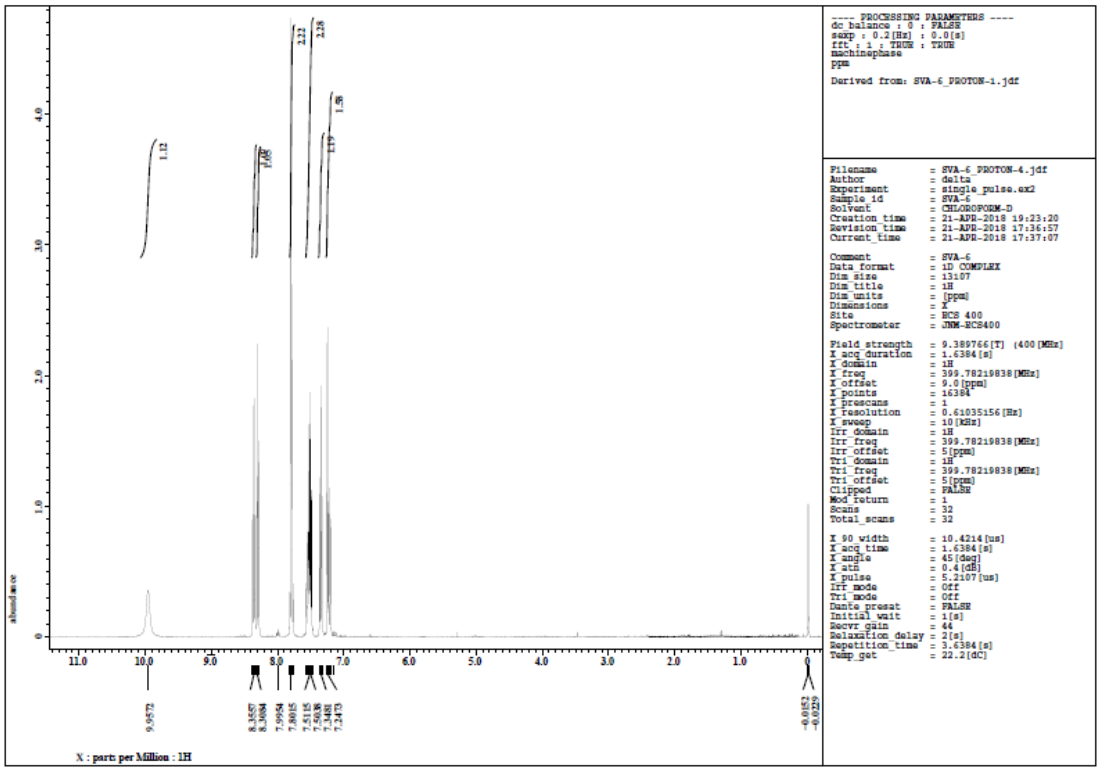

Figure 23: ^{1}H Spectrum of compound SVA-6

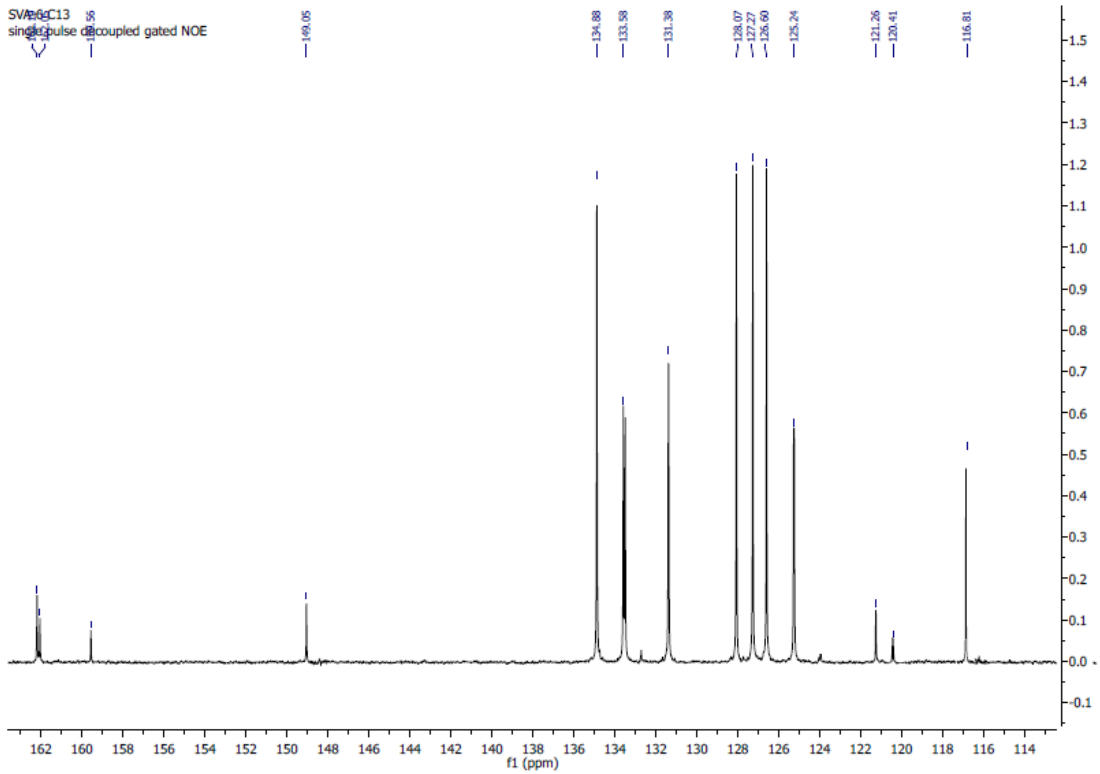

Figure 24: ^{13}C Spectrum of compound SVA-6

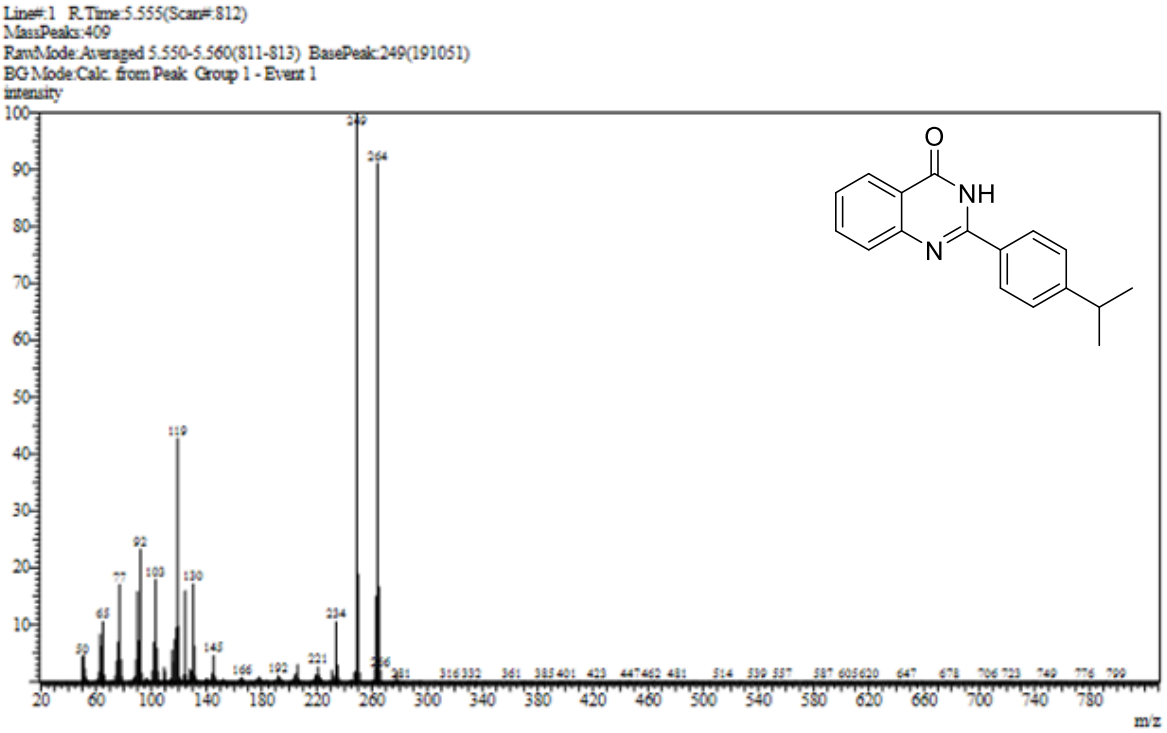

Figure 25: Mass spectrum of compound SVA-7

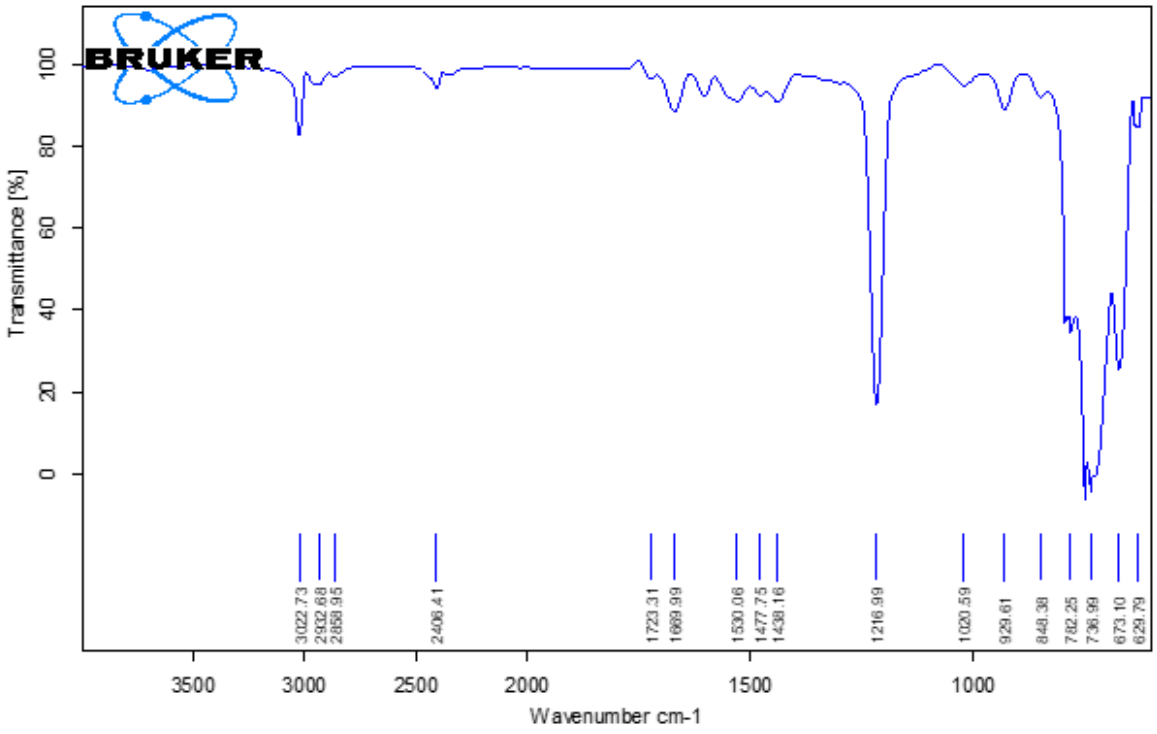

Figure 26: I.R. spectrum of compound SVA-7

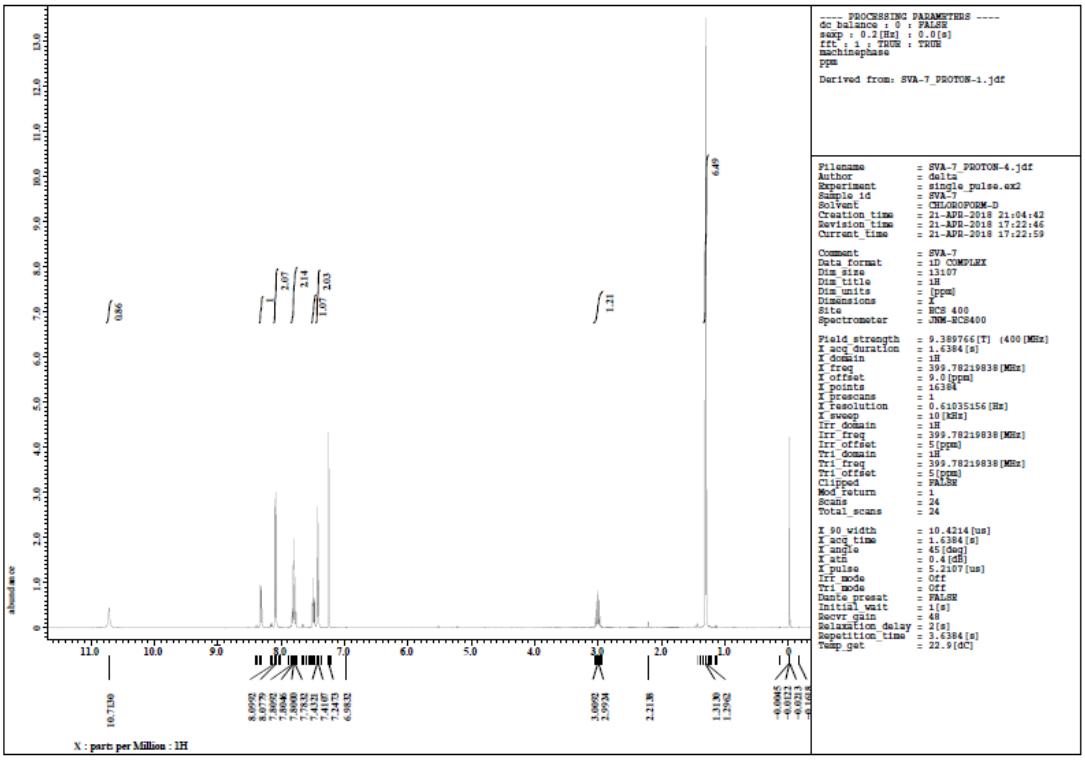

Figure 27: ^{1}H Spectrum of compound SVA-7

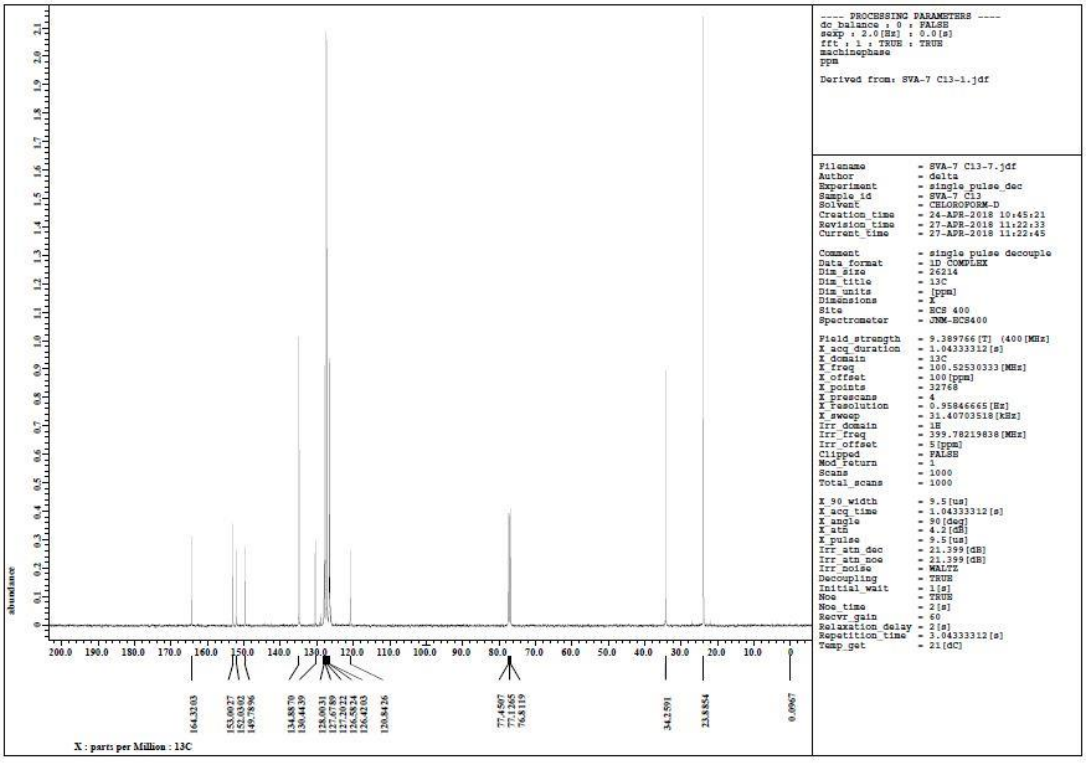

Figure 28: ^{13}C Spectrum of compound SVA-7

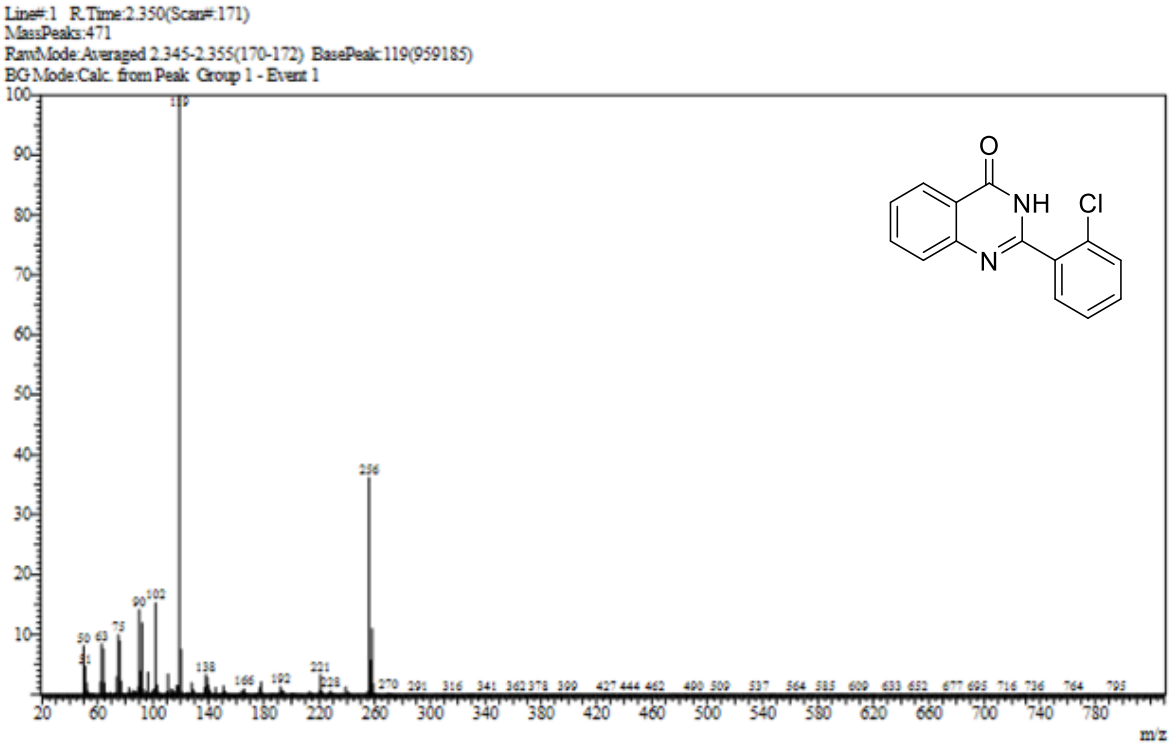

Figure 29: Mass spectrum of compound SVA-8

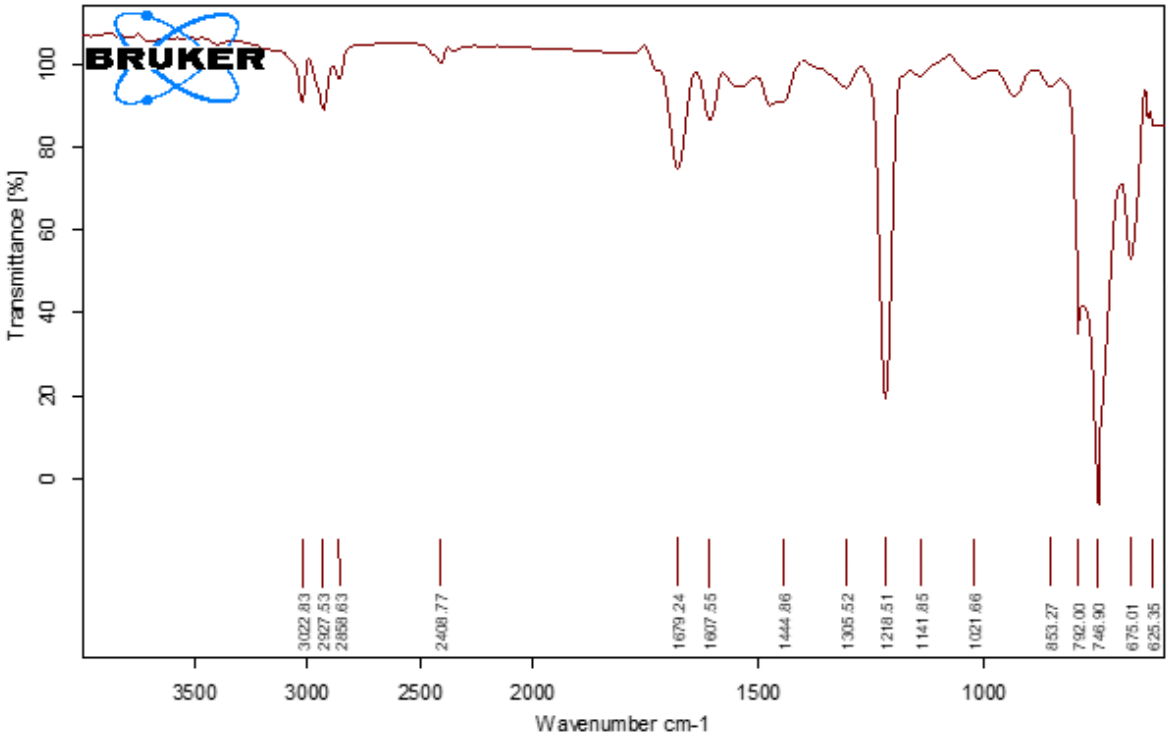

Figure 30: I.R. spectrum of compound SVA-8

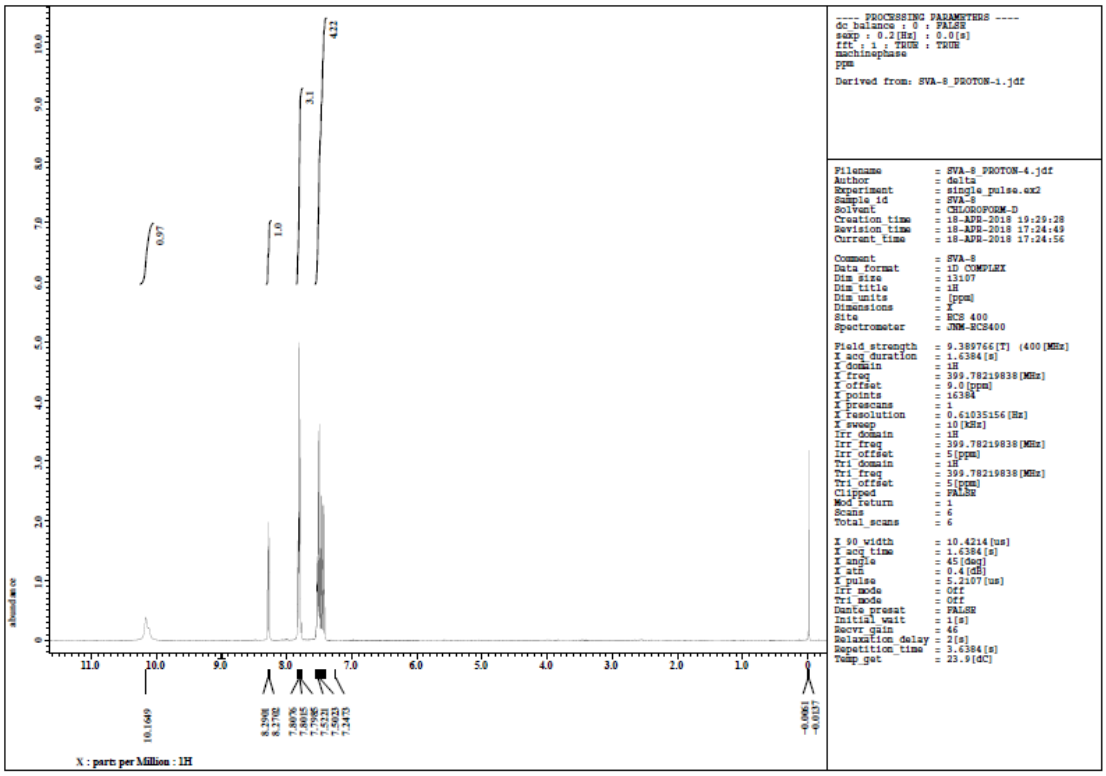

Figure 31: ^{1}H Spectrum of compound SVA-8

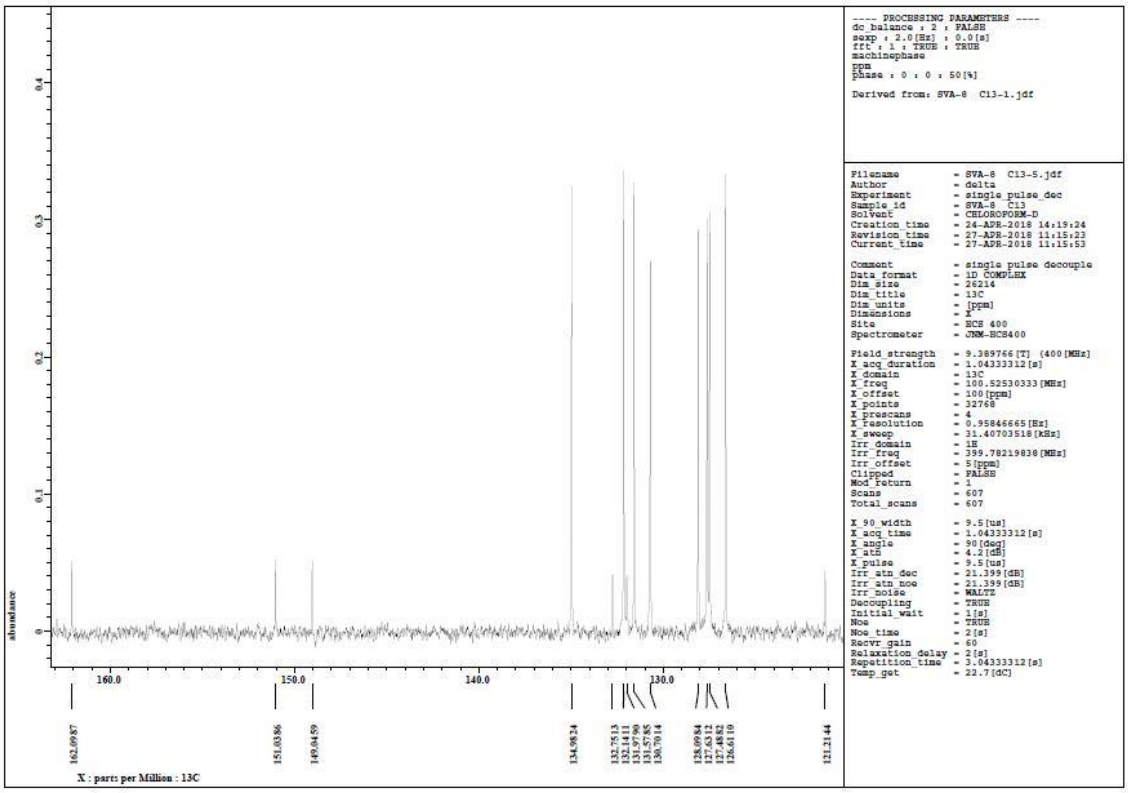

Figure 32: ^{13}C Spectrum of compound SVA-8

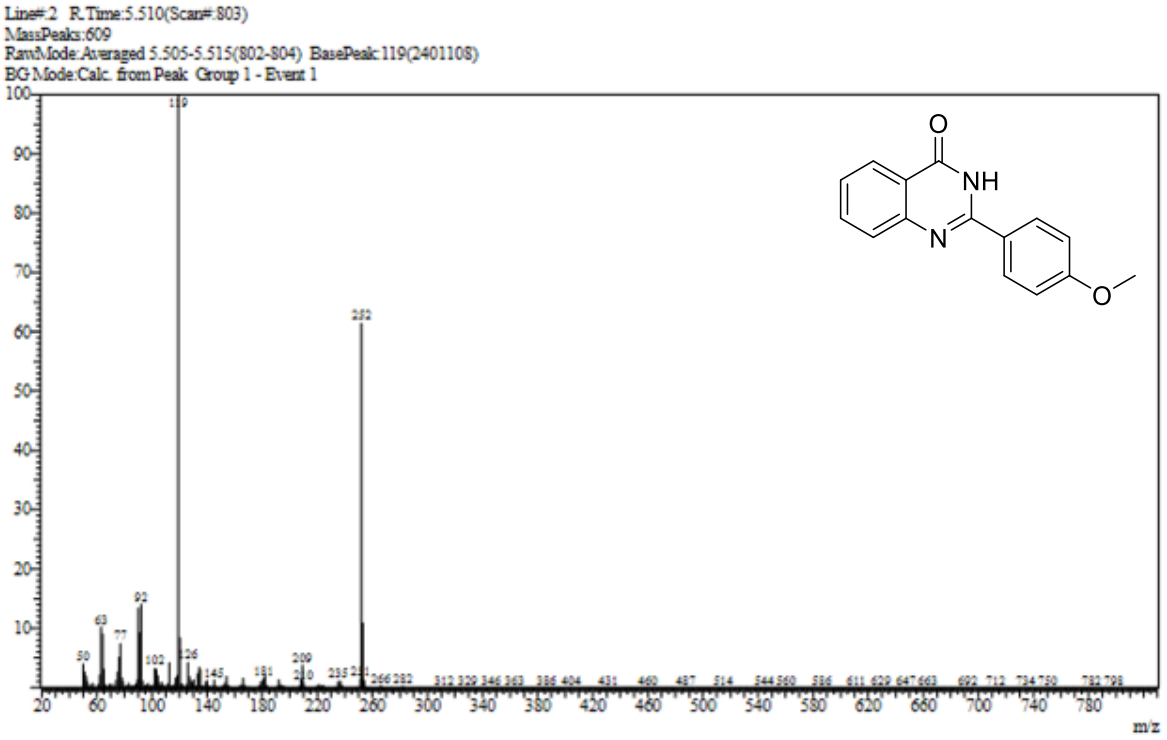

Figure 33: Mass spectrum of compound SVA-9

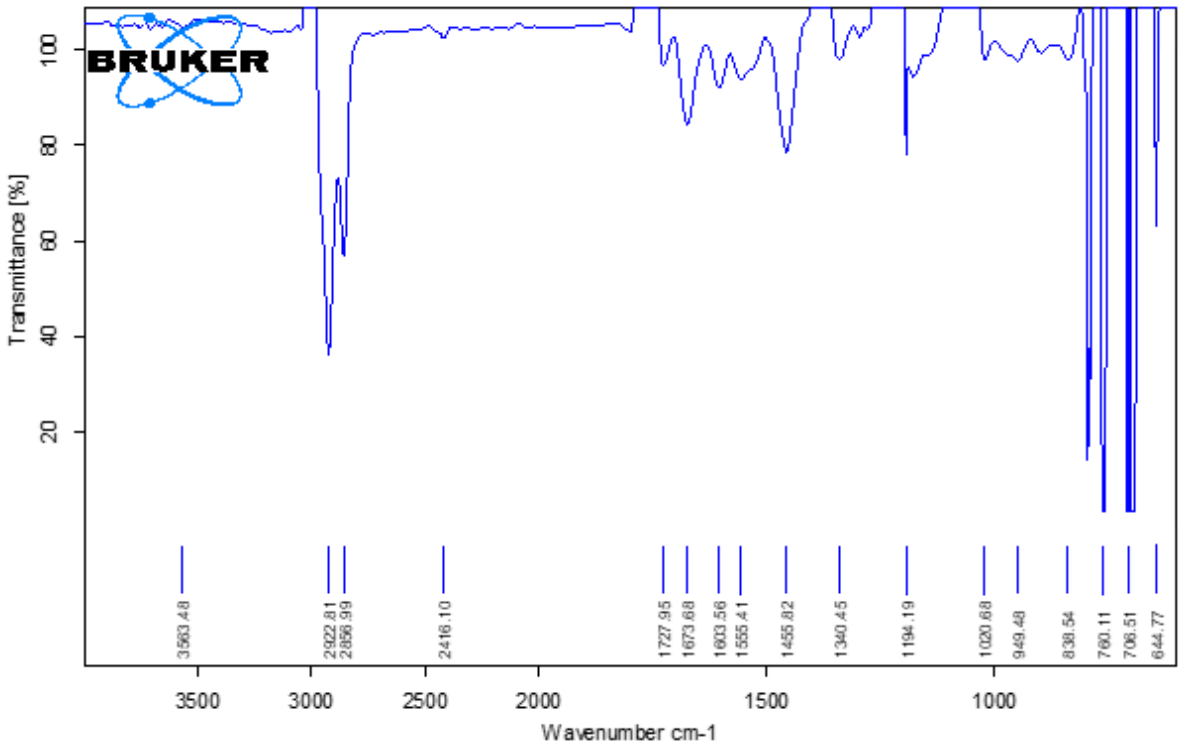

Figure 34: I.R. spectrum of compound SVA-9

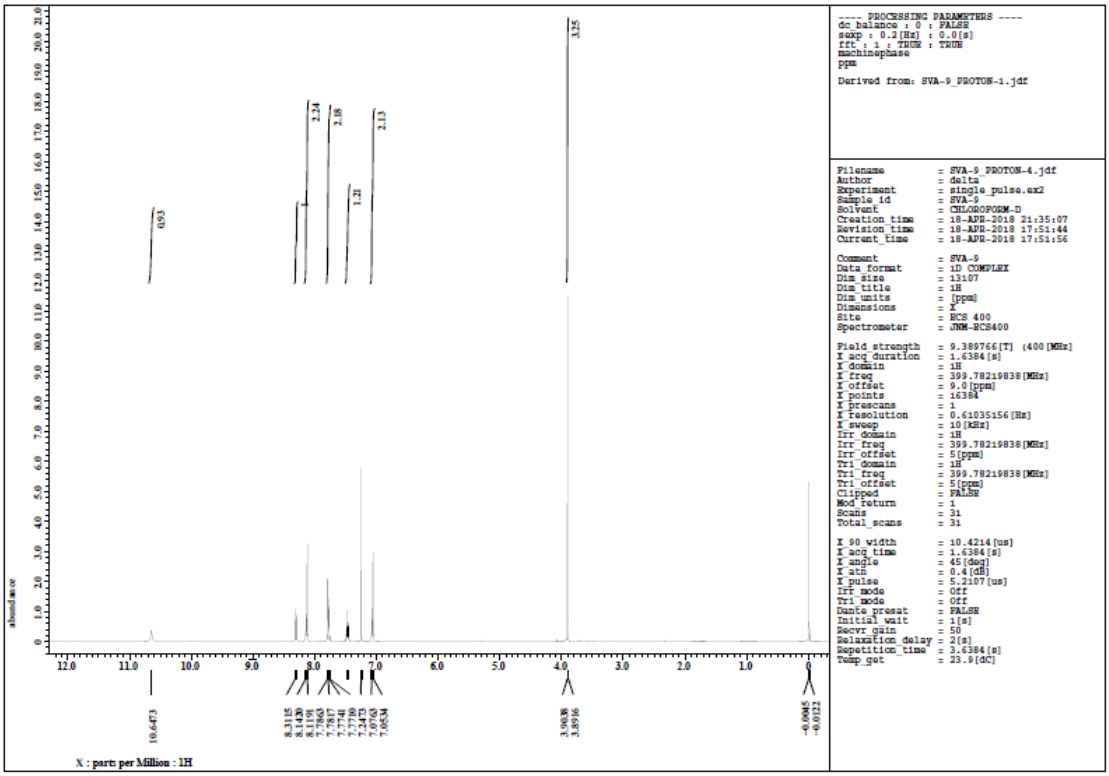

Figure 35: ^{1}H Spectrum of compound SVA-9

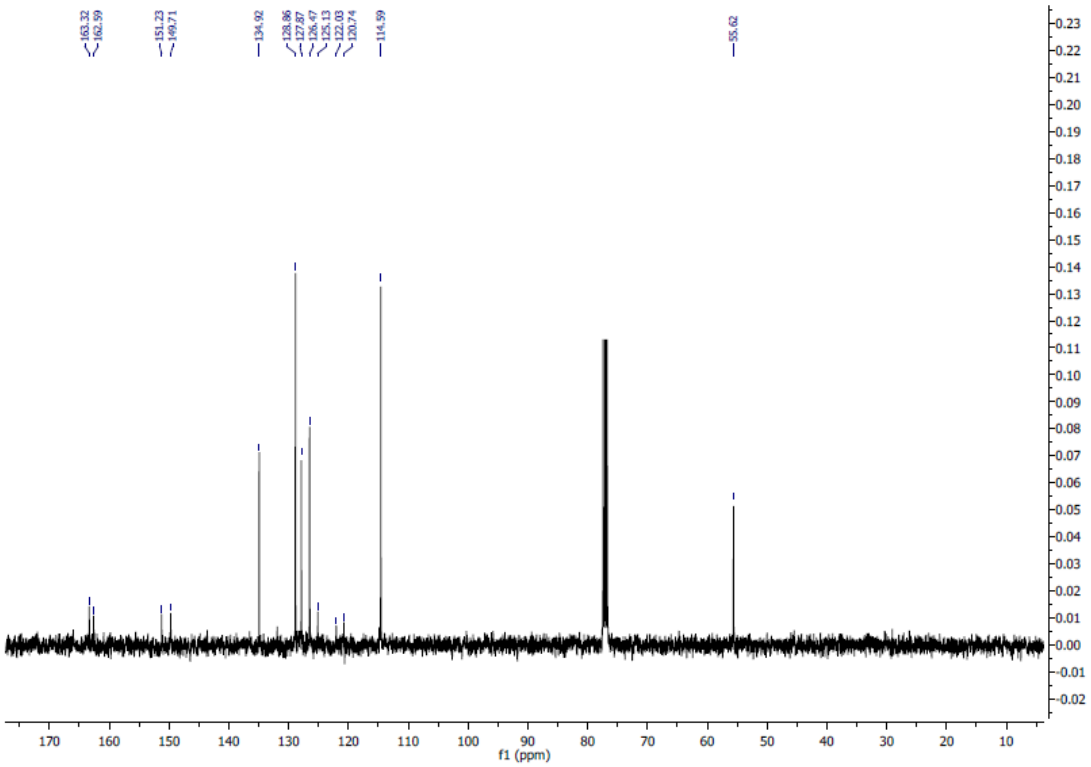

Figure 36: ^{13}C Spectrum of compound SVA-9

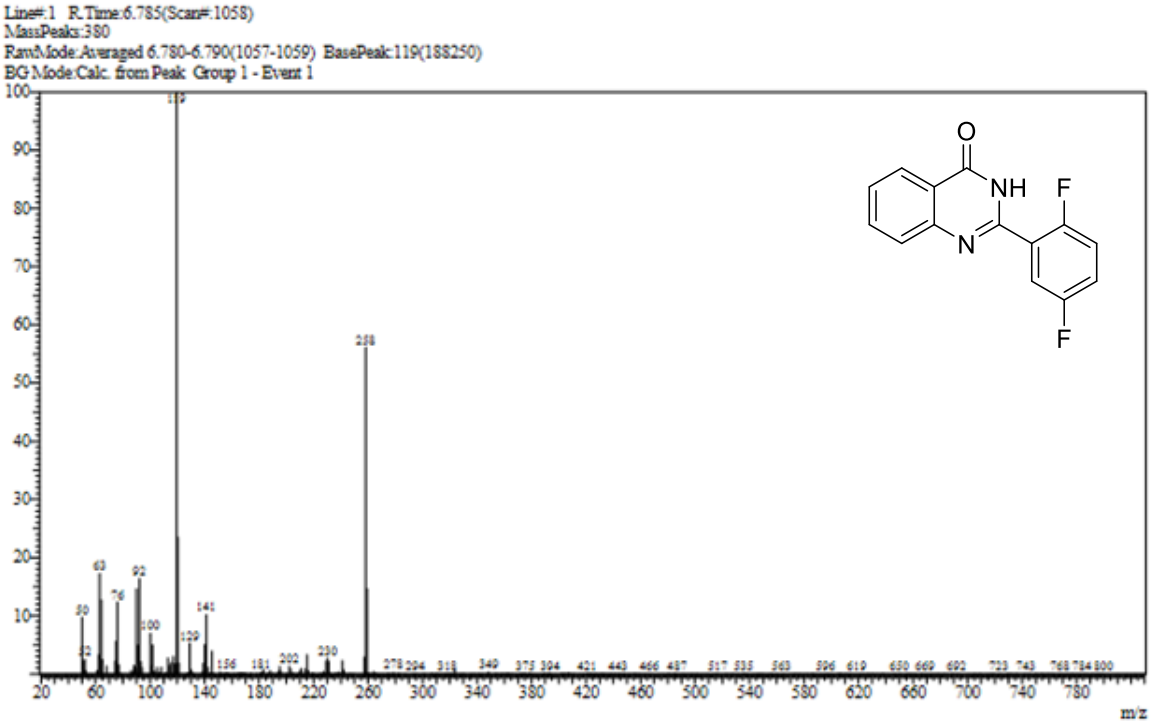

Figure 37: Mass spectrum of compound SVA-10

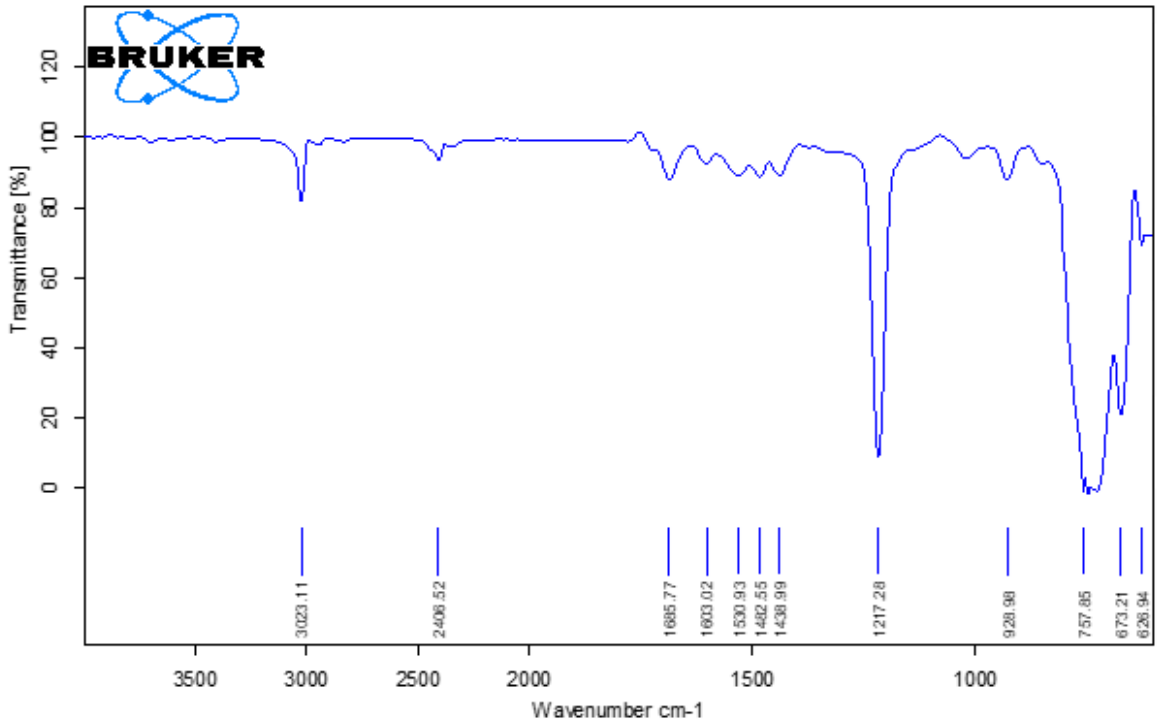

Figure 38: I.R. spectrum of compound SVA-10

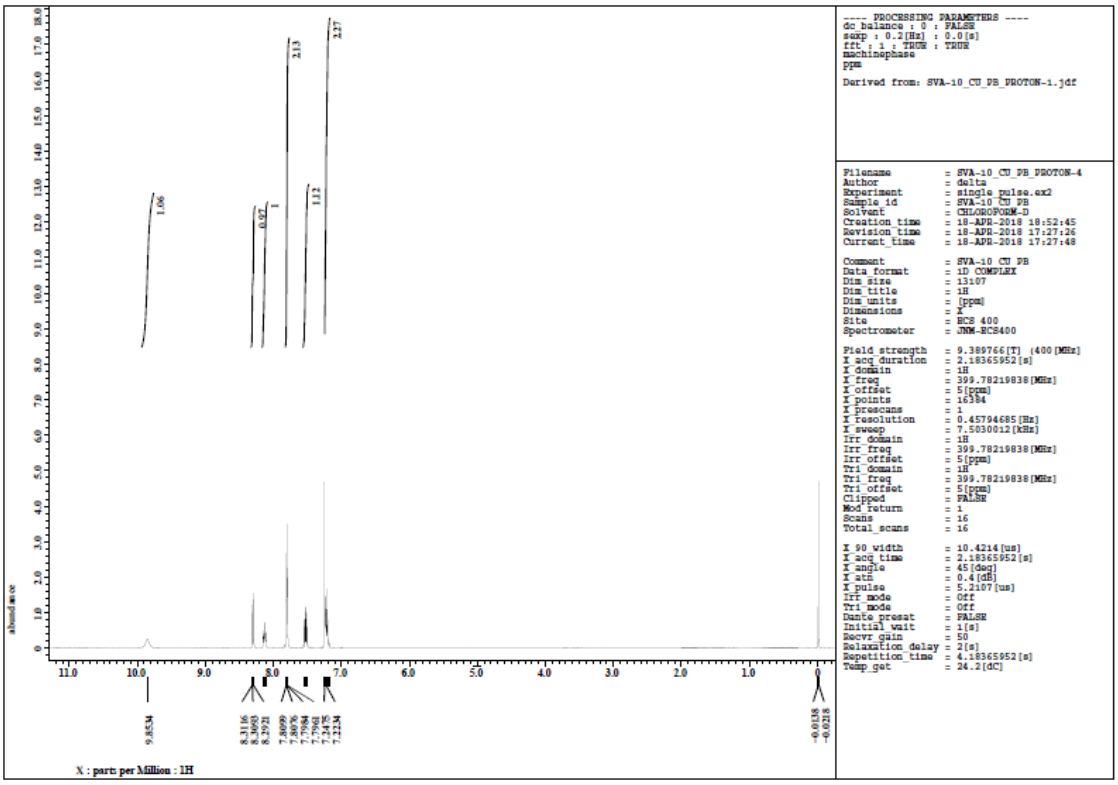

Figure 39: ^{1}H Spectrum of compound SVA-10

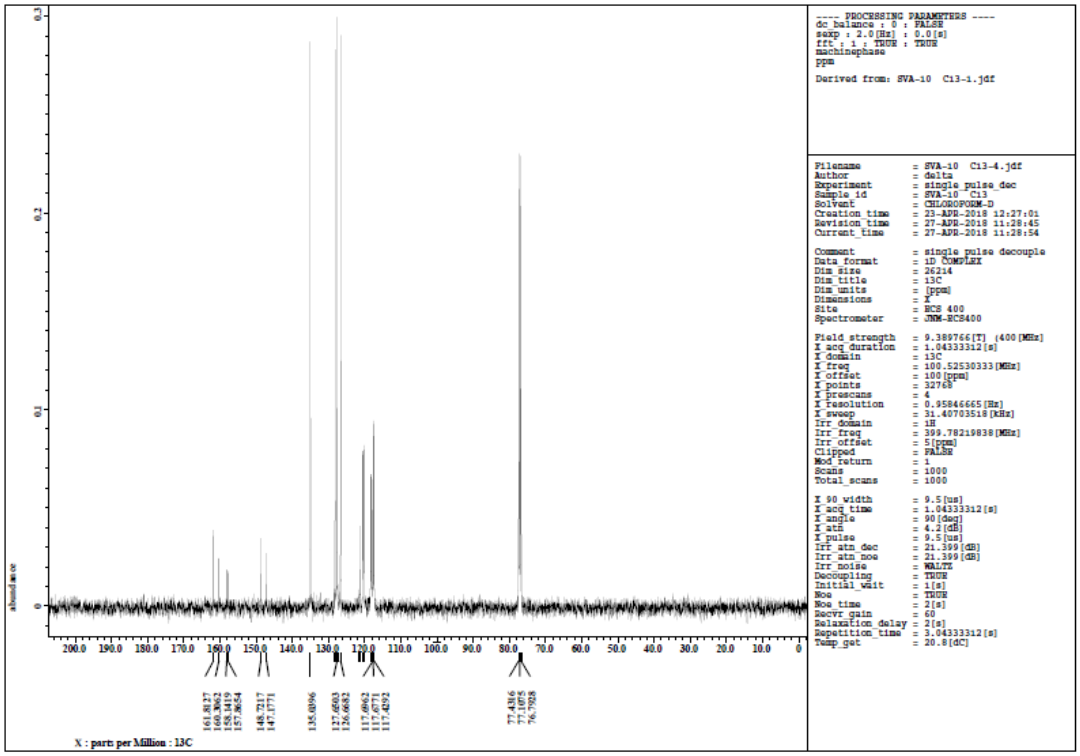

Figure 40: ^{13}C Spectrum of compound SVA-10

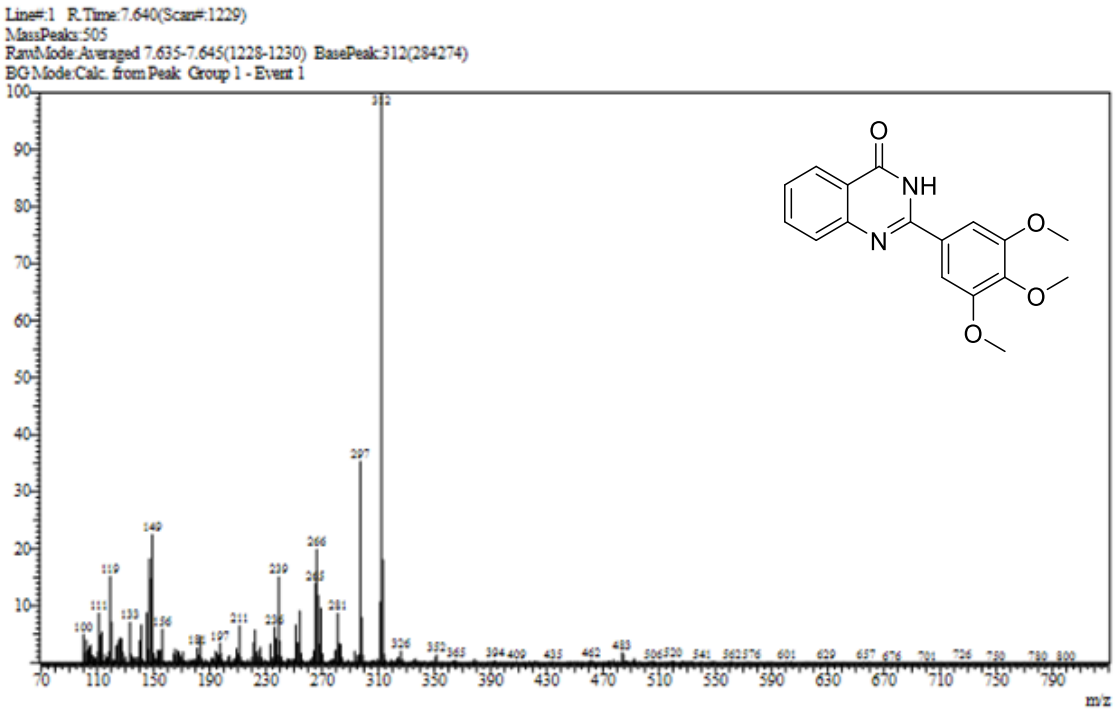

Figure 41: Mass spectrum of compound SVA-11

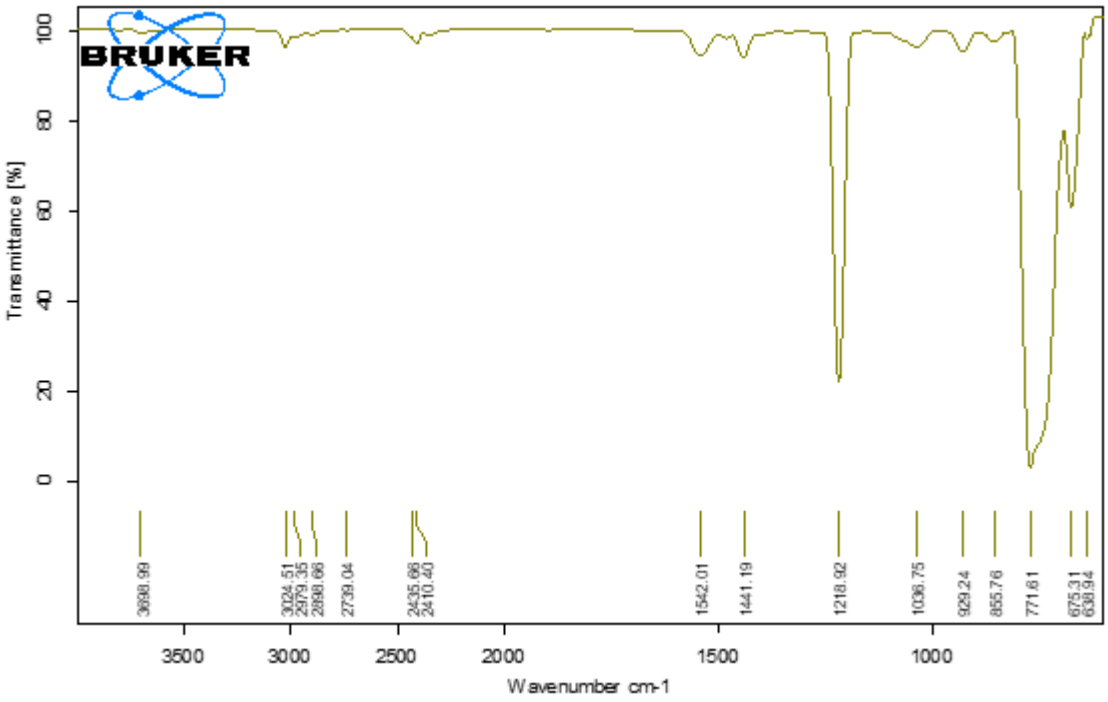

Figure 42: I.R. spectrum of compound SVA-11

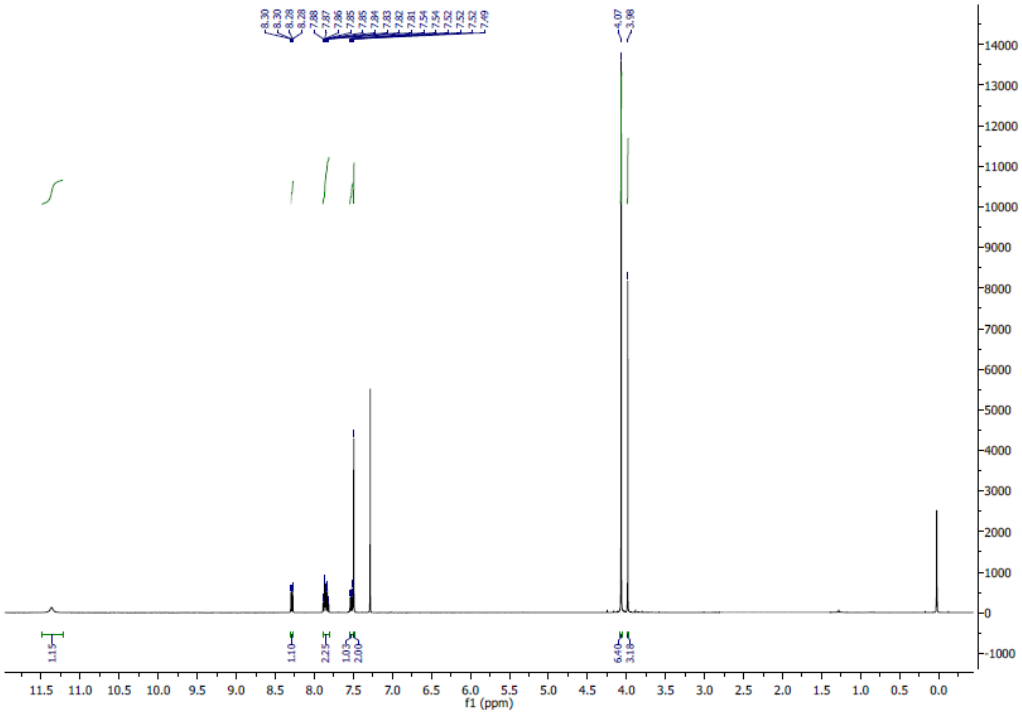

Figure 43: ^{1}H Spectrum of compound SVA-11

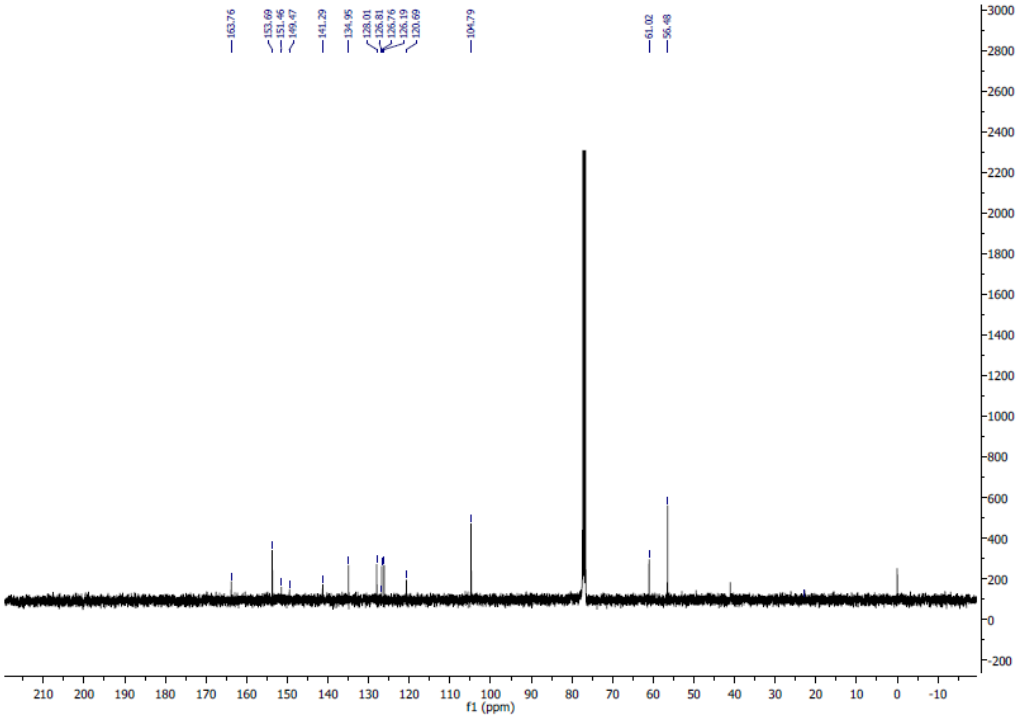

Figure 44: ^{13}C Spectrum of compound SVA-11